

Four-Mode Broadband PLC-based Converter-(de)Multiplexer

Hao Sun

A Thesis

in

The Department

of

Electrical and Computer Engineering

Presented in Partial Fulfillment of the Requirements

For the Degree of Master of Applied Science at

Concordia University

Montreal, Quebec, Canada

May 2019

© Hao Sun, 2019

**CONCORDIA UNIVERSITY
SCHOOL OF GRADUATE STUDIES**

This is to certify that the thesis prepared

By: Hao Sun

Entitled: Four-Mode Broadband PLC-based Converter-(de)Multiplexer

and submitted in partial fulfillment of the requirements for the degree of

Master of Applied Science

Complies with the regulations of this University and meets the accepted standards with respect to originality and quality.

Signed by the final examining committee:

| | |
|----------------------|--------------------|
| _____ | Chair |
| Dr. Zahangir Kabir | |
| _____ | Examiner, External |
| Dr. Pablo Bianucci | To the Program |
| _____ | Examiner |
| Dr. Zahangir Kabir | |
| _____ | Supervisor |
| Dr. John Xiupu Zhang | |
| _____ | Co-Supervisor |
| Dr. | |

Approved by: _____
Dr. W. E. Lynch, Chair
Department of Electrical and Computer Engineering

| | |
|-------|---|
| _____ | _____ |
| 20 | Dr. Amir Asif, Dean |
| | Gina Cody School of Engineering and Computer Science |

ABSTRACT

Mode-division (de)multiplexing (MDM) is one of the technologies that are being developed to increase the transmission capacity in optical communication. Signals are transmitted through different modes in such a system, and each mode is a channel. Generally speaking, in an MDM system, the fundamental mode is first converted into higher modes, then multiplexed into one few-mode fibre (FMF) or waveguide, and finally demultiplexed after the transmission in order to retrieve the original signals. Therefore, mode converters and (de)multiplexers are the key devices in the MDM system.

Mode converting and (de)multiplexing can be realized through varying methods and technologies. Initially, devices based on free-space optics have been studied. These devices use phase masks to match input modes to output modes. Free-space optics based devices are more wavelength independent but too complex to apply and are accompanied by high insertion loss. Other approaches are through fibre and other waveguides, which include all-fibre structure, tapered fibre, fibre grating, planar lightwave circuit (PLC), photonic crystal fibre (PCF) and Y-junction. These devices have high conversion efficiency and are more compact thus easier to apply in practice.

In this thesis, a broadband four-mode converter-(de)multiplexer based on silica planar lightwave circuit using two assistant waveguides is designed and analyzed under simulation.

First of all, a two-mode converter-(de)multiplexer is designed to justify the mode coupling method using N_{eff} matching. Because the waveguides utilized in all designs are weak waveguides, the power in one waveguide transmitting as mode 1 can be transferred to another waveguide while converting to mode 2. The key to mode converting is that the value of N_{eff} for the two different modes at each waveguide should be manipulated to be as close as possible, which can be achieved by changing the structure width. Insertion loss over the entire S, C, L-band is less than 1.5 dB, and less than 0.2 dB at the central wavelength of 1550 nm. The extinction ratio over the S, C, L-band is higher than 22 dB.

Next, a four-mode converter-(de)multiplexer designed for TE_0 , TE_1 , TE_2 and TE_3 mode over entire S, C, L-band is demonstrated. The structure includes six waveguides and two of them serve as assistant waveguides. At the end of process, four inputs of TE_0 mode are converted and multiplexed to the central waveguide in the form of TE_0 , TE_1 , TE_2 and TE_3 mode. The insertion loss over the C-band when converting and (de)multiplexing TE_0 mode to TE_1 , TE_2 and TE_3 mode is less than 0.5 dB. And over the S, C, L-band, the insertion loss for conversion between TE_0 , TE_1 , TE_2 mode is less than 2 dB. Moreover, the extinction ratio for TE_0 , TE_1 , TE_2 and TE_3 mode over the S, C, L -band is over 17 dB, and is higher than 23 dB for the C-band. Furthermore, the insertion loss between TE_0 and TE_3 is less than 0.5 dB for the C-band with the extinction ratio higher than 32 dB in the same range. The crosstalk between the TE_0 , TE_1 , TE_2 and TE_3 mode is below 0.4 dB over the C-band and below 1.1 dB over the S, C, L-band.

Index Terms: MDM, PLC, mode converter, mode (de)multiplexer

ACKNOWLEDGEMENTS

I would like to express my sincere gratitude to Professor John Xiupu Zhang for his insightful advice, help and great support for me to finish my thesis.

I would also like to express my appreciation to my colleague Dr. Hakim Mellah for his patient help and advice.

I would also like to thank Xiaoran Xie, Weijie Tang and Zijian Cheng for their help.

I am very grateful to my parents for their endless love, understanding and support.

I would like to say a big thanks to my girlfriend for her deep love and support.

Table of Contents

| | |
|--|------|
| Four-Mode Broadband PLC-based Converter-(de)Multiplexer..... | i |
| Table of Contents | vi |
| List of Figures | viii |
| List of Tables..... | xii |
| List of Acronyms..... | xiii |
| Chapter 1 Introduction..... | 1 |
| 1.1 Optical Communication and Mode-Division Multiplexing..... | 1 |
| 1.2 Motivations and Contributions | 4 |
| 1.3 Organization of Thesis..... | 4 |
| Chapter 2 Literature Review..... | 6 |
| 2.1 Introduction | 6 |
| 2.2 Mode Converters and (de)Multiplexers..... | 6 |
| 2.2.1 Free Space Mode Converters and (de)Multiplexers | 6 |
| 2.2.2 Fibre and Waveguide-Based Mode Converters and (de)Multiplexers | 7 |
| Chapter 3 Proposed Two-Mode converter-(de)multiplexer | 16 |
| 3.1 Introduction | 16 |
| 3.2 Introduction to RSoft..... | 16 |
| 3.2.1 BeamPROP..... | 16 |
| 3.2.2 MOST Optimizer..... | 23 |
| 3.3 Proposed Two-Mode converter-(de)multiplexer Structure | 24 |
| 3.4 Performance of the Two-Mode Design | 28 |

| | | |
|--|---|----|
| 3.4.1 | Input from Left Port..... | 28 |
| 3.4.2 | Input from Right Port | 30 |
| 3.4.3 | Input from Both Ports | 32 |
| 3.4.4 | Two-Mode Backward Conversion and Demux | 35 |
| 3.5 | Summary..... | 38 |
| Chapter 4 Proposed Four-Mode converter-(de)multiplexer | | 39 |
| 4.1 | Introduction | 39 |
| 4.2 | Proposed Four-Mode converter-(de)multiplexer structure..... | 39 |
| 4.2.1 | Overview of the Four-Mode Structure | 39 |
| 4.2.2 | Design of the Two Assistant Waveguides..... | 42 |
| 4.3 | Performance of the Four-Mode Design | 53 |
| 4.3.1 | Input from Port 1 | 53 |
| 4.3.2 | Input from Port 2 | 55 |
| 4.3.3 | Input from Port 3 | 57 |
| 4.3.4 | Input from Port 4 | 60 |
| 4.3.5 | Input from All 4 Ports..... | 62 |
| 4.3.6 | Four-Mode Backward Conversion and Demux..... | 65 |
| Chapter 5 Conclusion | | 71 |
| 5.1 | Conclusion..... | 71 |
| 5.2 | Future work..... | 72 |
| References | | 73 |

List of Figures

| | |
|---|----|
| Figure 1-1 The evolution of transmission capacity [1] | 1 |
| Figure 1-2 MCF approach for SDM [1] | 2 |
| Figure 1-3 FMF [1] | 3 |
| Figure 2-1 Mode conversion using LCOS [3]..... | 6 |
| Figure 2-2 MDM using phase plate [4] | 7 |
| Figure 2-3 All-Fibre Broadband LP02 Mode Converter [11] | 8 |
| Figure 2-4 Mode Rotator and Multiplexer [12] | 8 |
| Figure 2-5 Taper Fibre-based Mode Converter [13] | 9 |
| Figure 2-6 Mode converter based on fibre grating [14] | 9 |
| Figure 2-7 PCF Mode Converter [15] | 10 |
| Figure 2-8 LP11 mode rotator [18] | 10 |
| Figure 2-9 PLC-based mode converter-(de)multiplexer field transition [18] | 11 |
| Figure 2-10 PLC-based mode converter-(de)multiplexer [18] | 11 |
| Figure 2-11 Silicon-based mode converter-(de)multiplexer [22] | 12 |
| Figure 2-12 Y-junction based (de)multiplexer [29] | 12 |
| Figure 2-13 Mode (de)multiplexer based on waveguide arrays [28] | 13 |
| Figure 2-14 Schematic configuration of the three-channel device [30]..... | 13 |
| Figure 2-15 Four TM mode device [31]..... | 14 |
| Figure 2-16 Eight-channel hybrid (de)multiplexer [32]..... | 14 |
| Figure 3-1 Global Settings Window..... | 17 |
| Figure 3-2 Properties for Segment | 18 |
| Figure 3-3 Launch Parameters | 19 |
| Figure 3-4 Pathway | 20 |
| Figure 3-5 Monitor Options | 21 |
| Figure 3-6 Mode Calculation Options..... | 21 |
| Figure 3-7 Gaussian Offset | 22 |

| | |
|--|----|
| Figure 3-8 Mode Calculation Parameters..... | 22 |
| Figure 3-9 Warning | 23 |
| Figure 3-10 MOST Parameters | 23 |
| Figure 3-11 Two-Mode Structure (Front) | 24 |
| Figure 3-12 Two-Mode Structure (Top) | 25 |
| Figure 3-13 Two-Mode Structure (3D)..... | 25 |
| Figure 3-14 Mode Coupling and N_{eff} Matching [17]..... | 26 |
| Figure 3-15 Resonance..... | 27 |
| Figure 3-16 Two-Mode Input at Left | 28 |
| Figure 3-17 Two-Mode IL In- TE_0 Out- TE_0 | 29 |
| Figure 3-18 Two-Mode ER TE_0 | 30 |
| Figure 3-19 Two-Mode Input at Right..... | 31 |
| Figure 3-20 Two-Mode IL In- TE_0 Out- TE_1 | 31 |
| Figure 3-21 Two-Mode ER TE_1/TE_0 | 32 |
| Figure 3-22 Two-Mode Input All..... | 33 |
| Figure 3-23 Two-Mode XT TE_0 | 34 |
| Figure 3-24 Two-Mode XT TE_1 | 34 |
| Figure 3-25 Two-Mode Demux | 35 |
| Figure 3-26 Two-Mode Demux IL In- TE_0 Out- TE_0 | 36 |
| Figure 3-27 Two-Mode Demux IL In- TE_1 Out- TE_0 | 36 |
| Figure 3-28 Two-Mode Demux XT TE_0 | 37 |
| Figure 3-29 Two-Mode Demux XT TE_1 | 38 |
| Figure 4-1 Four-Mode Structure (Front)..... | 39 |
| Figure 4-2 Four-Mode Structure (Top) | 40 |
| Figure 4-3 Four-Mode Structure (3D)..... | 41 |
| Figure 4-4 N_{eff} and waveguide width for modes | 42 |
| Figure 4-5 TE_0 to TE_1 N_{eff} Matching Map..... | 43 |
| Figure 4-6 TE_0 to TE_2 mode N_{eff} Matching Map | 44 |

| | |
|---|----|
| Figure 4-7 TE ₀ to TE ₃ mode N _{eff} Matching Map..... | 44 |
| Figure 4-8 ΔN_{eff} for 48 μm waveguide..... | 45 |
| Figure 4-9 Design of Assistant Waveguide..... | 46 |
| Figure 4-10 N _{eff} Matching Map for the other research [19] | 46 |
| Figure 4-11 Comparison of ER TE ₃ /TE ₀ | 47 |
| Figure 4-12 Comparison of ER TE ₃ /TE ₁ | 47 |
| Figure 4-13 Comparison of ER TE ₃ /TE ₂ | 48 |
| Figure 4-14 Four-Mode design with TE ₀ to TE ₁ to TE ₃ N _{eff} matching map | 48 |
| Figure 4-15 Four-Mode design with TE ₀ to TE ₁ N _{eff} matching map..... | 49 |
| Figure 4-16 Four-Mode via input3..... | 50 |
| Figure 4-17 Reverse-transfer between TE ₁ and TE ₀ | 51 |
| Figure 4-18 Four-Mode N _{eff} matching | 52 |
| Figure 4-19 Four-Mode input at port 1 | 53 |
| Figure 4-20 Four-Mode IL In-TE ₀ Out-TE ₂ | 54 |
| Figure 4-21 Four-Mode ER TE ₂ | 55 |
| Figure 4-22 Four-Mode input at port 2 | 56 |
| Figure 4-23 Four-Mode IL In-TE ₀ Out-TE ₀ | 56 |
| Figure 4-24 Four-Mode ER TE ₀ | 57 |
| Figure 4-25 Four-Mode input at port 3 | 58 |
| Figure 4-26 Four-Mode IL In-TE ₀ Out-TE ₁ | 59 |
| Figure 4-27 Four-Mode ER TE ₁ | 59 |
| Figure 4-28 Four-Mode input at port 4 | 60 |
| Figure 4-29 Four-Mode IL In-TE ₀ Out-TE ₃ | 61 |
| Figure 4-30 Four-Mode ER TE ₃ | 61 |
| Figure 4-31 Four-Mode input all..... | 62 |
| Figure 4-32 Four-Mode XT TE ₀ | 63 |
| Figure 4-33 Four-Mode XT TE ₁ | 63 |
| Figure 4-34 Four-Mode XT TE ₂ | 64 |

| | |
|---|----|
| Figure 4-35 Four-Mode XT TE ₃ | 64 |
| Figure 4-36 Four-Mode Demux | 65 |
| Figure 4-37 Four-Mode Demux IL In-TE ₀ Out-TE ₀ | 66 |
| Figure 4-38 Four-Mode Demux IL In-TE ₁ Out-TE ₀ | 66 |
| Figure 4-39 Four-Mode Demux IL In-TE ₂ Out-TE ₀ | 67 |
| Figure 4-40 Four-Mode Demux IL In-TE ₃ Out-TE ₀ | 67 |
| Figure 4-41 Four-Mode Demux XT TE ₀ | 68 |
| Figure 4-42 Four-Mode Demux XT TE ₁ | 68 |
| Figure 4-43 Four-Mode Demux XT TE ₂ | 69 |
| Figure 4-44 Four-Mode Demux XT TE ₃ | 69 |

List of Tables

Table 1 Summary of different techniques 15

Table 2 Two-Mode Metrics..... 25

Table 3 Four-Mode Metrics (Width)..... 40

Table 4 Four-Mode Metrics (Gap) 40

Table 5 Four-Mode Metrics (Length) 40

List of Acronyms

| | |
|-------------------------|---------------------------------------|
| EDFA | Erbium-Doped Fibre Amplifier |
| MCF | Multi-Core Fibre |
| MDM | Mode-Division Multiplexing |
| MMF | Multi-Mode Fibre |
| FMF | Few-Mode Fibre |
| LCOS | Liquid Crystal on Silicon |
| PLC | Planar Lightwave Circuit |
| PCF | Photonic Crystal Fibre |
| SDM | Space-Division Multiplexing |
| SMF | Single Mode Fibre |
| WDM | Wavelength-Division Multiplexing |
| LP | Linear Polarized |
| Δn | Refractive index difference |
| N_{eff} | Effective refractive index |
| ΔN_{eff} | Effective refractive index difference |
| IL | Insertion Loss |
| ER | Extinction Ratio |

XT

Crosstalk

Chapter 1 Introduction

1.1 Optical Communication and Mode-Division Multiplexing

Though serving as a critical foundation to the global network and information-driven society for the past 40 years, transmission capacity has become a major challenge to traditional coaxial cable. In the world of modern telecommunication, optical communication has assumed an increasingly important role, thanks to the capacity increase brought by optical frequency band.

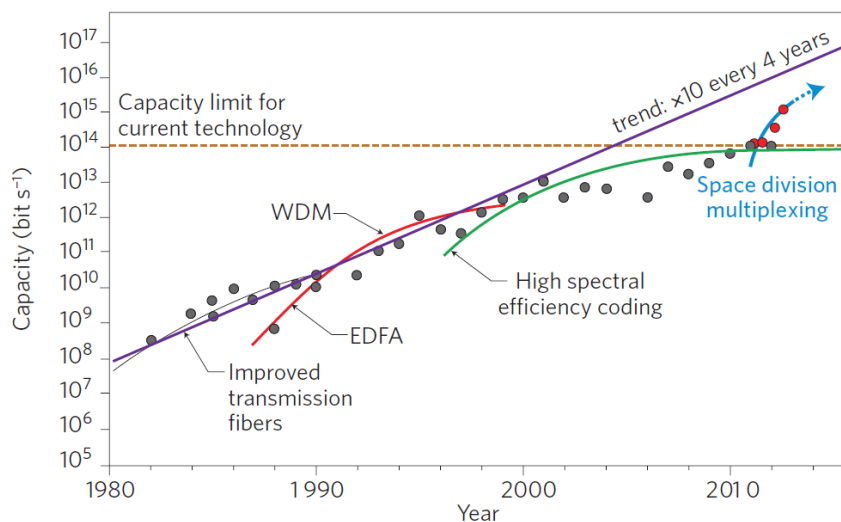


Figure 1-1 The evolution of transmission capacity [1]

Optical communication technologies have been developed and implemented since the first usable fibre was made by Corning Inc [1]. In the mid-70's, stable room-temperature semiconductor laser was invented, which laid the foundation of the usable light source in optical communication. In the 80's, improved fabrication technology allowed the invention of Single Mode Fibre (SMF), through which remarkable 0.2dB low-loss was achieved at 1550 nm window. Since then, transmission capacity has been increasing at a speed of approximately 10 times every four years. In the 90's, both Erbium-Doped Fibre Amplifier (EDFA) and Wavelength-Division Multiplexing (WDM) were developed and created a boom in the industry. By then, the transmission capacity had reached the level of 10¹¹-10¹² bits/s. Benefiting from

improved high spectral efficient coding, the capacity of an SMF reached a limit at around 100Tbits/s. However, that limit cannot be overcome by modulation mechanism because it's derived from the nature of Shannon capacity limit [2]. In order to carry more signals on fibre, we need to use multiple fibres. But this in turn introduces more costs directly associated with the level of capacity, which is not efficient in the long term. With the growing desire for a greater capacity of worldwide telecommunication transmission generated by the booming information technology era, optical communication industry had reached a point where it is ultimately essential to implement Space-Division Multiplexing (SDM) technology.

Since 2010, SDM has gained massive attention from researchers for its ability to break the capacity limit of transmission. SDM is also known as the following two types of technologies: transmission using Multi-Core Fibres (MCF), and Mode-Division Multiplexing (MDM) in the waveguide that supports multi-mode transmission. Both technologies use multiple spatial transmission paths to establish different communication channels. The goal for SDM is to integrate as many components as possible to achieve better performance with compacter device size, by combining these existing technologies with WDM and EDFA,

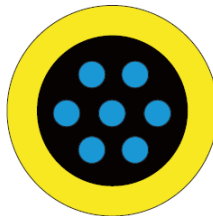


Figure 1-2 MCF approach for SDM [1]

First technological approach is through MCF, in which signal channels are separated by physical fibre path. To reduce the crosstalk between different cores, either the distance between fibre cores needs to be far enough, or the physical properties of the fibre need to be adjusted in a certain way to ensure that energy within one core is not able to crossover into the neighbour cores. Increasing the distance between multiple cores is the simplest method. However, to achieve optimal result, the diameter of the final MCF product will be too big for practical situations, which can bring problems such as reduced structure strength when facing potential

fracture. Figure 1-2 shows a typical seven-core MCF, which includes six neighbour-cores for the centre core. 12-core and 19-core MCFs also appeared in various researches.

Second approach is by employing Multi-Mode Fibres (MMF), Few-Mode Fibres (FMF) and other multi-mode waveguides as components of and in conjunction with converters and multiplexers according to each its own structures. Before the introduction of FMF, MMF reported with core/cladding diameters of 50/125 μm and 62.5/125 μm can support more than 100 modes. [1] However, due to group dispersion, the amount of travel time within the fibre varies for each signal in different modes. With more modes transmitting together, further time delay is expected and should be dealt with. In the case of MMF, performance of long links will suffer greatly from high group dispersion. In order to receive the original signal accurately, DSP is generally used. However, it increases complexity and cost of the system. Consequently, FMF is developed to limit support modes and find an optimum balance between mode count and group dispersion. Figure 1-3 shows the sectional view of an FMF with a core dimension/numerical aperture set to guide a restricted number of modes.

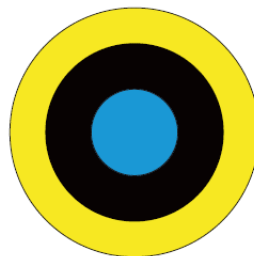


Figure 1-3 FMF [1]

To utilize the advantage of mode-division multiplexing, fundamental modes from inputs need to be converted to the higher modes and transmitted together. This process involves two techniques, mode converting and (de)multiplexing. Even though they are generally seen as two independent procedures, combining them together in fact reduces complexity of the device, which leads to easier installment and ultimately greater efficiency.

Since easy integration is one advantage of planar waveguide, silica and silicon planar waveguides has become one of the main platforms to perform mode-division multiplexing. The different technologies used for mode converting and (de)multiplexing are discussed in the next chapter.

1.2 Motivations and Contributions

Mode-division multiplexing are based on several key components, two of them are mode converters and mode multiplexers. Originally the two components were introduced as two separate devices, which result in increased system complexity and applying cost. By combine those two techniques together into one device, multiple processes can operate together to increase efficiency. The performance, in terms of insertion loss, extinction ratio and crosstalk are affecting the system when considered to apply such techniques.

In this thesis, the design is mainly focused to implement a fundamental method to strengthen the performance of extinction ratio by adding assistant waveguides to the structure. The contributions of this thesis are to design the two assistant waveguides and the physical narrowing process at the end of the assistant waveguides. After implementing one of the assistant waveguides in the two-mode structure to construct a novel three-mode structure, the extinction ratio is improved more than 8 dB at wavelength of 1550 nm, and it's improved greatly over a broad band. Finally, two assistant waveguides are implemented to the four-mode structure with total six waveguides to perform mode converting and (de) multiplexing.

1.3 Organization of Thesis

The rest of the thesis is organized as follows:

In chapter 2, literature review is presented for the free space optics and fibre/waveguide-based mode converters and (de)multiplexers.

Chapter 3 begins with introduction to the proposed two-mode converter-(de)multiplexer along with the simulation tool RSoft. It is then followed by a performance examination of two different light injection scenarios: injection from either port and injection from both ports. In the meantime, insertion loss for each mode is measured against wavelength scans above S, C, L-band for broadband performance evaluation. Extinction ratio and crosstalk are also measured to assess mode purity. Moreover, reverse light path is also examined for de-multiplexing and converting performance.

In chapter 4, the proposed four-mode converter-(de)multiplexer is introduced. Device design is based on the same metrics described in the previous chapter, but expanded to conduct converting and (de)multiplexing for more modes with two assistant waveguides. Same wavelength scan above S, C, L-band is performed to assess the quality on broadband.

Chapter 5 summarizes the results from this research and suggests potential future work.

Chapter 2 Literature Review

2.1 Introduction

In this chapter, existing mode converters and (de)multiplexers from other researches are presented. Since the introduction of Mode-division multiplexing (MDM) technology, mode converter and (de)multiplexer have been used to generate high order modes and combine multiple modes together. As the key parts of the MDM system, such devices have been widely researched. Based on the material in which power of different modes travels through, the devices can be classified into two general categories, free space optics based and fibre/waveguide based.

2.2 Mode Converters and (de)Multiplexers

2.2.1 Free Space Mode Converters and (de)Multiplexers

Free space optics based devices utilize input-output profile matching process based on phase masks programmed on liquid crystal on silicon (LCOS) spatial modulators. For example, a mode converter and multiplexer based on LCOS designed to convert LP_{01} to LP_{11a} and LP_{11b} mode has 6 dB conversion loss and 16 dB multiplexing loss overall [3].

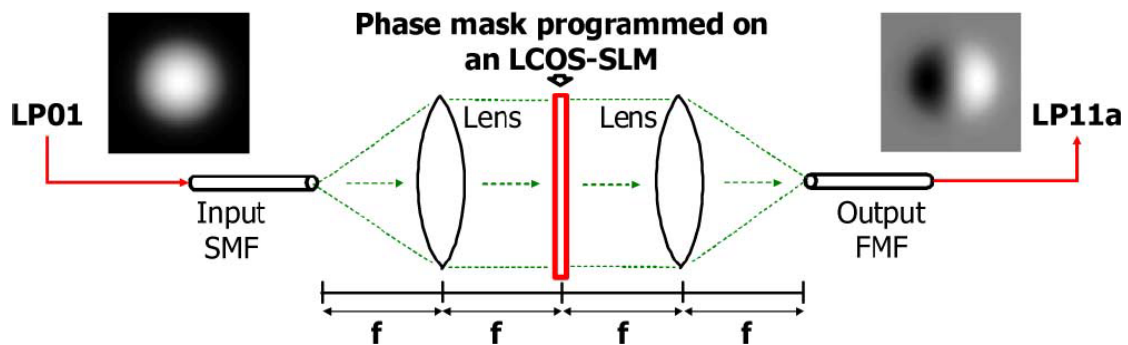


Figure 2-1 Mode conversion using LCOS [3]

Another research using phase plate with mirrors and lenses also successfully converted LP_{01} to LP_{11a} and LP_{11b} mode. The insertion loss for LP_{01} to LP_{11a} mode is 9 dB and 7.8 dB for LP_{01} to LP_{11b} modes [4].

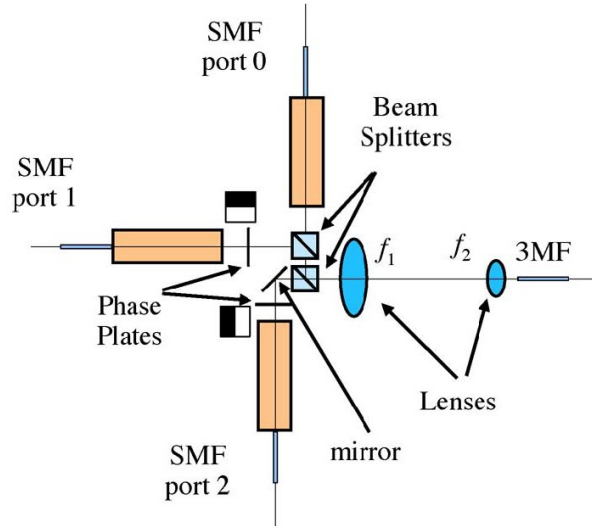


Figure 2-2 MDM using phase plate [4]

Mode converters and (de)multiplexers based on free space optics is broadband, therefore less sensitive to wavelength. However, besides the high insertion loss, the deployment for those technologies is also impractical. It usually involves optical alignment and can hardly be integrated.

2.2.2 Fibre and Waveguide-Based Mode Converters and (de)Multiplexers

Apart from free space mode converters and (de)multiplexers, devices based on optical waveguides have become the major trend of the academic research. Such structures include optical fibre [5], grating [6], photonic lantern [7], Y-junctions [8], planar lightwave circuit (PLC) [9] and photonic crystal fibre (PCF) [10].

One research used multimode fibre (MMF) by inserting it between a single mode fibre (SMF) and an few mode fibre (FMF) to build a combined device to convert LP_{01} to LP_{02} mode.

Based on the simulation results, it has an insertion loss lower than 2.4 dB over the S, C, L-band and the extinction ratio is 55 dB at the wavelength of 1550 nm [11].

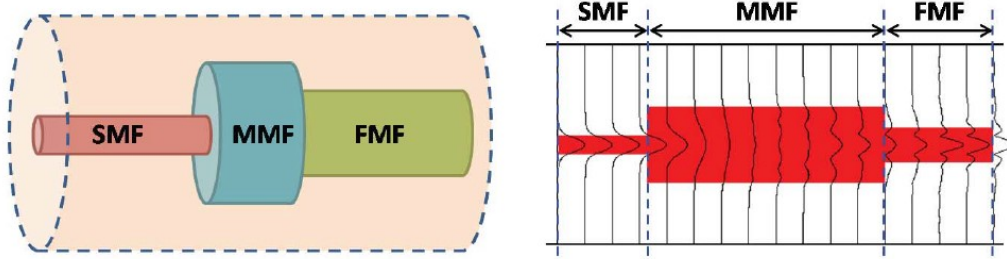


Figure 2-3 All-Fibre Broadband LP02 Mode Converter [11]

In another research [12], a fibre-based degenerate mode rotator is designed using a special 2-core-fibre. The simulation results of rotation efficiencies from 1450 to 1650 nm wavelength is more than 97% and 95% for LP₁₁ and LP₂₁ mode respectively. Overall rotation efficiency for LP_{11a}, LP_{11b}, LP_{21a}, LP_{21b} is higher than 70%. Extinction ratio is more than 20 dB.

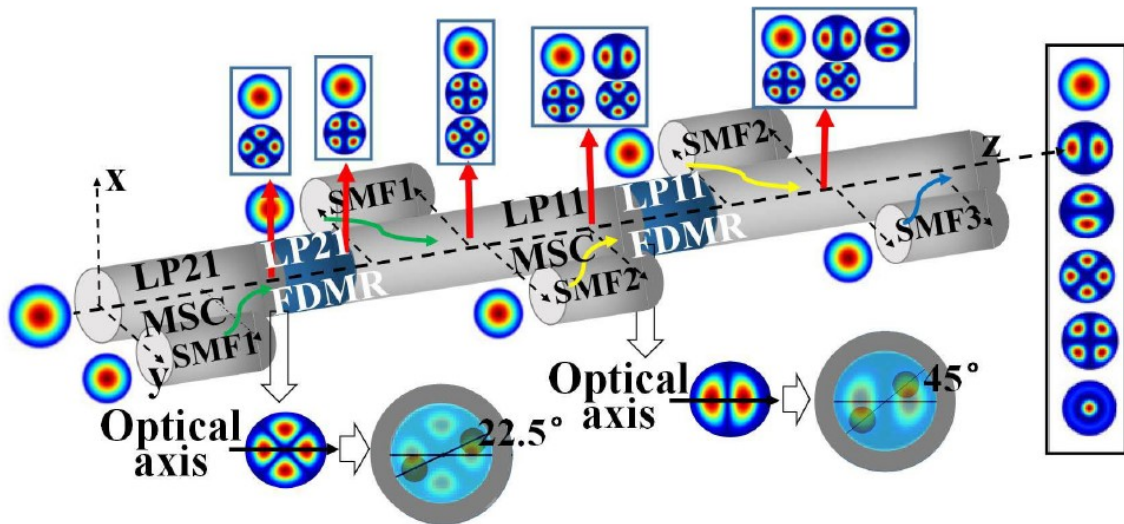


Figure 2-4 Mode Rotator and Multiplexer [12]

Taper fibre can also be used in mode conversion. Research [13] demonstrates simulation performance regarding mode converters between LP₀₁ and LP_{0m} using two-stage taper fibre. In the case of LP₀₁ to LP₀₂ mode conversion, the insertion loss is less than 0.2 dB from 1530-1560 nm. For LP₀₁ to LP₀₃ mode conversion, the insertion loss is less than 0.55 dB over the same

band. Furthermore, the same metric is less than 0.66 dB for the conversion between LP_{01} and LP_{04} mode. Overall the insertion loss is less than 0.7 dB, and the extinction ratio is higher than 15 dB.

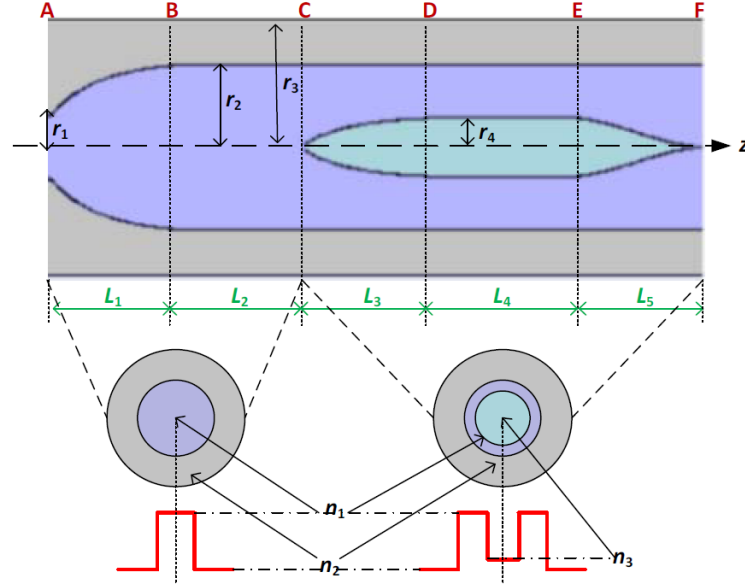


Figure 2-5 Taper Fibre-based Mode Converter [13]

Long-period fibre gratings also can be used to perform mode conversion. Research [14] utilizes mechanical pressure to generate fibre grating. Based on experimental results, the device can achieve 90% conversion efficiency for LP_{01} to LP_{11} conversion over the 30 nm bandwidth with a center at 1550 nm.

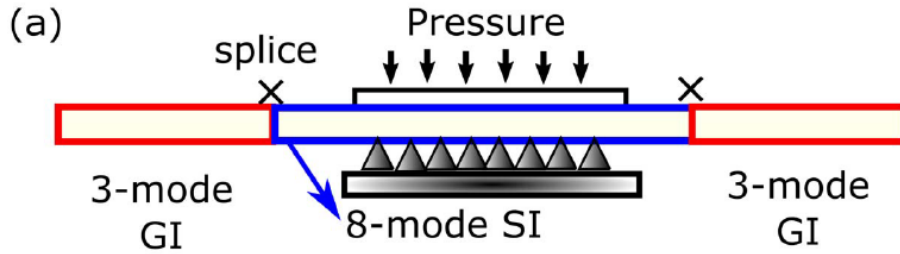


Figure 2-6 Mode converter based on fibre grating [14]

A mode converter based on photonic crystal fibre is analyzed numerically in article [15]. The mode conversion is achieved using air-hole structures of PCF, in which one air-hole is

plugged with glue and others are filled with specific gas. For the LP_{01} to LP_{11a} mode conversion, the coupling efficiency is more than 95% over the C-band. For the LP_{01} to LP_{11b} and LP_{01} to LP_{21} mode conversion the efficiency is higher than 95% and 90% over the S, C, L-band.

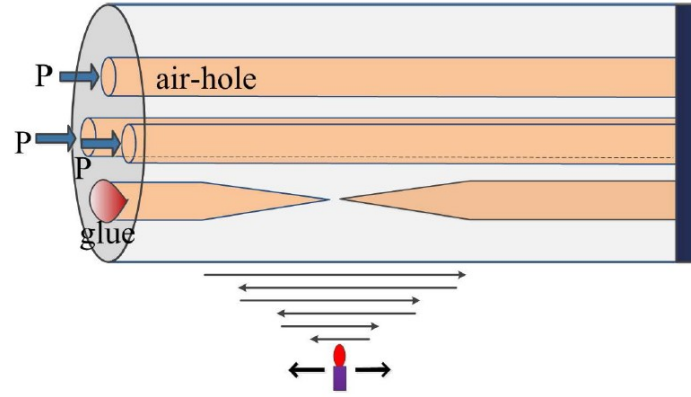


Figure 2-7 PCF Mode Converter [15]

Waveguides other than fibre coms with more possible physical shapes, which can be utilized in designs to suit different needs. Silica PLC is used in several researches [16] [17] [18] [19] [20] [21]. Under research [18], LP_{01} mode is converted to LP_{11a} , LP_{11b} and LP_{21a} mode. And a LP_{11} mode rotator is also included in the design using PLC.

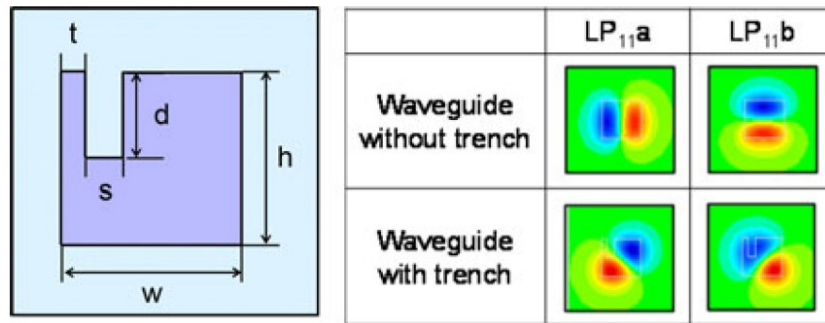


Figure 2-8 LP_{11} mode rotator [18]

The schematic of the device is shown below in Figure 2-9 and Figure 2-10. Three out of the four input LP_{01} modes are each converted into a different higher mode and all four modes are multiplexed based on N_{eff} matching for the different modes in different waveguides. The experiment result of overall insertion loss is less than 3.5 dB over 1530-1560 nm. The extinction ratio is higher than 12 dB over the same range.

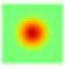
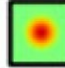
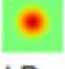




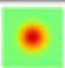

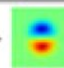
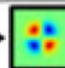
| Input port | Electrical field transition |
|------------|--|
| Port 1 |  \longrightarrow  $LP_{01} \longrightarrow LP_{01}$ |
| Port 2 |  \longrightarrow  $LP_{01} \longrightarrow LP_{11a}$ |
| Port 3 |  \longrightarrow  \longrightarrow  $LP_{01} \longrightarrow LP_{11a} \longrightarrow LP_{11b^*}$ *rotate LP_{11a} 90 degrees. |
| Port 4 |  \longrightarrow  \longrightarrow  \longrightarrow  $LP_{01} \longrightarrow LP_{11a} \longrightarrow LP_{11b^*} \longrightarrow LP_{21a}$ *rotate LP_{11a} 90 degrees. |

Figure 2-9 PLC-based mode converter-(de)multiplexer field transition [18]

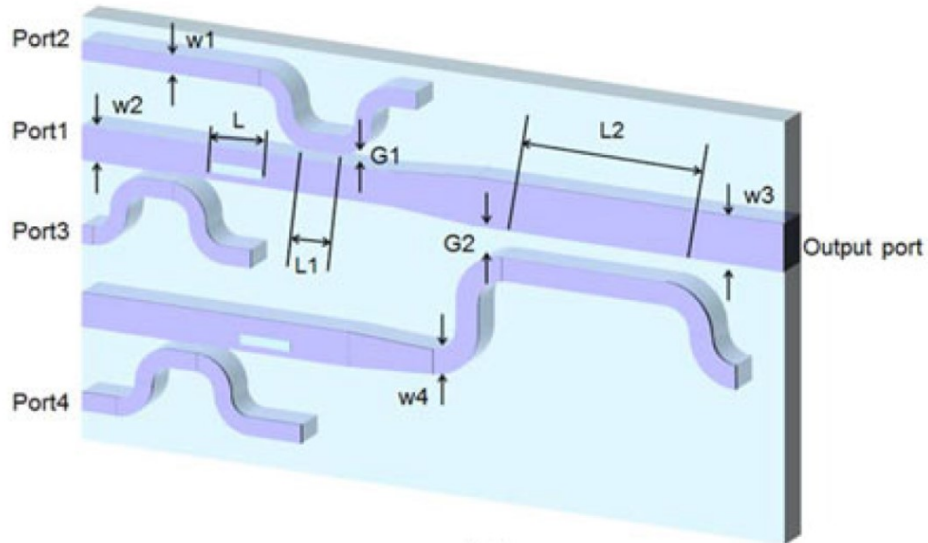


Figure 2-10 PLC-based mode converter-(de)multiplexer [18]

Silicon-based mode converters have been researched widely in the following articles [22] [23] [24] [25] [26] [27]. In research [22], mode converter-(de)multiplexer between TE_0 and TE_1 mode based on mode evolution counter-tapered couplers is designed and fabricated. The insertion loss is less than -1 dB over a band of 180 nm, and extinction ratio (described as crosstalk in the article) is higher than 13 dB.

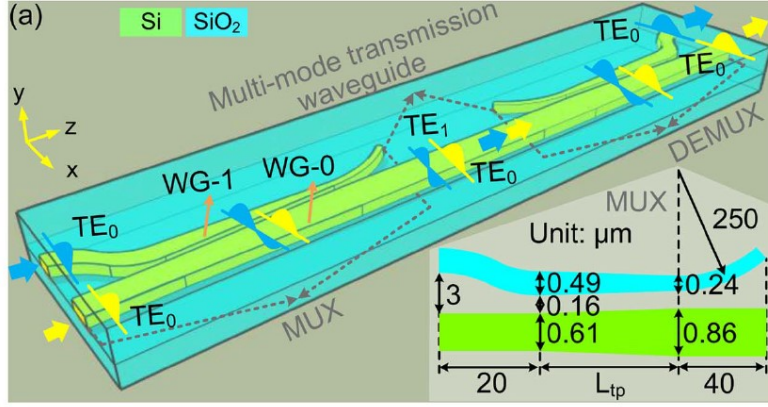


Figure 2-11 Silicon-based mode converter-(de)multiplexer [22]

Waveguide arrays are also utilized in a three-mode multiplexer design according to research [28]. By manipulating the width, the efficient refractive index is set differently for three waveguides. Insertion loss for the (de)multiplexing is less than 0.05 dB and extinction ratio (described as crosstalk in the article) is higher than 20 dB over 100 nm band with a center wavelength of 1550 nm.

A three-mode (de)multiplexer based on two cascaded Y-junctions is introduced in this research [29]. Within a bandwidth from 1537 to 1566 nm, the insertion loss is less than 5.7 dB, and extinction ratio (described as crosstalk in the article) is higher than 9.7 dB.

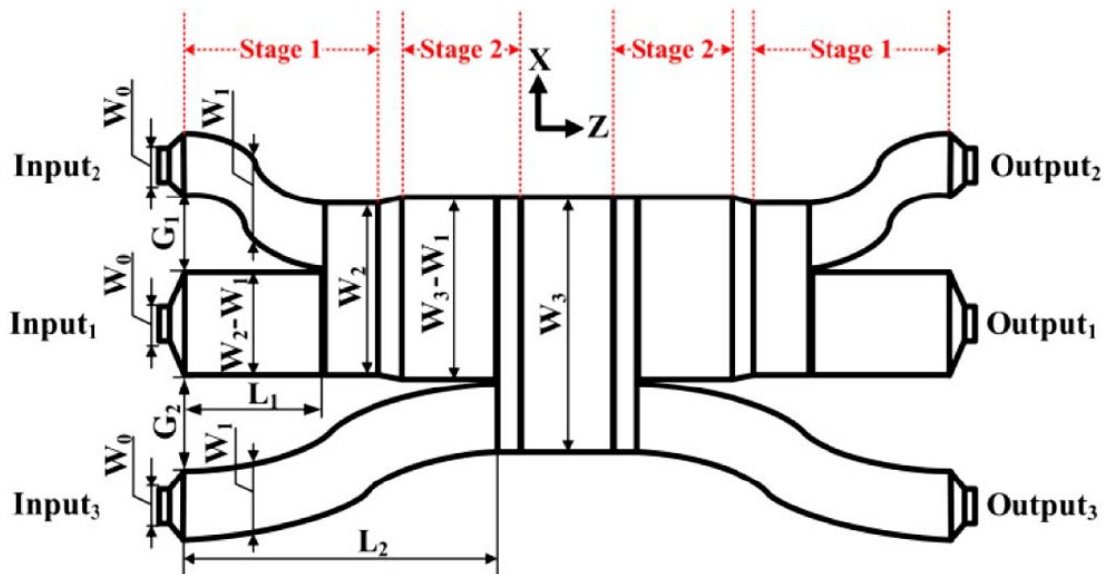


Figure 2-12 Y-junction based (de)multiplexer [29]

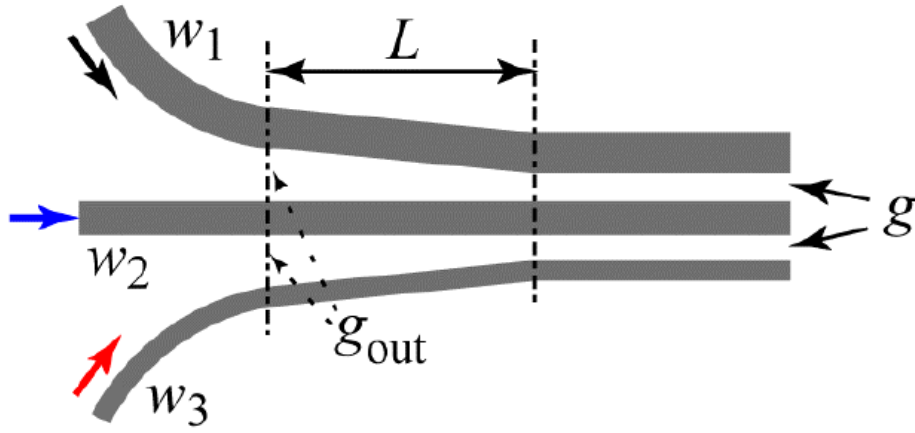


Figure 2-13 Mode (de)multiplexer based on waveguide arrays [28]

In article [30], a three-mode converter-(de)multiplexer is designed based on SOI waveguides. The device can conduct mode converting and demultiplexing process from TE_0 , TE_1 and TE_2 to three TE_0 modes at the output. Also, the reciprocal process can be done from three TE_0 modes to different outputs. As an experimental result, insertion loss is less than 0.2 dB over 65 nm and extinction ratio (described as crosstalk in the article) is higher than 20 dB over the same bandwidth.

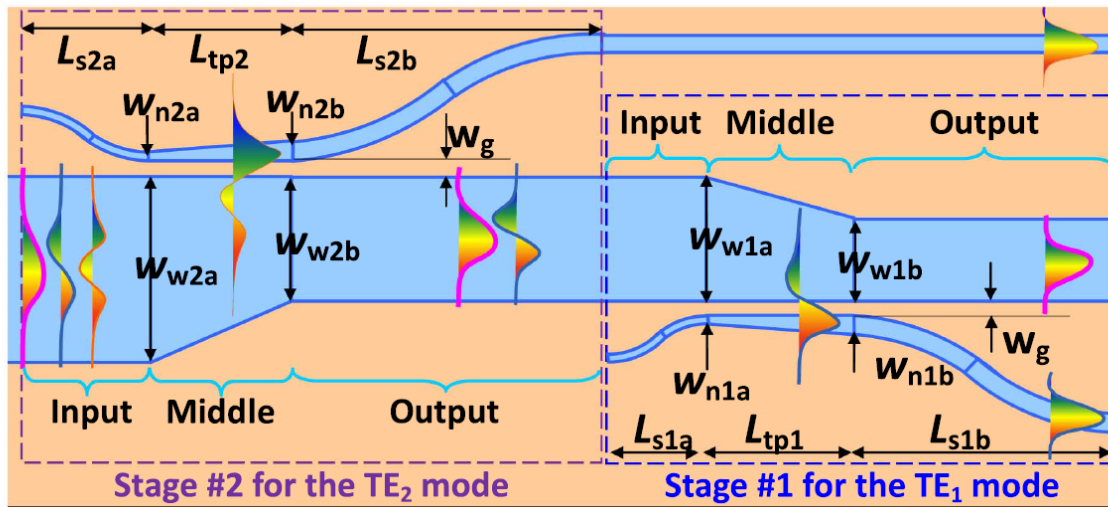


Figure 2-14 Schematic configuration of the three-channel device [30]

Another research [31] uses similar structure to execute mode converting and (de)multiplexing process for TM_0 , TM_1 , TM_2 and TM_3 mode. An insertion loss of 2-5 dB is achieved in the experiment and extinction ratio is higher than 20 dB over 1525-1555 nm.



Figure 2-15 Four TM mode device [31]

Furthermore, an eight-channel hybrid (de)multiplexer based on former research is studied in article [32]. Eight modes including TM_0 , TM_1 , TM_2 , TM_3 , TE_0 , TE_1 , TE_2 and TE_3 mode is converted and (de)multiplexed in the process as shown in Figure 2-16. Extinction ratio (described as crosstalk in the article) is higher than 10 dB for eight modes over a 30 nm wavelength range and the insertion loss is lower than 2 dB.

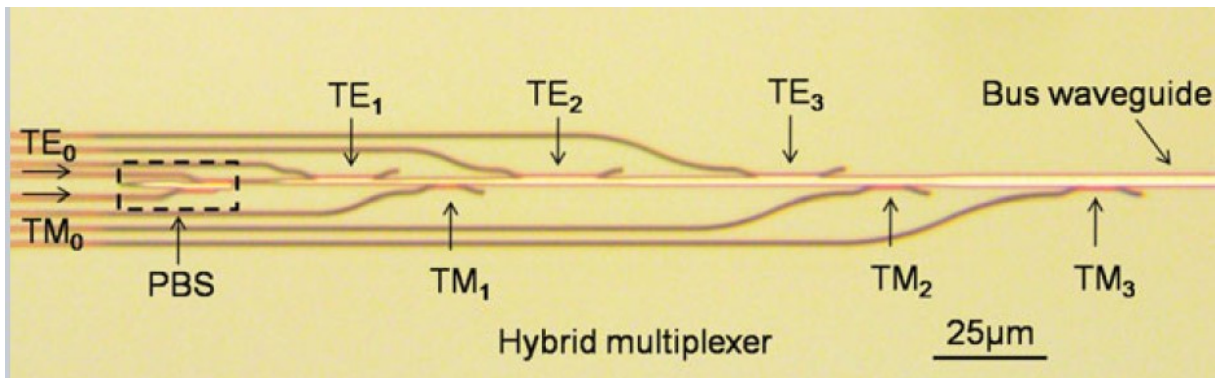


Figure 2-16 Eight-channel hybrid (de)multiplexer [32]

Table 1 below shows the summary of different techniques to achieve mode converting (MC) and/or (de)multiplexing (MUX) with simulation (SIM) or experiment (EXP) result given.

Table 1 Summary of different techniques

| Techniques | Applications | IL (dB) or Efficiency (%) | ER (dB) | Band/Wave length (nm) |
|------------|---|---------------------------|---------|-----------------------|
| Fibre | LP ₀₁ to LP ₀₂ (MC) (SIM) [11] | 2.4 | 55 | S, C, L-band |
| | LP ₀₁ , LP ₁₁ , LP ₂₁ , LP ₀₂ (MC&MUX) (SIM) [12] | 70% | 20 | 1450-1650 |
| | LP ₀₁ , LP ₀₂ , LP ₀₃ and LP ₀₄ (MUX) (SIM) [13] | 0.7 | 15 | 1530-1560 |
| Grating | LP ₀₁ , LP ₁₁ (MC&MUX) (EXP) [14] | 90% | NA | 1535-1545 |
| PCF | LP ₀₁ to LP _{11a} , LP _{11b} and LP ₂₁ (MC) (SIM) [15] | 90% | NA | S, C, L-band |
| Y-Junction | TE ₀ , TE ₁ and TE ₂ (MC&MUX) (EXP) [28] | 5.7 | 9.7 | 1537-1566 |
| PLC | LP ₀₁ to LP _{11a} , LP _{11b} and LP _{21a} (MC&MUX) (EXP) [18] | 3.5 | 12 | 1530-1560 |
| | TE ₀ , TE ₁ and TE ₂ (MC&MUX) (EXP) [22] | 1 | 10 | 1460-1640 |
| | Three modes (MC&MUX) (SIM) [28] | 0.05 | 20 | 1500-1640 |
| | TE ₀ , TE ₁ and TE ₂ (MC&MUX) (EXP) [30] | 0.2 | 20 | 1520-1585 |
| | TM ₀ , TM ₁ , TM ₂ and TM ₃ (MC&MUX) (EXP) [31] | 5 | 20 | 1525-1555 |
| | TM ₀ , TM ₁ , TM ₂ , TM ₃ , TE ₀ , TE ₁ , TE ₂ and TE ₃ (MC&MUX) (EXP) [32] | 2 | 10 | 30 nm in the C-band |

Chapter 3 Proposed Two-Mode converter-(de)multiplexer

3.1 Introduction

In this chapter, the two-mode converter-(de)multiplexer is designed and simulated with RSoft in three dimensions. The principles to design a mode-related passive optical component in RSoft using channel waveguide is studied and demonstrated.

3.2 Introduction to RSoft

RSoft Photonics CAD Suite is a bundle of multiple effective design tools for photonic device and circuit designs for various purposes.

In our simulation, mainly two tools from the RSoft suite were used: BeamPROP and MOST Optimizer. The former tool is used for fundamental structure building, simulation as well as result monitoring and documentation. The latter is for optimizing the target design regarding to different changeable parameters.

3.2.1 BeamPROP

3.2.1.1 Global Settings

Global settings are meant to be configured at the beginning of the design. Some fundamental parameters used in this simulation are presented in the following figure.

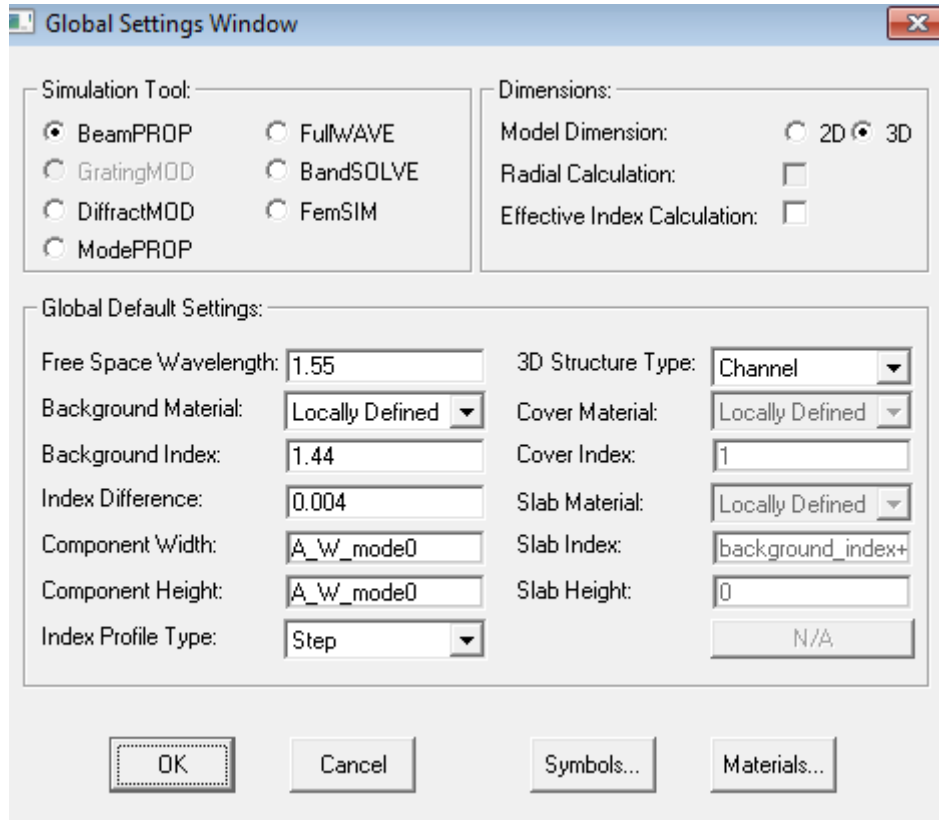


Figure 3-1 Global Settings Window

As shown in Figure 3-1, free space wavelength is set to 1550 nm, and the background index is set to 1.44 for cladding. The index difference Δn , which is the refractive index difference between cladding and core is set to 0.4%. BeamPROP solves electromagnetic fields within a given domain, which can be 2D or 3D. It provides two different 3D structure types, Fibre and Channel. Fibre structure is literally fibre-like circular waveguide that supports Linear Polarized (LP) modes, and channel structure is rectangular waveguide that supports normal TE, TM modes. Simulations of this thesis are all based on 3D Channel structures. The default segment width and height can be set in the Global Settings Window. For each segment, width and height can be overridden individually in its own properties setting window. All parameters can be defined as symbols so that equations can be used to define multiple parameters for convenient use in position planning or optimization.

3.2.1.2 Properties for Segment

For each segment, BeamPROP provides the option to adjust each parameter individually in Properties for Segments window.

Figure 3-2 Properties for Segment

As shown in Figure 3-2, each segment has its own parameters related to structure, position and other physical properties. Among these parameters, mainly component width and position are designated for each segment in simulations. Thanks to the symbols function in the software, some parameters can be defined using equations involving other parameters.

The position of segments can be defined by an offset to another segment, which means two or more segments can be virtually linked together, so that we can move a group of segments together without losing their relative position relationship with each other. As for the Z-axis, the reference type “angle” can be defined to set various tilt positions for segments.

3.2.1.3 Launch Parameters

After parameters for all segments are setup, launch field parameters are required for the software to launch desired input for simulations.

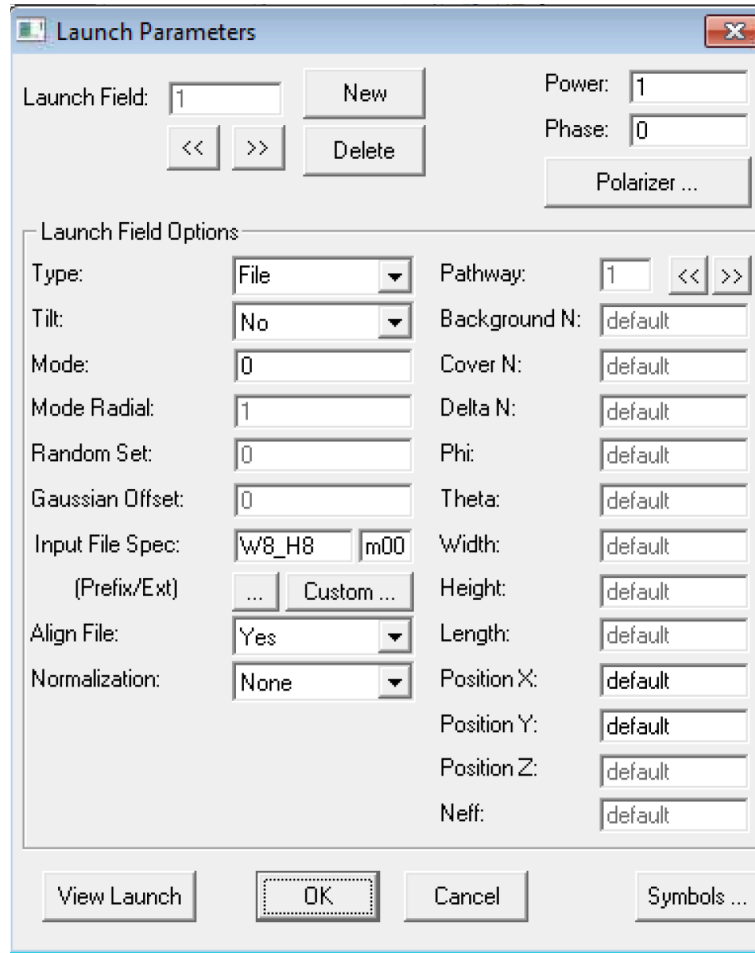


Figure 3-3 Launch Parameters

From Figure 3-3, multiple launch fields can be set in one simulation in BeamPROP, each launch field is easy to manage and has its own setting page and parameters. One important parameter, wavelength, is already setup via Global Setting Window mentioned before, so it is not required in the launch field settings. But launch field type, which is one of the most relevant parameters to simulations, can be set up in this window. There are several types available in this software. Type “fibre” can be used to directly generate fibre-based LP mode input, which is pre-calculated by software for convenience. There is also type “Gaussian”, under which Gaussian Offset option is used in mode calculation to excite different potential modes. Among other modes types, “file” type is used in this thesis because waveguide in this simulation is in the shape of a rectangular channel, which means we need to load user-calculated mode profiles from ASCII files. The specific file for modes can be loaded into Input File Spec field.

3.2.1.4 Pathway and pathway monitor

After launch field is determined, pathways can be set by choosing appropriate segments, as shown in Figure 3-4.

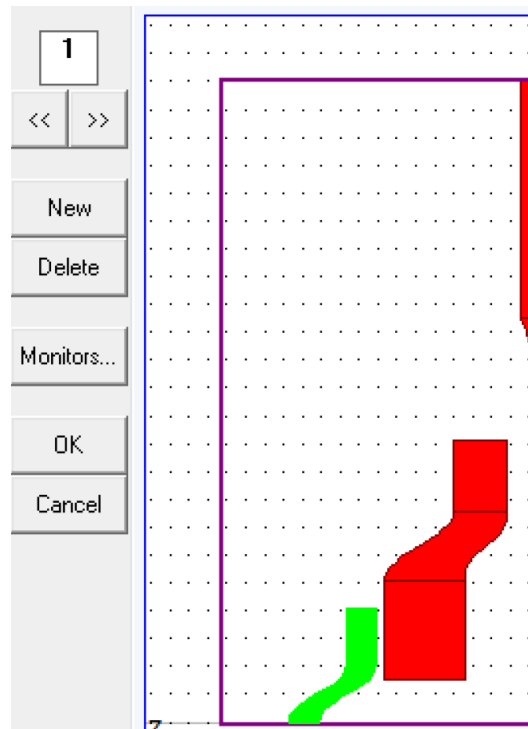


Figure 3-4 Pathway

Pathway monitors as displayed in Figure 3-5 can be designated to each pathway and are used to monitor different field parameters of the segment belonging to the pathways.

Type File Power is selected here to monitor dedicated mode power based on user-calculated mode profiles from input ASCII files, which are also used in the Launch Parameter settings.

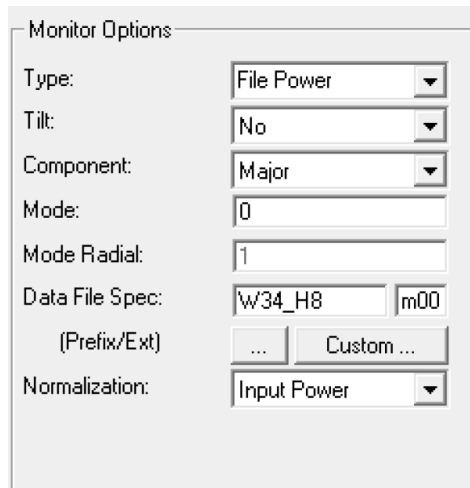


Figure 3-5 Monitor Options

With input power option selected for the normalization field, a relative ratio of output power to input power will be calculated to present the relationship between the two, which can also be exported as needed.

3.2.1.5 Mode Calculation

In the procedures described above, user-calculated mode profiles are used to precisely launch or monitor dedicated mode for the simulation. These profiles are generated by RSoft BeamPROP through its built-in mode-calculation function.

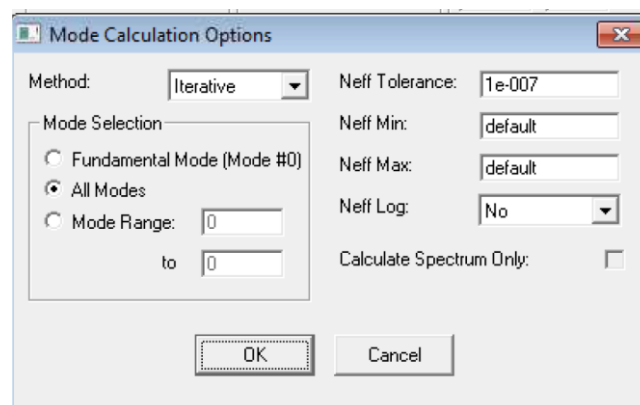


Figure 3-6 Mode Calculation Options

The iterative method is used in the simulation. RSoft calculates whether a certain mode can be found in the given structure of waveguide. If the effective refractive index (N_{eff}) for a mode is almost fixed after the calculation, which means the fluctuation range of the N_{eff} result

observed is less than N_{eff} Tolerance, then a certain mode is found in this waveguide. To excite as many modes as possible in the mode computation, the launch parameters need to be different from normal simulations. Offset Gaussian input combinations shown in Figure 3-7 is chosen to generate a required environment so that a variety of existing modes can be found in the segment.

| | |
|---|---------|
| Position X: | 0.2 |
| Position Y: | 0.2 |
| Position Z: | default |
| Neff: | default |
| <div> <div>Cancel</div> <div>Symbols ...</div> </div> | |

Figure 3-7 Gaussian Offset

As shown in Figure 3-8, BeamPROP uses user-defined grid size to efficiently calculate results in a given domain. Here, grid size “1” is chosen on Z-axis settings for the computation.

| | X | | | Y | | | Z | | |
|---------------|---------------|---------------|-------------------------------------|---------------|---------------|-------------------------------------|---------------|---------------|-------------------------------------|
| | Current Value | Default Value | Use Defs | Current Value | Default Value | Use Defs | Current Value | Default Value | Use Defs |
| Domain Min: | -96.2 | -96.2 | <input checked="" type="checkbox"/> | -21.6 | -21.6 | <input checked="" type="checkbox"/> | 0 | 0 | <input checked="" type="checkbox"/> |
| Domain Max: | 108.8 | 108.8 | <input checked="" type="checkbox"/> | 21.6 | 21.6 | <input checked="" type="checkbox"/> | 46100 | 46100 | <input checked="" type="checkbox"/> |
| Grid Size: | 0.2 | 0.2 | <input checked="" type="checkbox"/> | 0.2 | 0.2 | <input checked="" type="checkbox"/> | 1 | 50 | <input type="checkbox"/> |
| Slice Grid: | 0.6 | 0.6 | <input checked="" type="checkbox"/> | 0.2 | 0.2 | <input checked="" type="checkbox"/> | 115 | 115 | <input checked="" type="checkbox"/> |
| Monitor Grid: | | | | | | | 12 | 12 | <input checked="" type="checkbox"/> |

Figure 3-8 Mode Calculation Parameters

Generally speaking, larger the grid size, less time-consuming the simulation will be. However, a longer propagation length is needed to finish the computation. Otherwise, the computation will fail with a warning message shown in Figure 3-9:

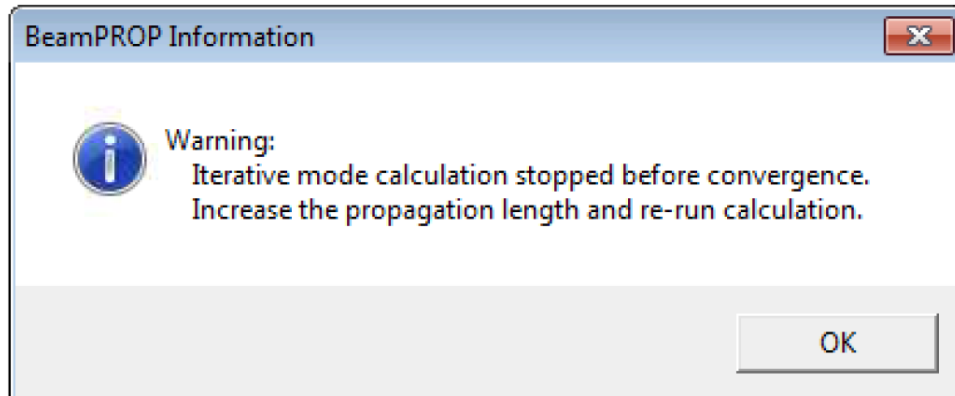


Figure 3-9 Warning

So, it's critical to find a balance between the appropriate grid size and the related propagation length to go through a successful computation within affordable time. After mode computation for segments of different width, the results are stored in ASCII files for future usage. File names are based on the related mode profile, e.g. example.m00, example.m01 and so on. Here "m00" represents the first mode that can be found in this segment.

3.2.2 MOST Optimizer

Besides setting up appropriate physical parameters for the segments, simulation result can be further optimized by RSoft built-in optimizer, MOST.

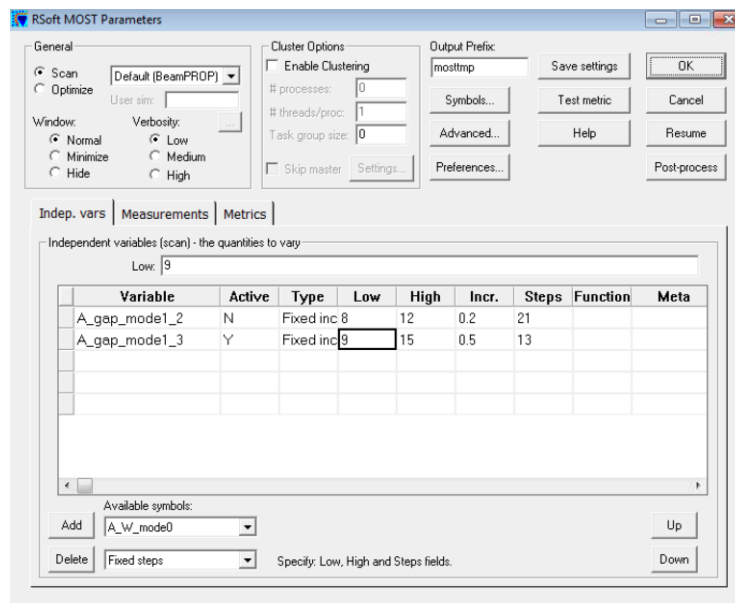


Figure 3-10 MOST Parameters

As shown in Figure 3-10, symbols can be selected to carry out step-by-step automatic simulations and metrics can be monitored to find the most desired result. Multiple symbols can be chosen together in one optimization for convenience. However, optimization complexity will increase exponentially with the growth of symbol count, which requires a much longer processing time. Thus, the symbols in an optimization process need to be chosen properly to efficiently optimize the design.

3.3 Proposed Two-Mode converter-(de)multiplexer Structure

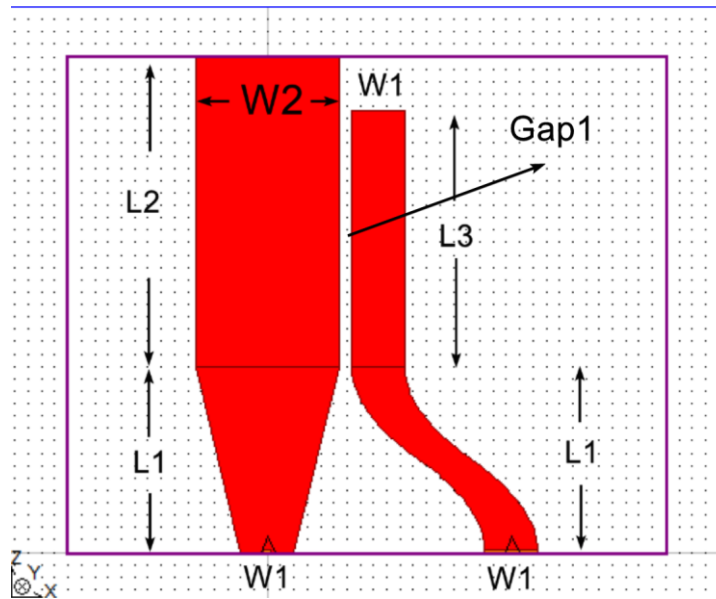


Figure 3-11 Two-Mode Structure (Front)

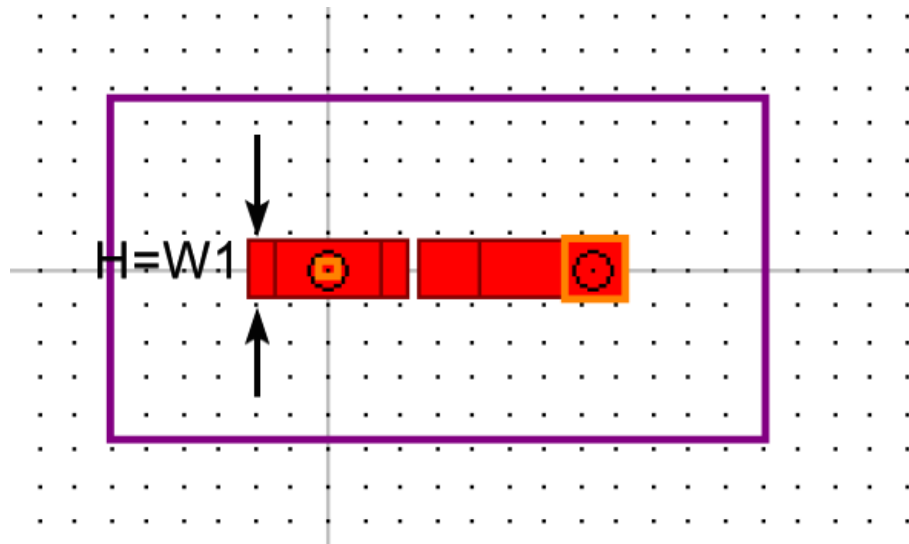


Figure 3-12 Two-Mode Structure (Top)

Table 2 Two-Mode Metrics

| | H=W1 | W2 | L1 | L2 | L3 | Gap1 |
|--------------------------|------|------|------|------|------|------|
| Length (μm) | 8 | 21.5 | 3000 | 5000 | 4130 | 2 |

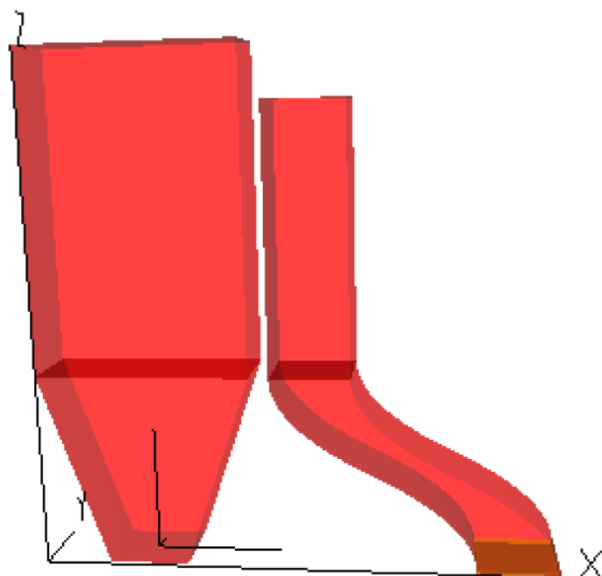


Figure 3-13 Two-Mode Structure (3D)

The structure shown in Figure 3-11, Figure 3-12 and Figure 3-13 is transformed at a ratio of 107:1 to be viewer-friendly. There are two segments in the design, and either of port at the bottom can be an input port to launch TE_0 mode. Table 2 summarizes the final parameters of the two-mode converter-(de)multiplexer.

Because the refractive index difference Δn is 0.4%, which is small enough, this is a weak waveguide system, which indicates that power not only travels in the core but also travels in the cladding. This phenomenon opens a window for the possibility that power in transmitting can travel between different waveguides that are small gaps apart. This is recognized as mode coupling.

As shown in Figure 3-14, the key for mode coupling is to manipulate N_{eff} of two waveguides. For example, by changing the shape, the structure width in this case, we can get same (or two N_{eff} with a negligible difference) N_{eff} for different modes at each waveguide. Because both are weak waveguides, the power in one waveguide transmitting as mode 1 can be transferred to another waveguide while converting to mode 2.

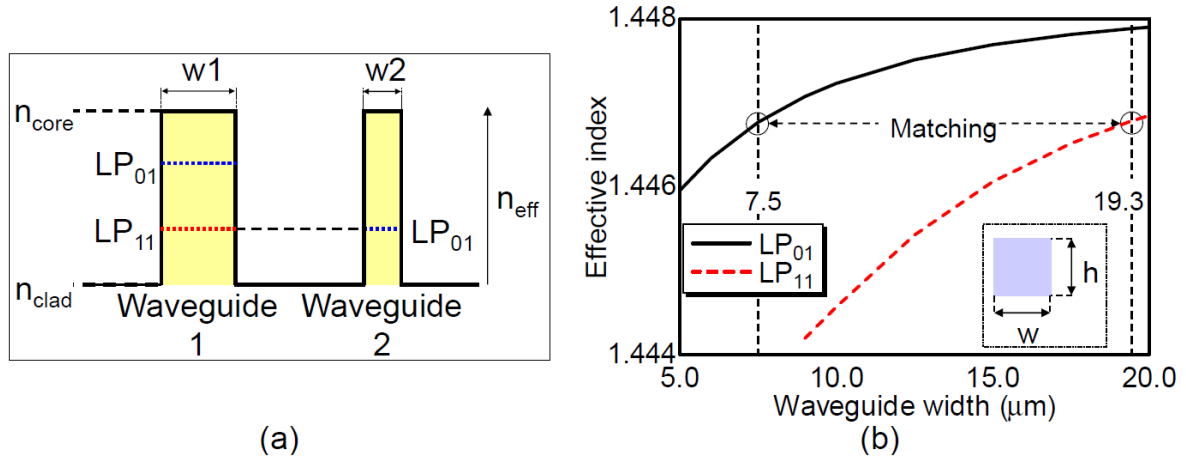


Figure 3-14 Mode Coupling and N_{eff} Matching [17]

In the proposed two-mode device, when the left port is used for TE_0 input, output will still be TE_0 except the mode shape will gradually transform to fit the endpoint of the same waveguide. When the right port is used for TE_0 input, the energy of TE_0 mode will be coupled

into the left waveguide. In this specific case, the N_{eff} for TE_1 mode in the left waveguide is manipulated by modifying the width of two waveguides to the same value as the N_{eff} for TE_0 mode in the right waveguide. As a result, when both ports are used for TE_0 input, this device acts as a mode converter-(de)multiplexer.

After the required N_{eff} for mode coupling is reached, power from the original waveguide will be coupled into target waveguide and transformed to target mode. During this process, power will travel between both waveguides periodically.

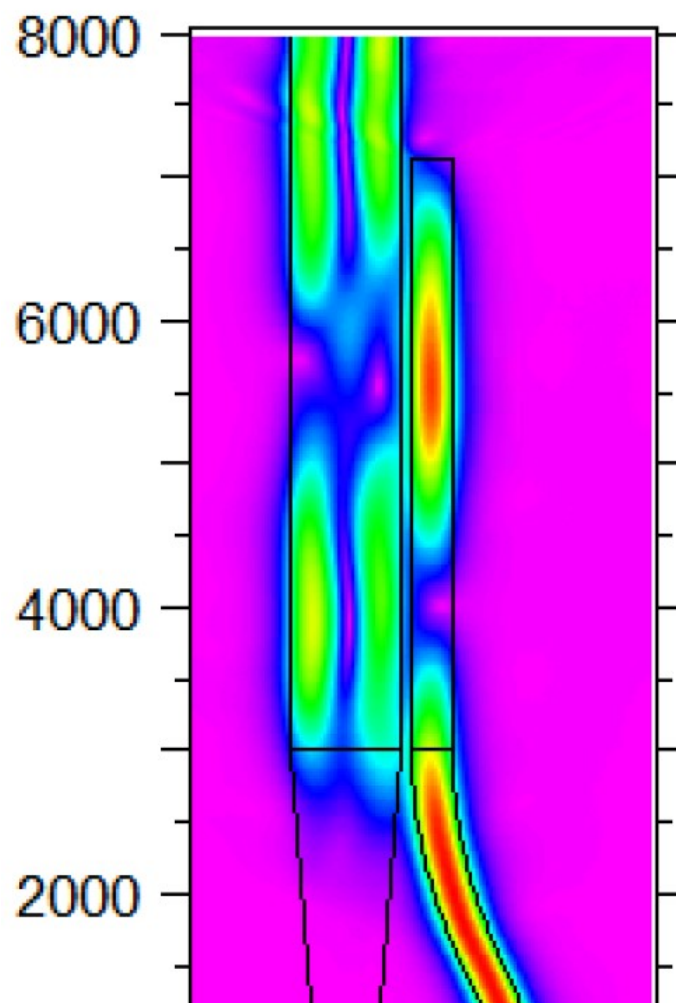


Figure 3-15 Resonance

The reason that final structure' length is chosen to include another power-travel-cycle, which means longer coupling distance, is based on MOST optimizer result. The gap between two waveguides also has an impact on final performance. A structure with larger gaps requires longer coupling distance of each cycle to achieve successful mode conversion for two waveguides, but will gain more coupling-resistance to other unwanted lower modes. This subject will be studied further in the next chapter on more complex structures.

3.4 Performance of the Two-Mode Design

3.4.1 Input from Left Port

For the performance evaluation, first only left port is used to inject TE_0 mode, as shown in Figure 3-16 below. Along the waveguide, it is clear that energy distribution of TE_0 mode gradually expands with the growth of waveguide width. Some energy travels cross the gap and returns. Almost pure TE_0 is received at output as the green line shown at the end of the right figure.

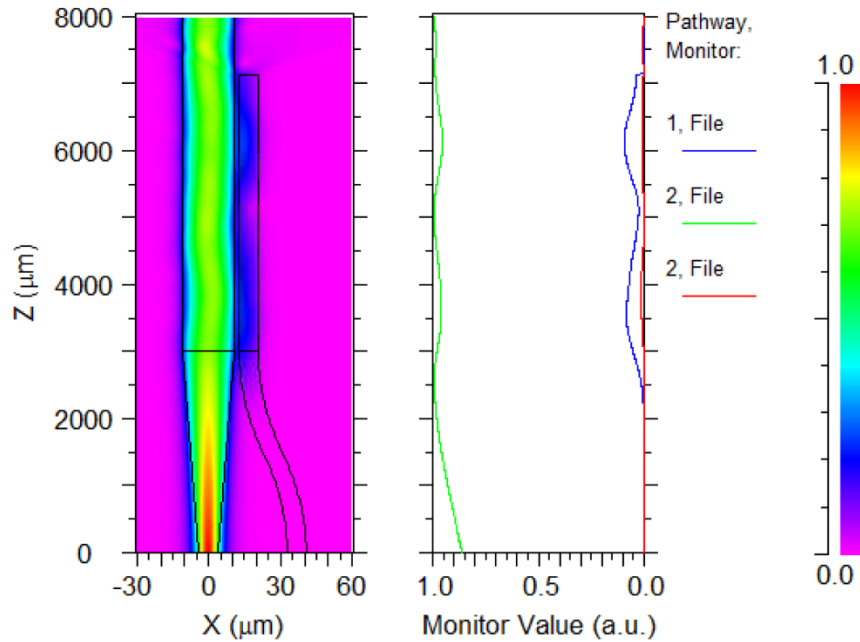


Figure 3-16 Two-Mode Input at Left

In order to evaluate the performance in a range of wavelength, we performed wavelength scan with MOST Optimizer. By comparing input mode power and target mode power at output we can get the value of Insertion Loss (IL):

$$IL = 10\log \frac{P_{TE_0,in}}{P_{TE_n,out}}$$

Where, $P_{TE_n,out}$ is optical power of output TE_n mode, and $P_{TE_0,in}$ is optical power of input TE_0 mode [11].

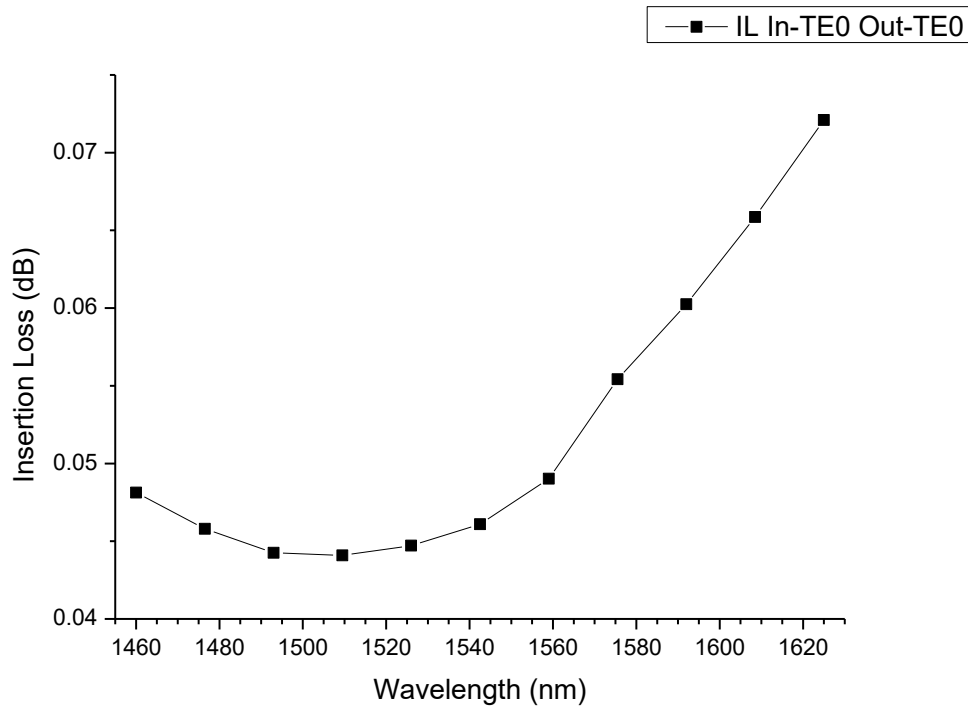


Figure 3-17 Two-Mode IL In- TE_0 Out- TE_0

Because the input and output are in the same waveguide and they are both TE_0 mode, there is no mode conversion in this case. From Figure 3-17 we can see there is almost no insertion loss over the S, C, L-Band.

Extinction Ratio (ER) can also be calculated to evaluate the result. It represents the purity of target mode compared to remaining input mode:

$$ER_{n,k} = 10 \log \frac{P_{TE_n,out}}{P_{TE_k,out}}$$

Where $P_{TE_n,out}$ is optical power of TE_n after the conversion at output, and $P_{TE_k,out}$ represents optical power of TE_k which is the remaining other modes after the conversion at output. [11] [13]

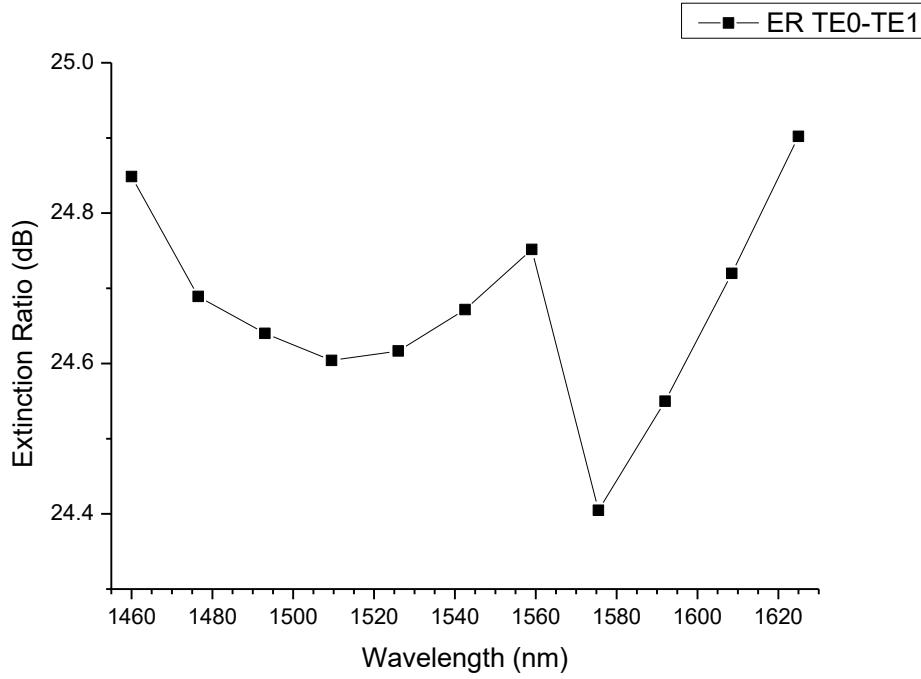


Figure 3-18 Two-Mode ER TE_0

From Figure 3-18, over the entire S, C, L-Band, it can be found the extinction ratio for TE_0 mode is larger than 24.4 dB.

3.4.2 Input from Right Port

To achieve mode conversion, optical power is injected into right port for extensive simulations.

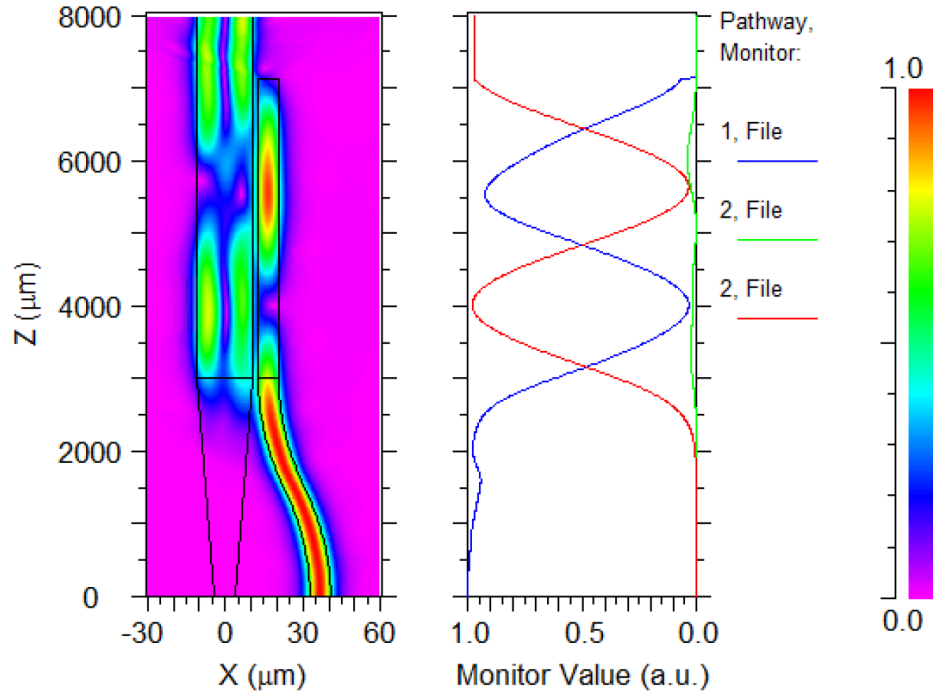


Figure 3-19 Two-Mode Input at Right

From Figure 3-19, we can see that the optical power of input TE_0 from right port is coupled to left waveguide and transforms into TE_1 mode. After extensive simulations for wavelength scanning, insertion loss is calculated over a broadband.

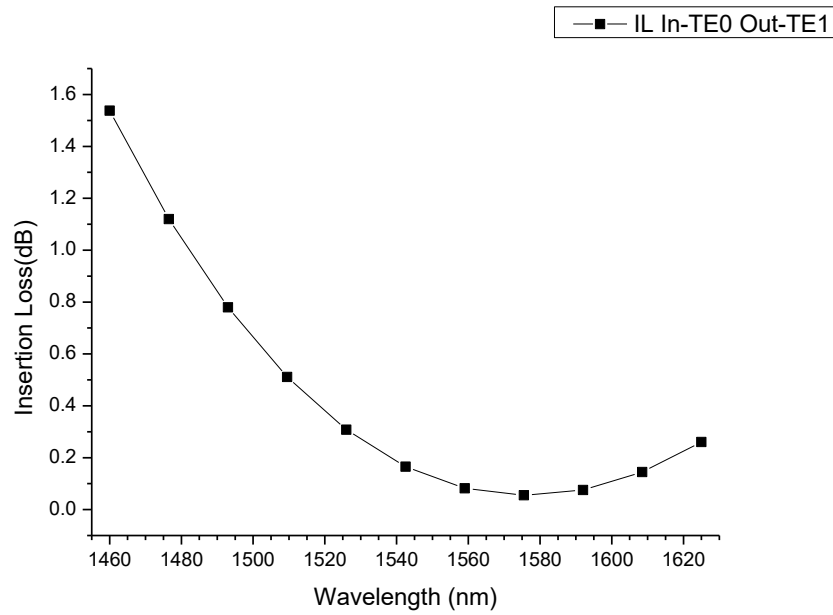


Figure 3-20 Two-Mode IL In- TE_0 Out- TE_1

Figure 3-20 shows that over the entire S, C, L-Band, the insertion loss is less than 1.5 dB, while at central wavelength of 1550 nm, the insertion loss is around 0.2 dB.

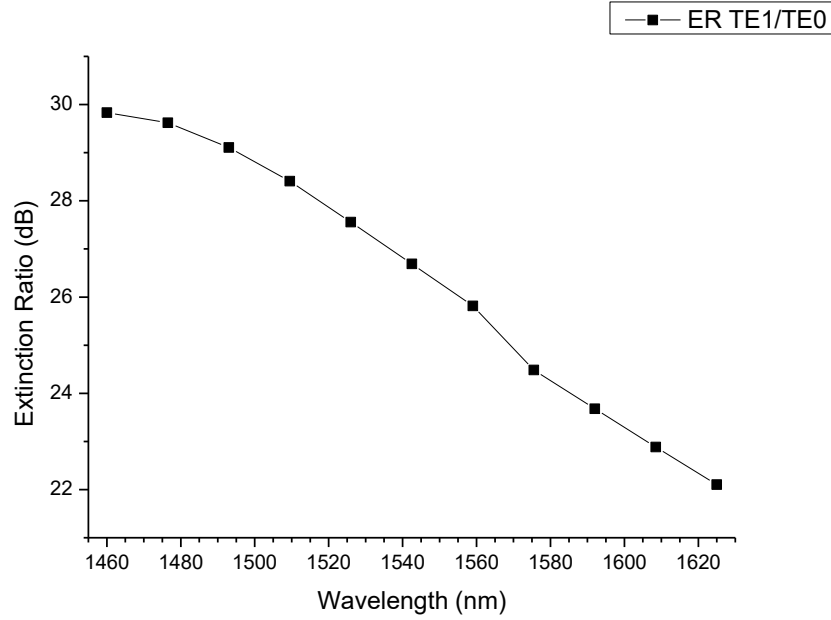


Figure 3-21 Two-Mode ER TE₁/TE₀

From Figure 3-21, it is clear that over the entire S, C, L-Band, the extinction ratio is larger than 22 dB. At the central wavelength of 1550 nm, we can get an extinction ratio around 26 dB.

3.4.3 Input from Both Ports

By injecting optical power into both ports, the device can function as a mode converter-multiplexer.

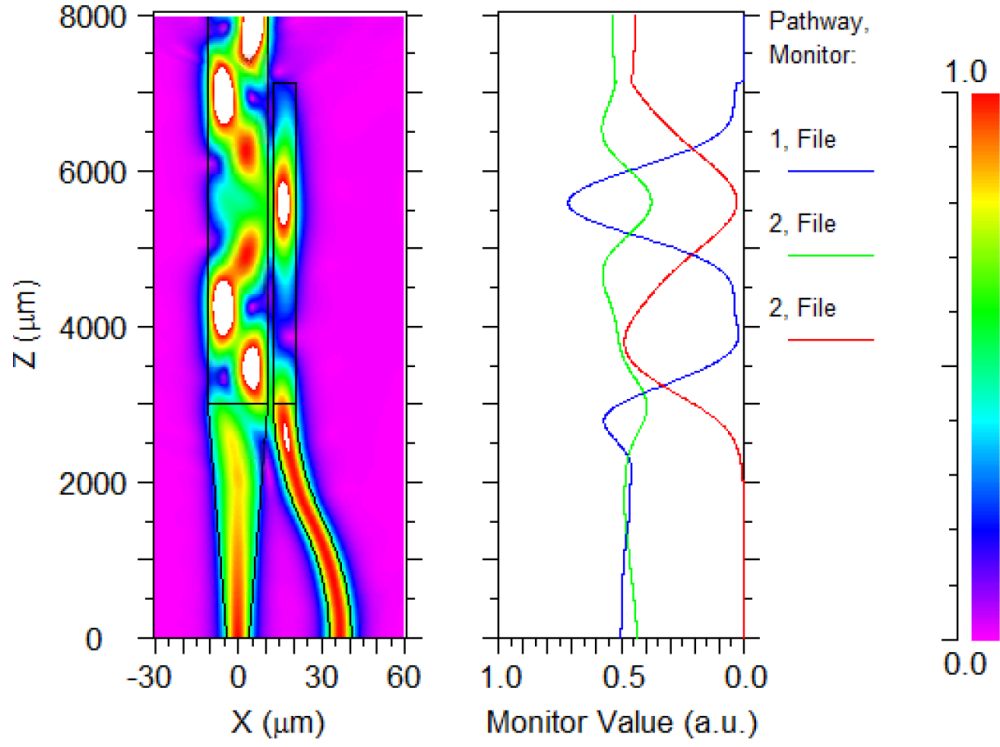


Figure 3-22 Two-Mode Input All

From Figure 3-22, the green line in right figure indicates TE_0 mode in the left waveguide and the red line indicates TE_1 mode in the left waveguide. Because there are two inputs in the simulation, mode power of both inputs are each normalized to 50%, so that together they contribute 100% of optical power. This also explains why the optical power of the output modes stays around 50% for both modes.

The optical power of TE_0 mode from the left port is combined with TE_1 mode converted from the right port. To evaluate the impact between both modes, crosstalk (XT) is calculated as follows:

$$XT = \left| 10 \log \frac{P_{TE_n,out}}{P'_{TE_n,out}} \right|$$

Where $P_{TE_n,out}$ is optical power for TE_n mode at output when the only input is the mode that converts to TE_n . And $P'_{TE_n,out}$ is optical power for TE_n mode at output when all the input modes are injected into the device.

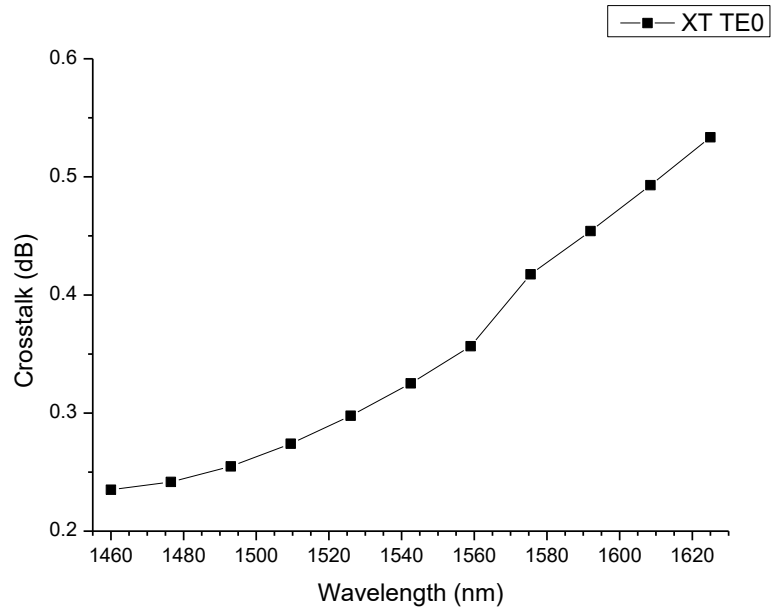


Figure 3-23 Two-Mode XT TE₀

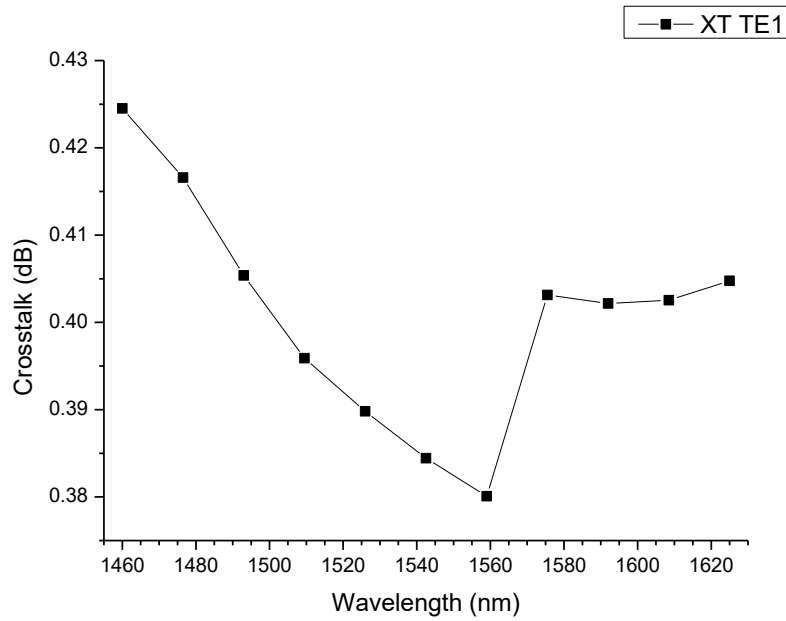


Figure 3-24 Two-Mode XT TE₁

From Figure 3-23 and Figure 3-24 above, we can find that for both TE₀ and TE₁ mode output, the crosstalk from other undesired modes is less than 0.5 dB. And at the central wavelength of 1550 nm, the crosstalk is less than 0.4 dB.

3.4.4 Two-Mode Backward Conversion and Demux

The device can also be used as mode converter-demultiplexer to perform backward conversion when injecting TE_0 and TE_1 mode from the original output port. It needs to be pointed out that since the structure only supports TE mode in this device, the input of light should pass a polarization controller to get efficient results.

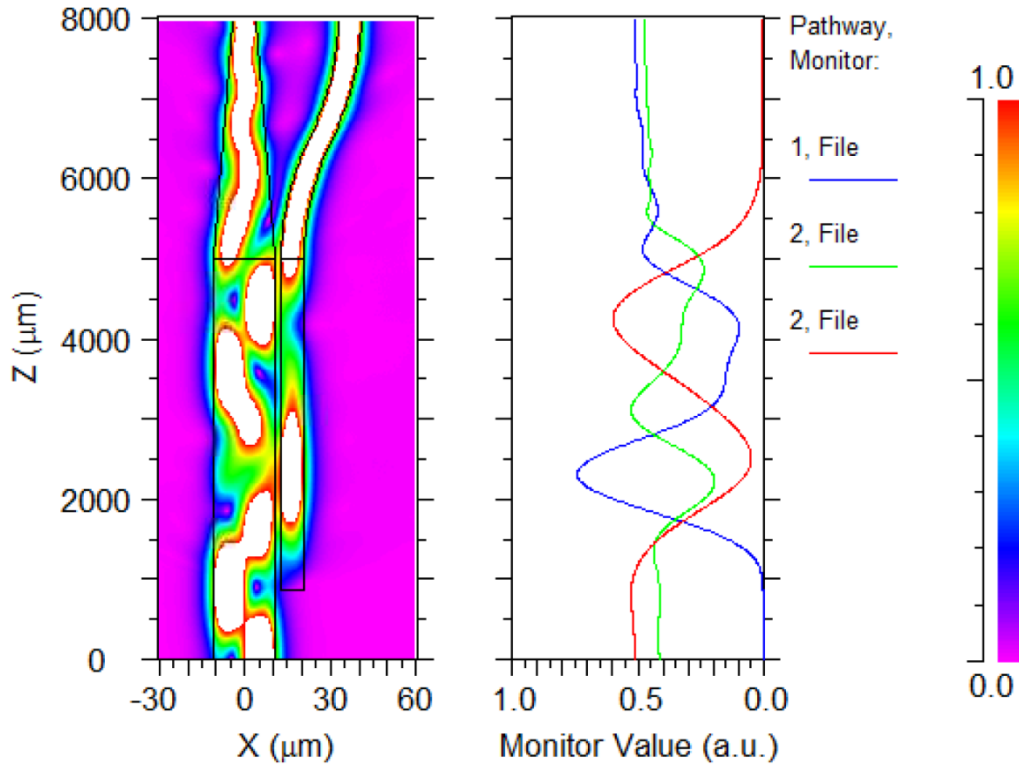


Figure 3-25 Two-Mode Demux

Figure 3-25 illustrates that the device can support backward conversion, and outputs will both be TE_0 modes. Extensive simulations with wavelength scan are executed. For each simulation, insertion loss is calculated.

Figure 3-26 represents the case where only TE_0 is injected back into the port:

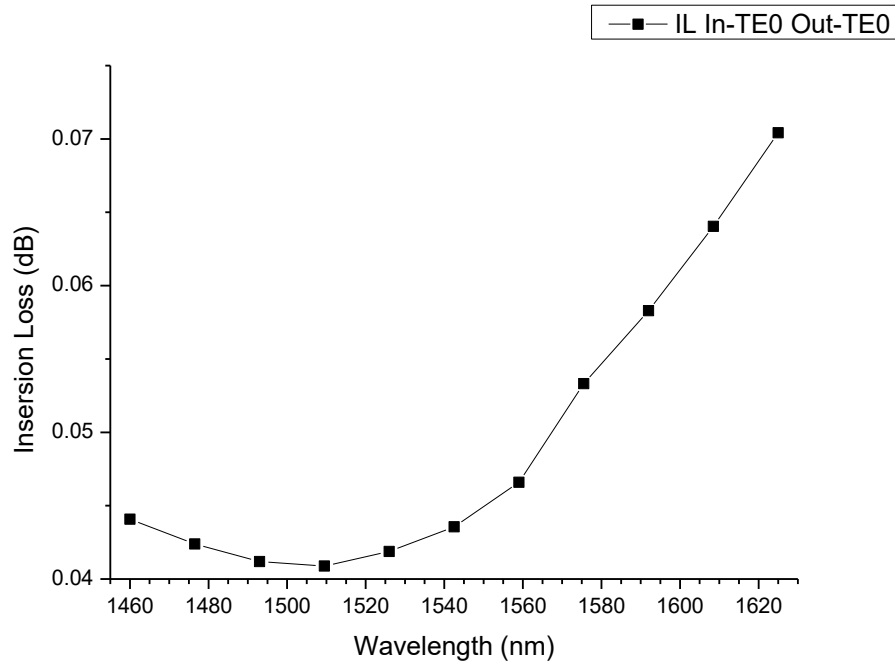


Figure 3-26 Two-Mode Demux IL In-TE₀ Out-TE₀

Figure 3-27 represents the case where only TE₁ is injected back into the port:

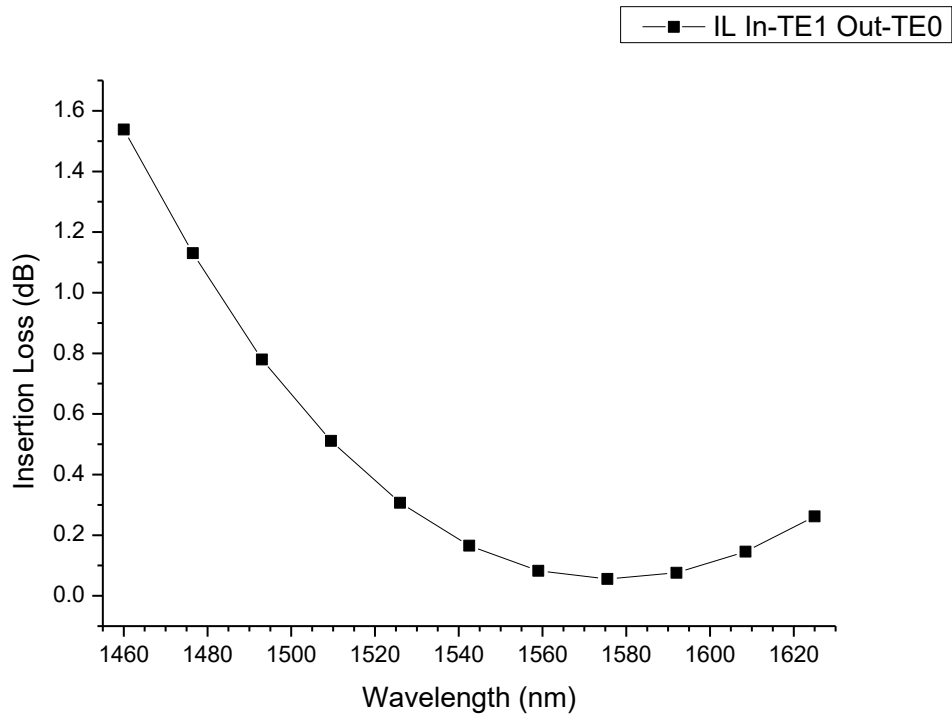


Figure 3-27 Two-Mode Demux IL In-TE₁ Out-TE₀

Figure 3-27 above indicates that for both TE_0 and TE_1 mode, the insertion loss is less than 1.5 dB, and at the central wavelength of 1550 nm, the insertion loss is around 0.2 dB. The extinction ratio is not measured because in the backward operation, the output structure only supports TE_0 mode. That means no other modes can stably exist in the waveguide, so there is no remaining input mode to compare with.

For the crosstalk measurement, because both outputs in backward operation are TE_0 modes, we measure certain output mode power when only one input port is used to launch TE_0 mode and compare them with the result where two input ports are utilized to inject TE_0 modes.

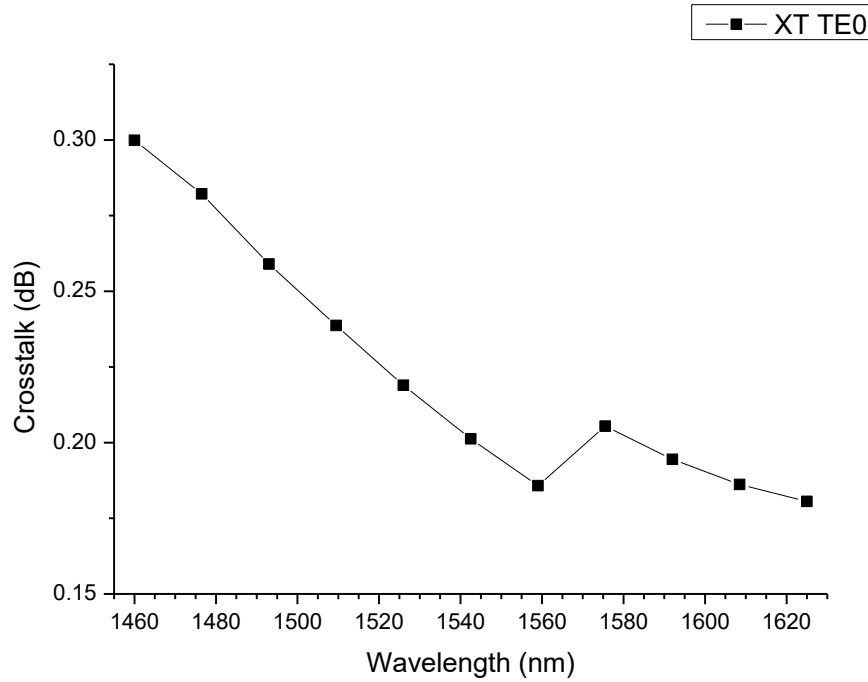


Figure 3-28 Two-Mode Demux XT TE_0

From Figure 3-28 and Figure 3-29 we can see that for the reciprocal operation, a similar general trend is observed as in the forward operation, because the converting-(de)multiplexing process is bi-directional. For the TE_0 input, a crosstalk below 0.55 dB is achieved over the S, C, L-band. And for the TE_1 input, the crosstalk is below 0.33 dB over the broadband.

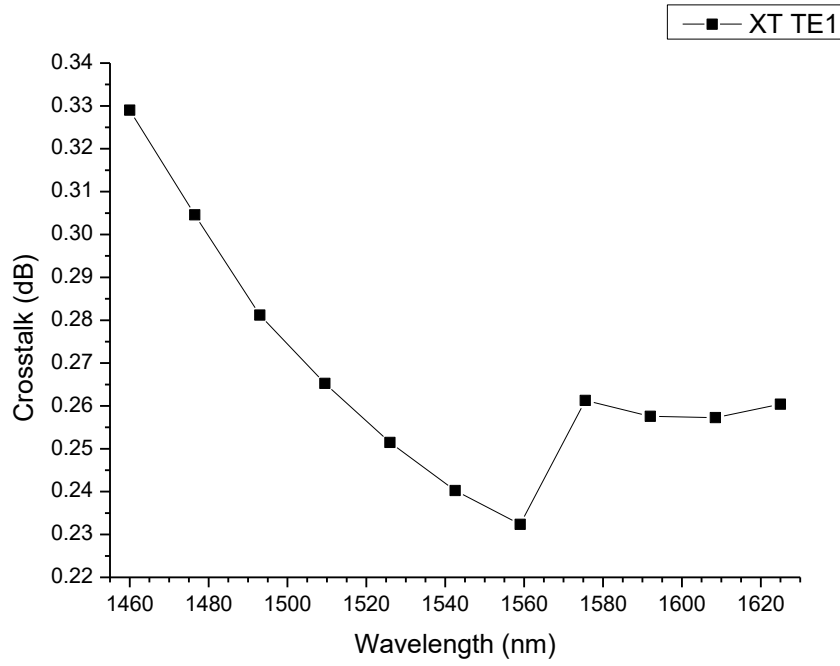


Figure 3-29 Two-Mode Demux XT TE₁

3.5 Summary

The two-mode converter-(de)multiplexer designed above shows great performance over S, C, L-band, especially in the C-band. This success proves that such design is fundamentally capable of mode converting and (de)multiplexing. This structure is re-used and expanded in Chapter 4 for higher modes design.

Chapter 4 Proposed Four-Mode converter-(de)multiplexer

4.1 Introduction

In the previous chapter, a two-mode converter-(de)multiplexer is designed using two pieces of channel waveguides. It functions as a basic mode converting and (de)multiplexing tool for TE_0 and TE_1 modes. The same structure is deployed as a key component in the following device including two assistant waveguides, extended to four modes: TE_0 , TE_1 , TE_2 and TE_3 .

4.2 Proposed Four-Mode converter-(de)multiplexer structure

4.2.1 Overview of the Four-Mode Structure

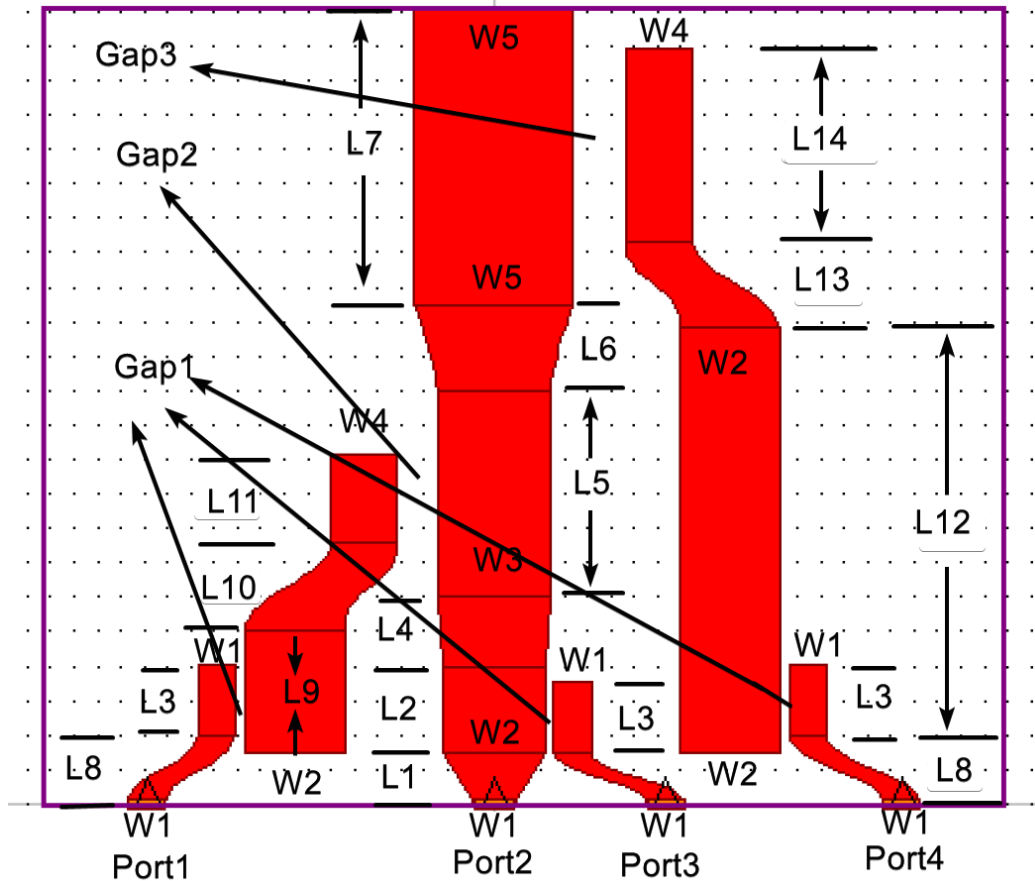


Figure 4-1 Four-Mode Structure (Front)

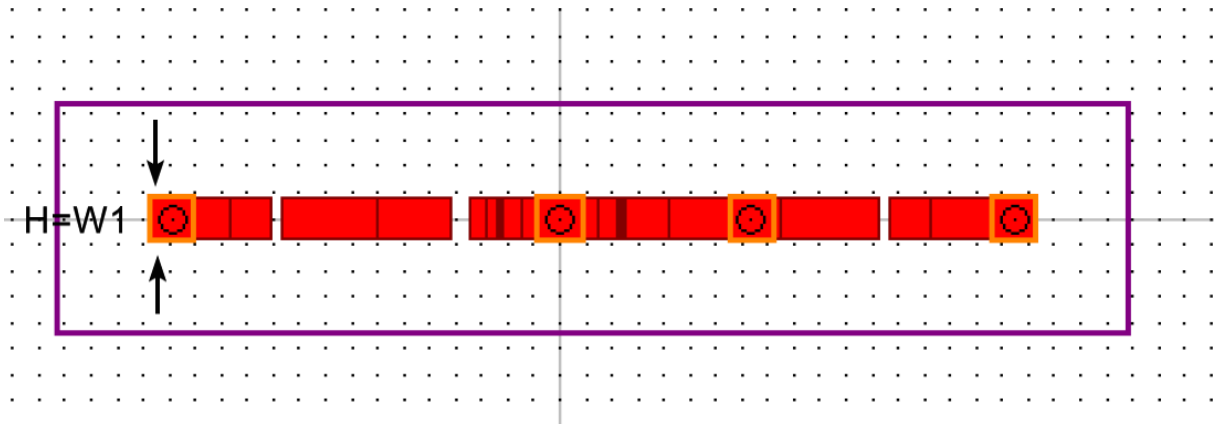


Figure 4-2 Four-Mode Structure (Top)

Table 3 Four-Mode Metrics (Width)

| | W1 | W2 | W3 | W4 | W5 |
|--------------------------|----|------|----|----|----|
| Length (μm) | 8 | 21.5 | 24 | 14 | 34 |

Table 4 Four-Mode Metrics (Gap)

| | Gap1 | Gap2 | Gap3 |
|--------------------------|------|------|------|
| Length (μm) | 2 | 8.8 | 11.5 |

Table 5 Four-Mode Metrics (Length)

| | L1 | L2 | L3 | L4 | L5 | L6 | L7 |
|--------------------------|------|------|------|------|-------|------|-------|
| Length (μm) | 3000 | 5000 | 4130 | 4000 | 12000 | 5000 | 17130 |
| | L8 | L9 | L10 | L11 | L12 | L13 | L14 |
| Length (μm) | 4000 | 7130 | 5000 | 5120 | 24630 | 5000 | 11208 |

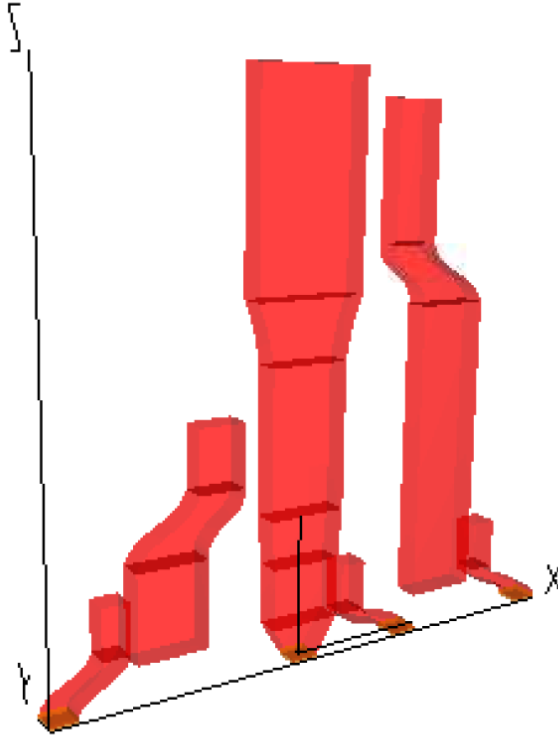


Figure 4-3 Four-Mode Structure (3D)

Structure of the final device shown above in Figure 4-1, Figure 4-2 and Figure 4-3 is transformed at a ratio of 271:1 to be viewer-friendly. It contains 6 pieces of channel waveguide, including two assistant waveguides. All of them are designed in unified height for easy fabrication. Table 3, Table 4 and Table 5 summarize the final parameters of the four-mode converter-(de)multiplexer. Some of the metrics are finalized after multiple rounds of optimization due to complexity of the design.

There are overall four potential input ports for the structure, and each of them can be used to input TE_0 mode separately or simultaneously. Light injected from port 1 transforms to TE_1 mode through the fundamental structure designed in the last chapter. Then the TE_1 mode is compressed through an assistant waveguide, which is a complex component involving binding and narrowing design. Afterwards, this TE_1 mode is transformed to a TE_2 mode while crossing over the gap to the reach central waveguide. Light from port 2 remains as TE_0 mode all the way to the output, only its mode width is expanded along the structure. TE_0 mode from port 3 is

transformed to TE_1 mode and remains the same throughout the central waveguide. Light from port 4 is first transformed to TE_1 mode, though another assistant waveguide, then finally converted to TE_3 mode when reaching the central waveguide. In conclusion, from the process introduced above, four TE_0 input modes are injected into the device, and four different modes are received at the output, which are TE_0 , TE_1 , TE_2 , TE_3 mode. In the design of this device, two assistant waveguides that involve narrowing procedure at the end are critical to the success of achieving these conversion results. These detailed design process will be explained further in the following subsections.

4.2.2 Design of the Two Assistant Waveguides

As introduced in the last chapter, when N_{eff} values are matching for two different modes in two different waveguides, mode coupling will take place. In a four-mode design, things are a lot more complex. Even though the same principal holds, there are some side effects that need to be dealt with.

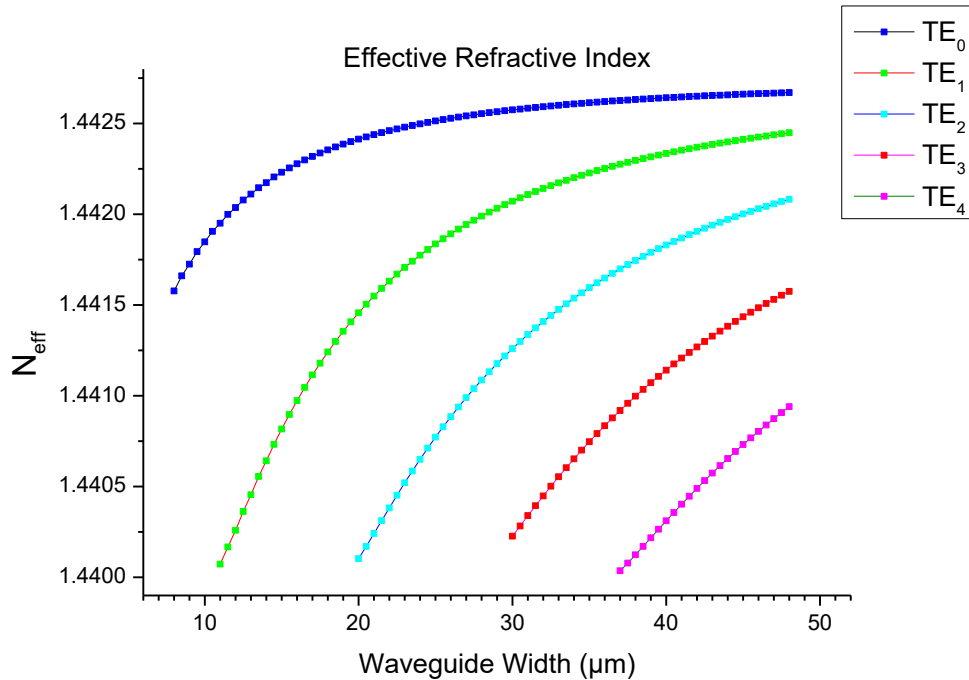


Figure 4-4 N_{eff} and waveguide width for modes

As shown in Figure 4-4, in waveguides with a predetermined width, only certain modes can exist. Consequently, higher the target mode is, wider the waveguide needs to be. The difficulty of mode converting is highly and positively correlated to ΔN_{eff} , the difference between effective refractive index of two waveguides. When we conduct the desired mode conversion, the two N_{eff} are manipulated by changing waveguide width so that their values are close enough to trigger the converting process.

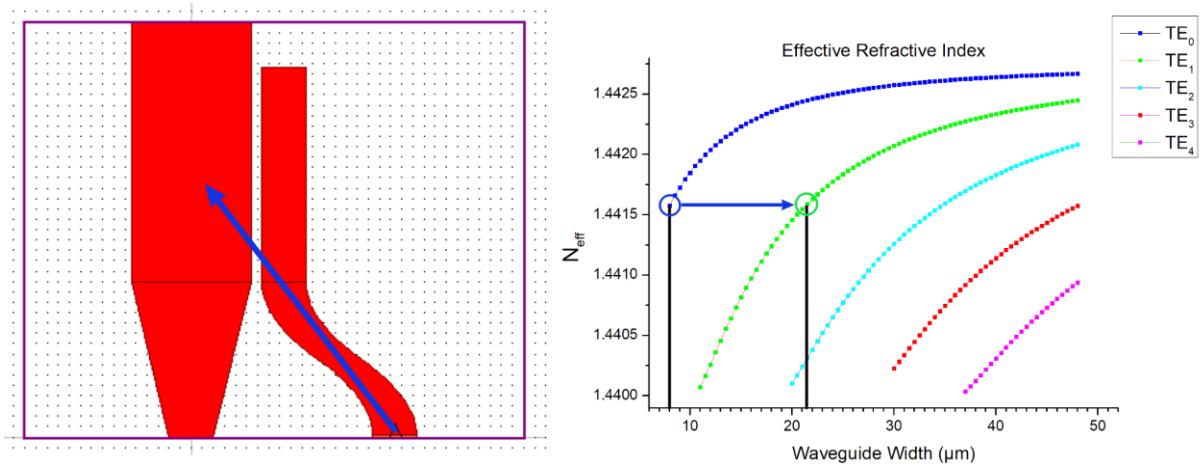


Figure 4-5 TE₀ to TE₁ N_{eff} Matching Map

As introduced in the previous chapter, when TE₀ mode is converted to TE₁ mode, the transition is only between two modes. The path marked with blue arrow from above Figure 4-5 illustrates the N_{eff} matching map for two-mode conversion, and the corresponding key points can be found in the map to the right. The circles represent certain modes that exist during the process, with each mode marked with a different colour. Blue indicates TE₀ mode, and green indicates TE₁ mode. The arrow lines in all maps specify the direction of conversion operations. Because the width for each assistant waveguide is fixed, N_{eff} is also fixed for each mode. To achieve mode conversion, N_{eff} for TE₀ and TE₁ modes in two waveguides are manipulated to the same value. The black lines indicate the corresponding width of each waveguide in this conversion.

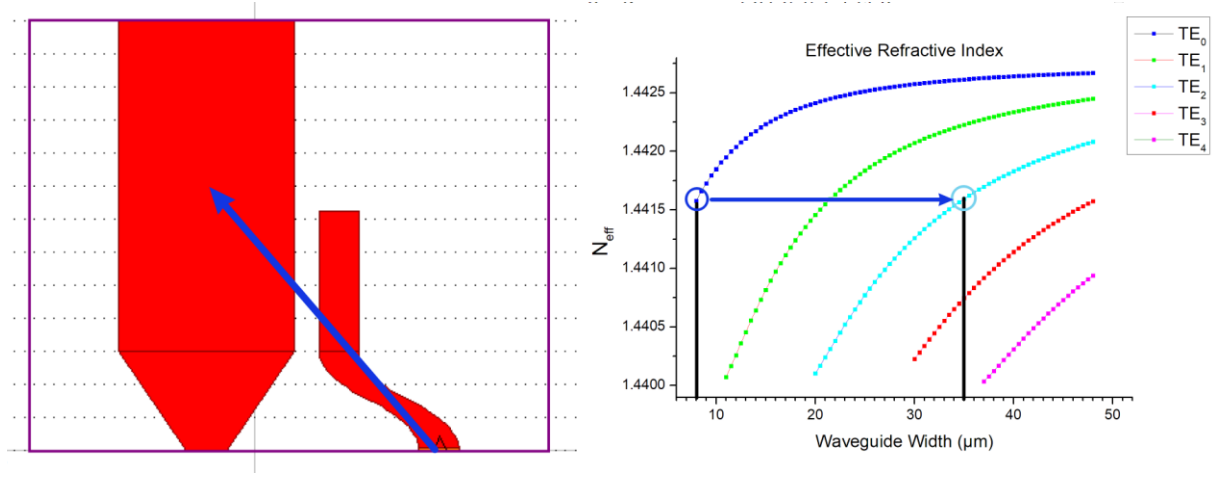


Figure 4-6 TE_0 to TE_2 mode N_{eff} Matching Map

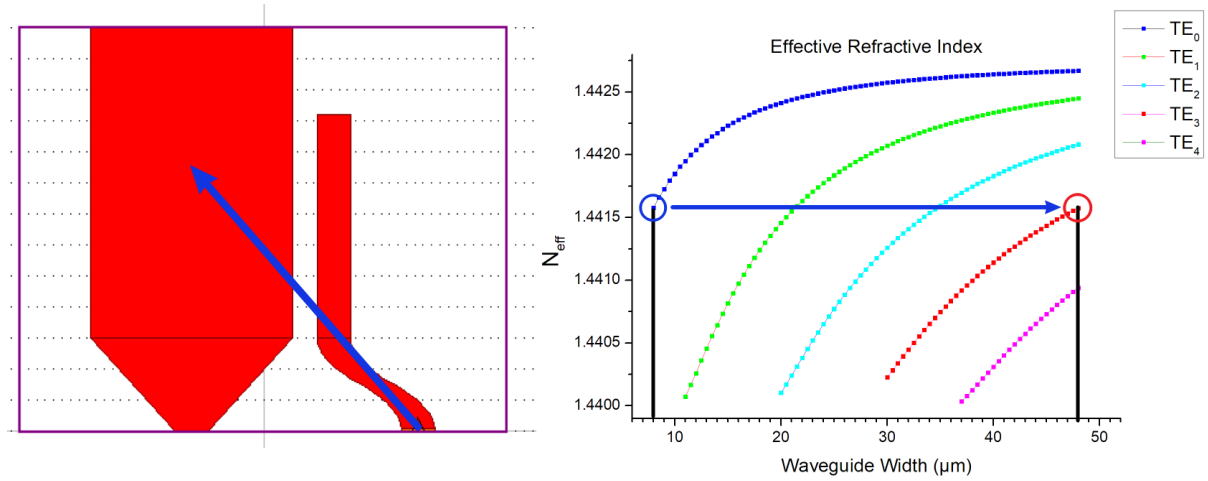


Figure 4-7 TE_0 to TE_3 mode N_{eff} Matching Map

When it comes to achieving the higher modes conversion, the easiest way is to directly manipulate width of two waveguides as shown in Figure 4-6 and Figure 4-7 above. Using the same structure from Figure 4-5, by altering the width of target waveguide from 21.5 to 35 μm , conversion between TE_0 and TE_2 mode is achieved. Followed by the same principle, TE_0 to TE_3 mode conversion can be obtained through changing the width further to 48 μm . However, as a consequence to such modification, a large width is required at the end of the device, which leads to more complex situation explained below.

One fundamental fact across all scenarios from Figure 4-4 to Figure 4-7 is that the slope of N_{eff} curve for multiple modes gets more moderate as the waveguide grows wider. As a result,

the distance between the corresponding N_{eff} -axis positions for different modes within a waveguide is getting shorter as the width grows, meaning that for a given waveguide width, effective refractive index difference ΔN_{eff} is smaller between different modes at the end of the device, as shown in Figure 4-8.

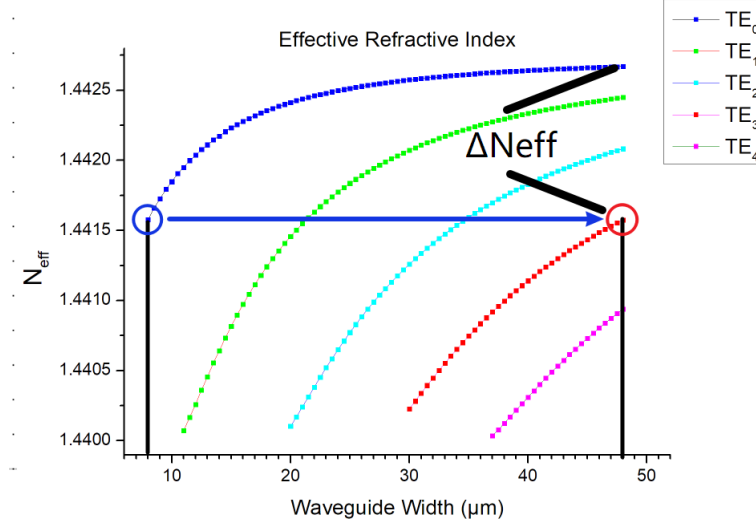


Figure 4-8 ΔN_{eff} for 48 μm waveguide

As mentioned before, the difficulty for mode conversion is related to ΔN_{eff} , and with a smaller ΔN_{eff} , the easier it would be for mode conversion to happen. In this case, a smaller ΔN_{eff} will also lead to easier unwanted mode coupling inside the target waveguide, which will have negative impact on output mode purity.

To improve mode purity, an assistant waveguide with narrowed end is applied to the above TE_0 to TE_3 mode device as an example. Following the arrows in Figure 4-9, we can see that at first TE_0 mode is converted to TE_1 mode. After the narrowing process by adjusting the width at the end of the assistant waveguide from 21.5 to 14 μm , the starting point for next conversion (TE_1 to TE_3 mode) is moved to a lower position on N_{eff} -axis. From the new position, TE_1 mode is eventually converted to TE_3 mode based on the same principle, but with reduced width for target waveguide compared to previous design, from 48 to 34 μm .

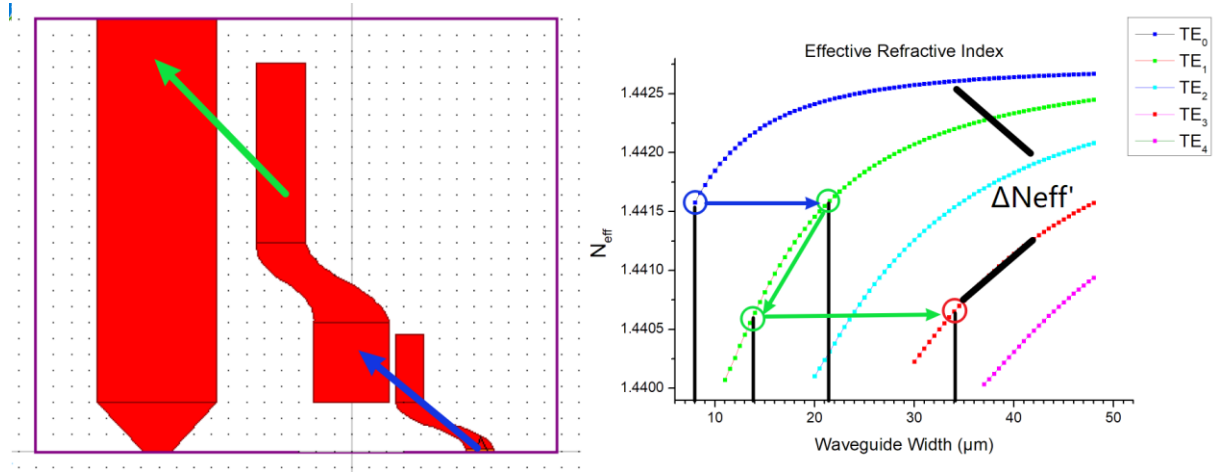


Figure 4-9 Design of Assistant Waveguide

As shown on the map to the right in Figure 4-9, it is clear that the new effective refractive index difference $\Delta N_{eff}'$ between different modes in the target waveguide is much larger than the ΔN_{eff} presented in the previous design. Under extensive simulations with wavelength scan, the improvement of extinction ratio is shown in following figures.

The reason that assistant waveguide is implemented here is to increase the performance of extinction ratio by making the $\Delta N_{eff}'$ larger than ΔN_{eff} , so that different modes have less chance to interfere with each other, which results in high extinction ratio. It needs to be pointed out that one research mentioned in the literature review also used assistant waveguide [18]. However, the implementation was totally for another reason, that in their design, LP_{01} mode cannot directly converted into LP_{21a} without multiple conversions with assistant waveguide.

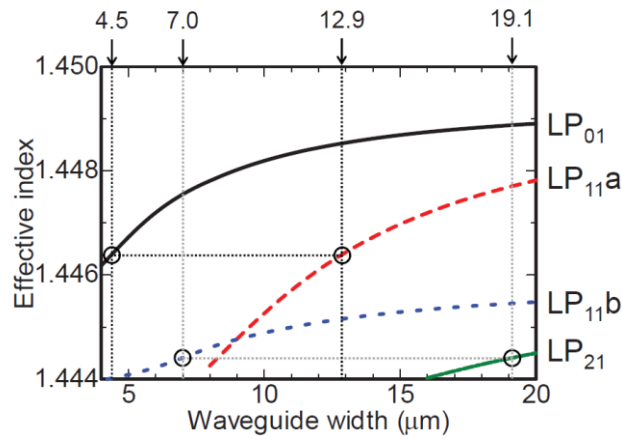


Figure 4-10 N_{eff} Matching Map for the other research [19]

As shown in Figure 4-10, the sole reason for the implementation of assistant waveguide in that research is that N_{eff} for LP_{21a} mode is lower than the N_{eff} starting point of LP_{01} mode, means that LP_{01} mode cannot be converted to LP_{21a} mode using the same N_{eff} matching method. So, the workaround is to convert LP_{01} mode to LP_{11a} mode and rotate it to LP_{11b} mode. Finally, LP_{11b} mode can be converted to LP_{21a} mode. The reason is not to strengthen the performance as that in this thesis.

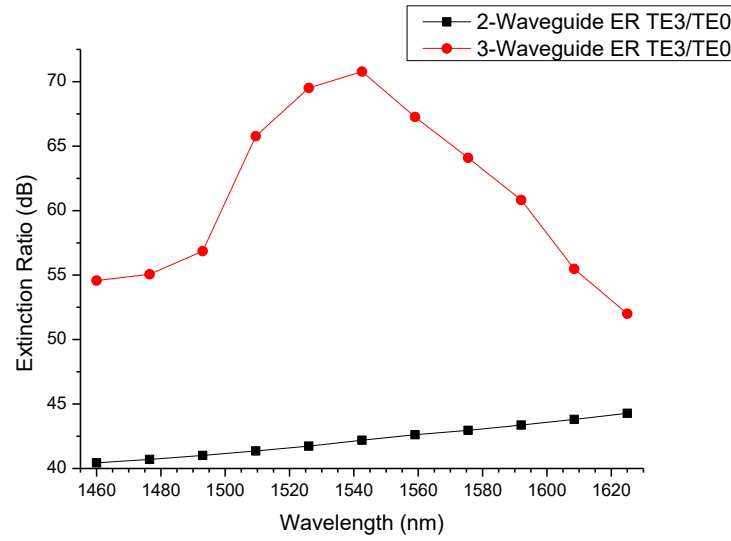


Figure 4-11 Comparison of ER TE₃/TE₀

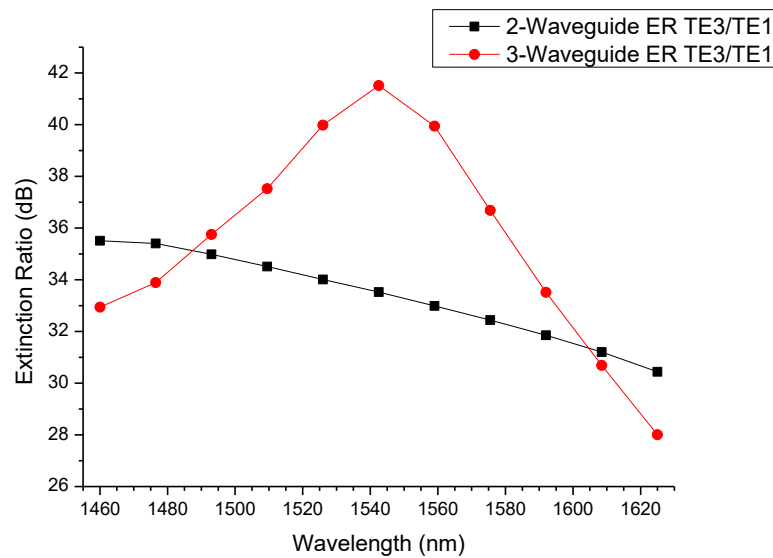


Figure 4-12 Comparison of ER TE₃/TE₁

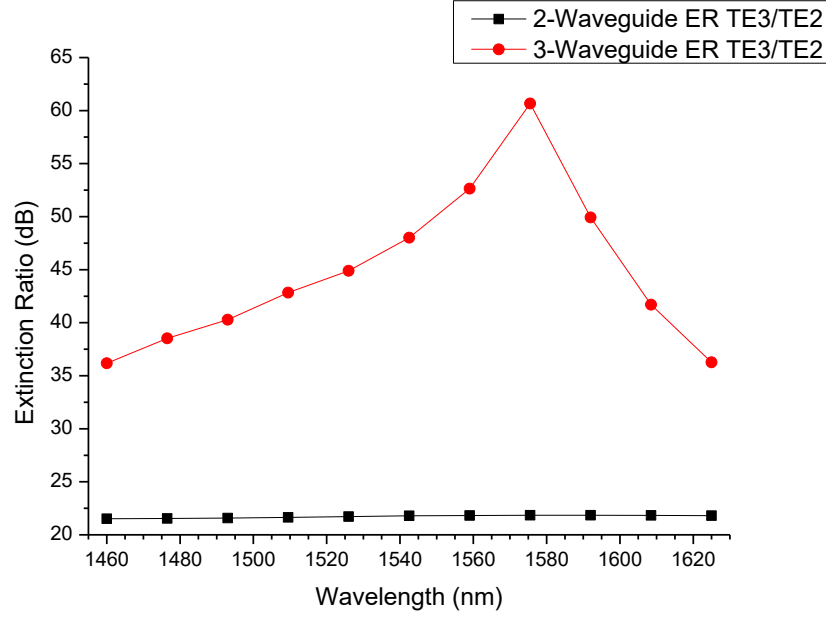


Figure 4-13 Comparison of ER TE₃/TE₂

Figure 4-11 illustrates that the TE₃/TE₀ mode extinction ratio of the three-waveguide device is increased by 28 dB compared to the two-waveguide device at the wavelength of 1550 nm, and overall improvement is more than 8 dB over the S, C, L-band. From Figure 4-12 it can be found that TE₃/TE₁ mode extinction ratio is improved by 8 dB at the wavelength of 1550 nm. Furthermore, TE₃/TE₂ mode extinction ratio of the three-waveguide device is increased by 38 dB at maximum and has an overall improvement of 13 dB over the S, C, L-band as shown in Figure 4-13.

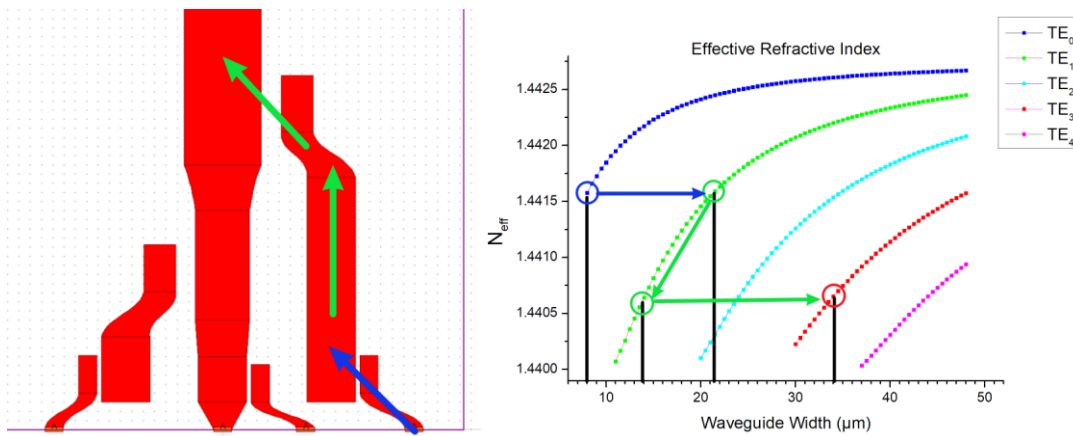


Figure 4-14 Four-Mode design with TE₀ to TE₁ to TE₃ N_{eff} matching map

By expanding the former design in chapter 3, four-mode converter-(de)multiplexer including two assistant waveguides is established and its structure with N_{eff} map is shown in Figure 4-14. To illustrate, $\text{TE}_0 \rightarrow \text{TE}_1 \rightarrow \text{TE}_3$ mode conversion is chosen as an example, and the corresponding key data at each stage of conversion can be found in the map to the right. Mode conversions in this device are set to occur at only specific positions of the structure by ensuring that each position's partial physical shape is dedicated to the one desired mode conversion only.

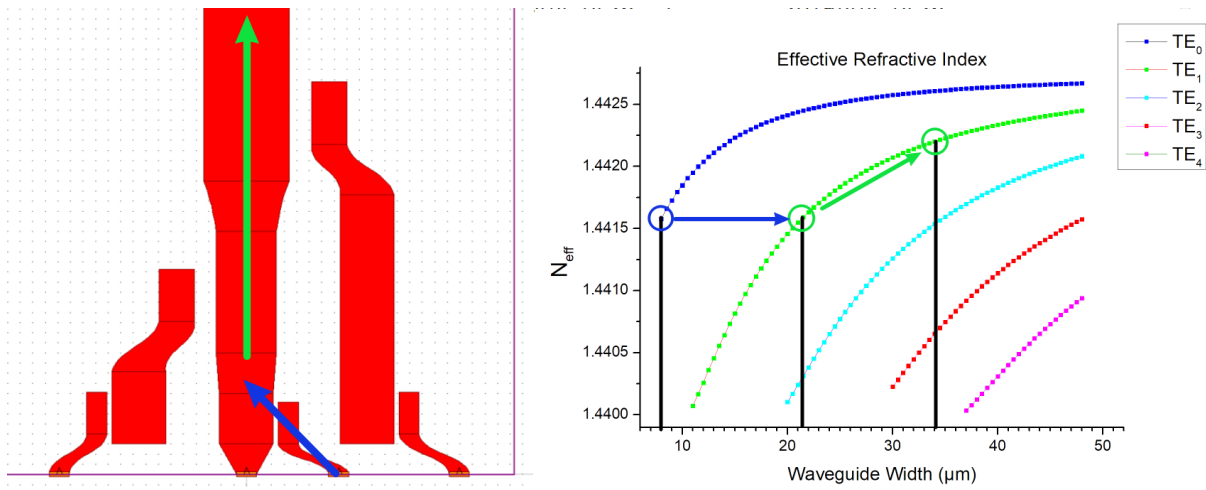


Figure 4-15 Four-Mode design with TE_0 to TE_1 N_{eff} matching map

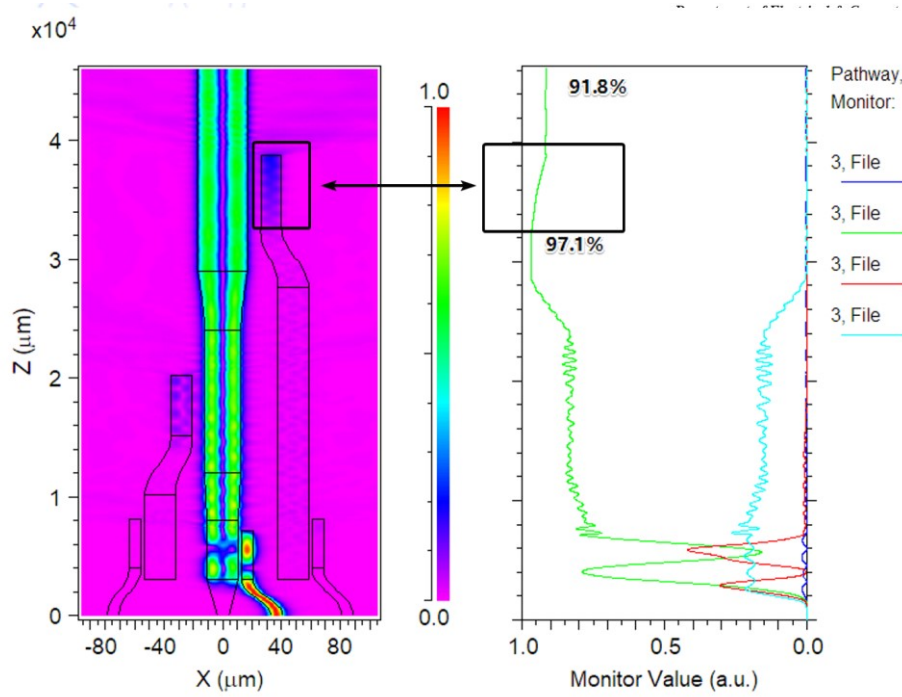


Figure 4-16 Four-Mode via input3

However, under the example of TE_0 to TE_1 mode conversion as shown in Figure 4-15 Figure 4-16, at the position marked with black triangular where TE_1 mode is supposed to transform into TE_3 mode from the assistant waveguide targeting the central waveguide, other modes irrelevant to this exact process already exist in the central waveguide. These irrelevant modes will leak from the central waveguide to the assistant waveguides when passing by the joint position, see example areas with TE_1 mode power losses in the central waveguide on the chart to the right, where only 91.8% of the power has reached output. This phenomenon will be referred to as reverse-transfer here for convenience, which has a major negative impact on final performance of the designed device. Therefore, it should be eliminated as much as possible in the design.

As mentioned before, the difference between effective refractive index ΔN_{eff} of two waveguides is crucial to the mode conversion. When we conduct the desired mode conversion, the two N_{eff} are manipulated by changing waveguide width so that their values are close enough to trigger the converting process. However, in the meantime, such physical shape of waveguide

may have increased the chance for other modes to reverse-transfer to the assistant waveguides, which is not wanted.

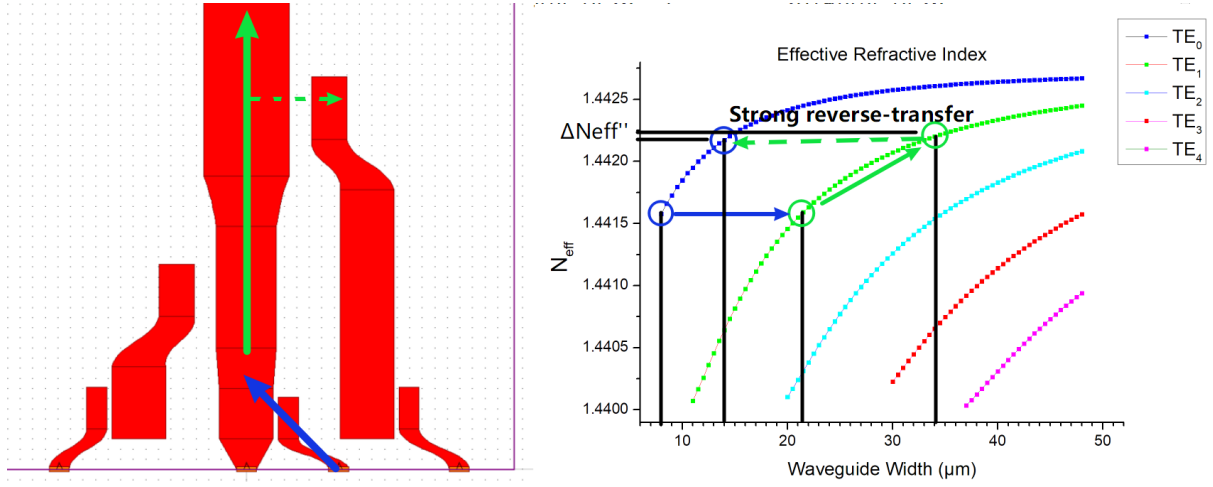


Figure 4-17 Reverse-transfer between TE₁ and TE₀

The dashed blue arrow in Figure 4-17 indicates the strong reverse-transfer from TE₁ mode in the central waveguide to TE₀ mode in the assistant waveguide. We can tell that when TE₁ mode in central waveguide passes by the conversion position, the effective refractive index difference $\Delta N_{eff}''$ between TE₁ mode in central waveguide and TE₀ mode in assistant waveguide is too small so that reverse-transfer will happen, which will result as negative impact on final performance.

Since the structure at the end of the assistant waveguide supports TE₀, TE₁ modes, other reverse-transfer will also occur at this position. Among all scenarios, the reverse-transfer from TE₁ mode in the central waveguide to TE₀ mode in the assistant waveguide is the most major issue that we need to tackle next to improve the design. Other transformations such as TE₁ mode in the central waveguide to TE₁ mode in the assistant waveguide are less likely to occur given the much larger ΔN_{eff} , thus will be ignored for the purpose of illustration.

To reduce reverse-transfer in scenarios represented by Figure 4-16 and Figure 4-17, the distance between the central waveguide and the assistant waveguide to the right is increased in final design as shown in Figure 4-1. However, larger gap could produce more side effects due

to longer conversion length. Therefore, a balance needs to be chosen carefully between obtaining a good enough result through a larger gap with longer conversion length and controlling power leakage arose from modifications. This part of the design requires the most meticulous optimization, since any change will affect other mode converting and multiplexing process between the waveguides.

The full N_{eff} matching map is shown in Figure 4-18 below, it contains all processes including mode conversions and mode-unchanged power transitions. Each colour represents a different mode ranging from TE_0 to TE_5 . The circles stand for all the modes within the simulation range. The arrows travelling between two circles but away from the dotted lines indicate mode conversion directions, and the ones along the dotted lines demonstrate variation in mode size of the same mode within the same waveguide. Furthermore, the footnotes describe the count of the same modes occurred during the simulation. Lastly for the result of this simulation, we can see from the figure that each of the four TE_0 modes finally turned into four different modes respectively in the wide central waveguide at output of the device.

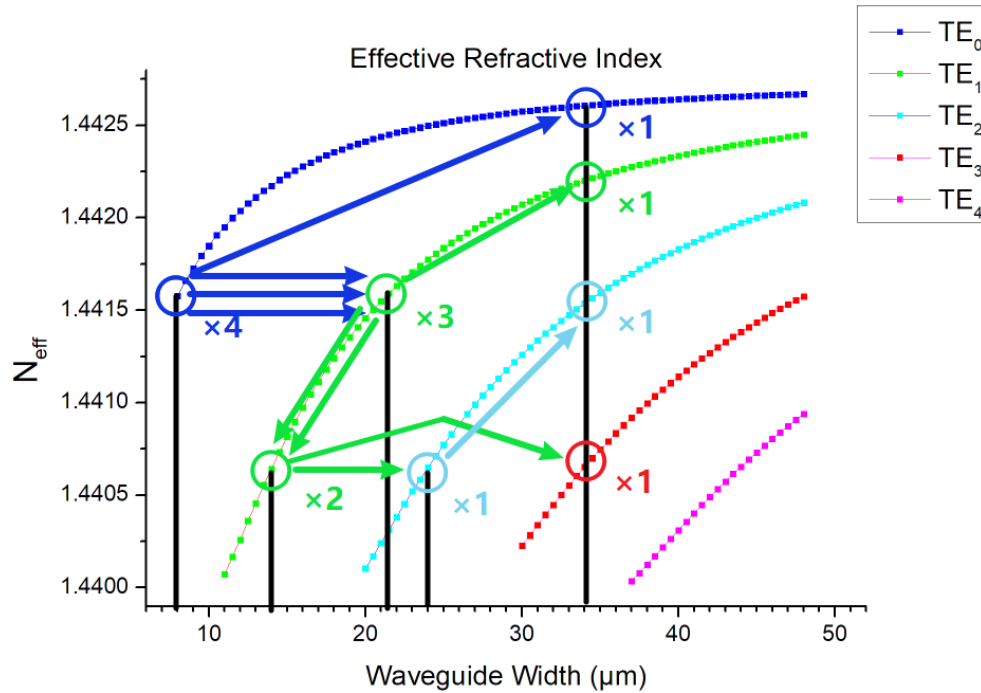


Figure 4-18 Four-Mode N_{eff} matching

4.3 Performance of the Four-Mode Design

Various performance results of the Four-Mode Design after optimization will be presented and evaluated below.

4.3.1 Input from Port 1

Under the first scenario, only TE_0 mode is injected into port 1. After the first conversion, we get TE_1 mode in the left assistant waveguide. Through the second conversion, it transforms into TE_2 mode in the central waveguide. The simulation result is shown in Figure 4-19. Extensive simulations with wavelength scan are further executed. For each simulation, insertion loss is calculated in Figure 4-20.

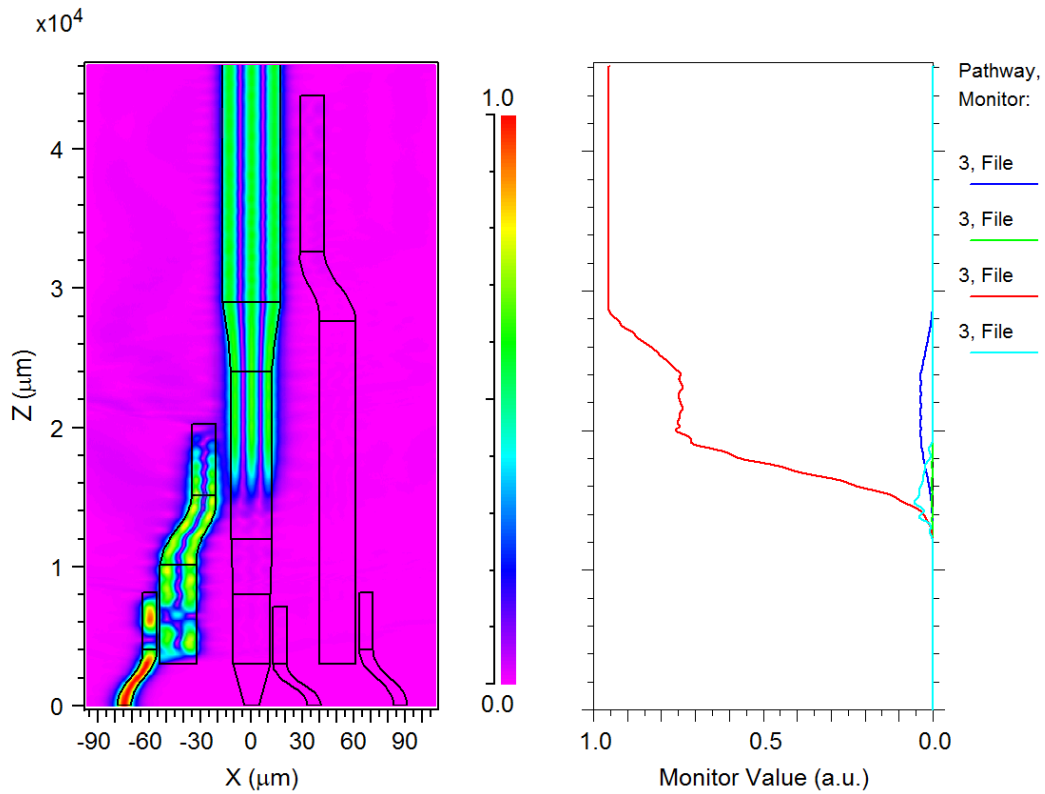


Figure 4-19 Four-Mode input at port 1

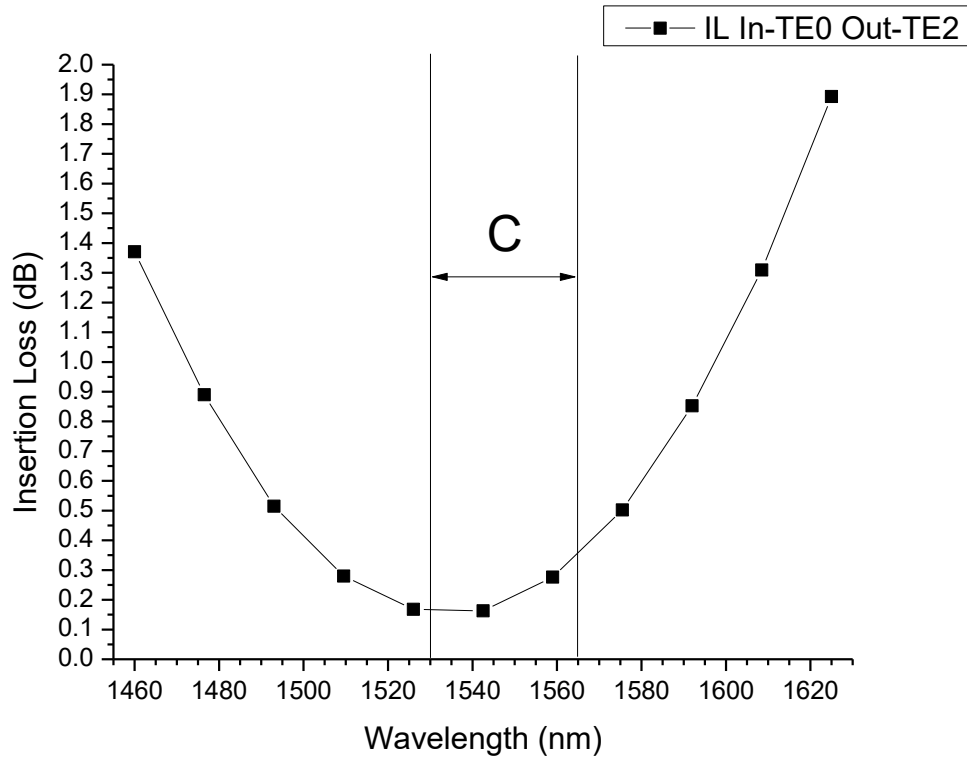


Figure 4-20 Four-Mode IL In-TE₀ Out-TE₂

Figure 4-20 indicates that insertion loss for TE₀ to TE₂ mode conversion is less than 2 dB over the S, C, L-band. For the C-band, a much better result with lower than 0.4 dB insertion loss is achieved. And at central wavelength 1550 nm, insertion loss is around 0.2 dB.

As introduced in the last chapter, we can calculate the extinction ratio to review mode purity level after simulations with wavelength scan.

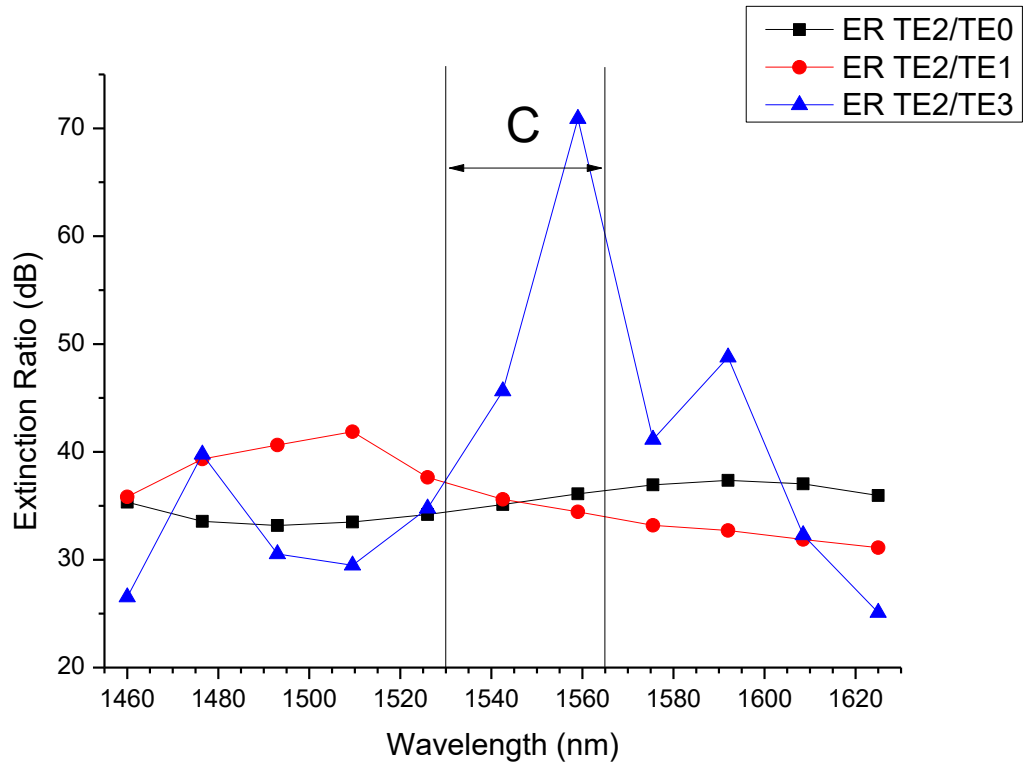


Figure 4-21 Four-Mode ER TE₂

From Figure 4-21, the extinction ratio for TE₂ mode when converted from TE₀ mode is above 25 dB over the whole S, C, L-band. Furthermore, it is over 32 dB in the C-band.

4.3.2 Input from Port 2

When optical power is injected at port 2, there is no mode conversion. TE₀ mode is received at the end of the device just with a wider power distribution as shown in Figure 4-22.

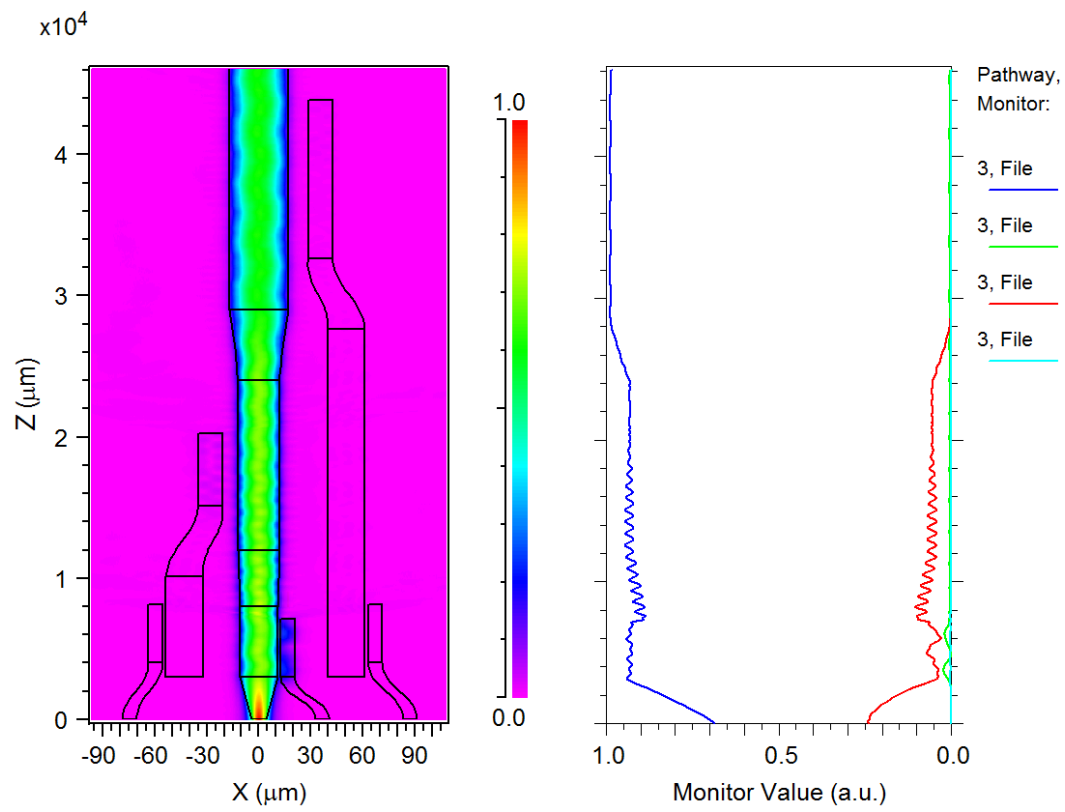


Figure 4-22 Four-Mode input at port 2

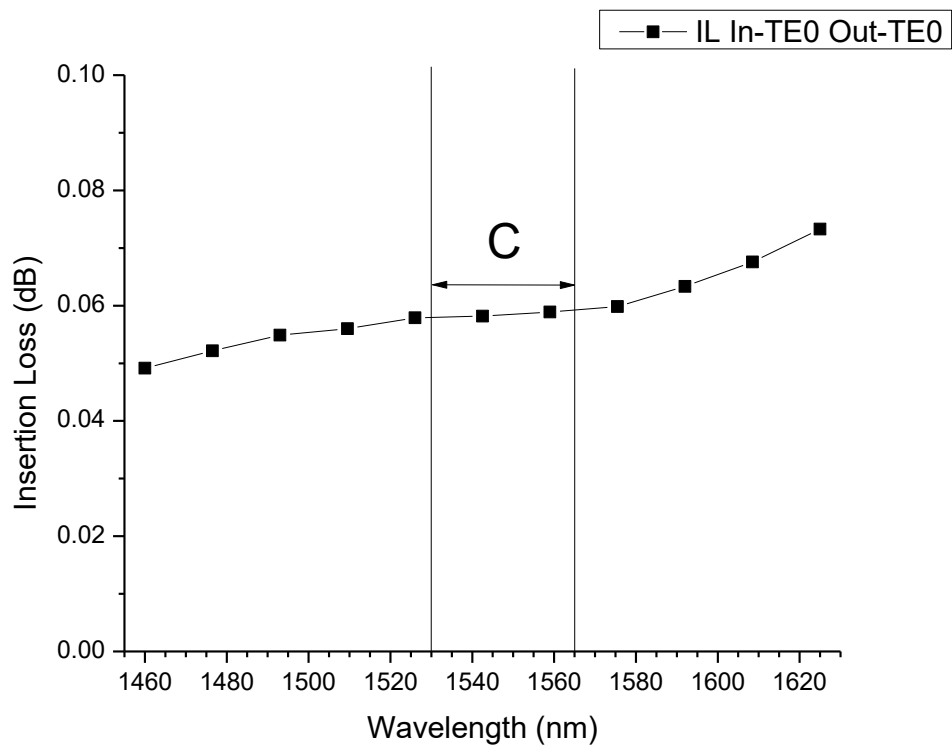


Figure 4-23 Four-Mode IL In-TE₀ Out-TE₀

Figure 4-23 shows that insertion loss is lower than 0.08 dB over the whole S, C, L-band. As shown in Figure 4-24, over the S, C, L-band, the extinction ratio of TE₀/TE₁ mode is over 23 dB. For TE₀/TE₂ mode and TE₀/TE₃ mode, it is higher than 32 dB and 37 dB respectively. Furthermore, for TE₀/TE₃ mode, the extinction ratio is higher than 52 dB over the C-band.

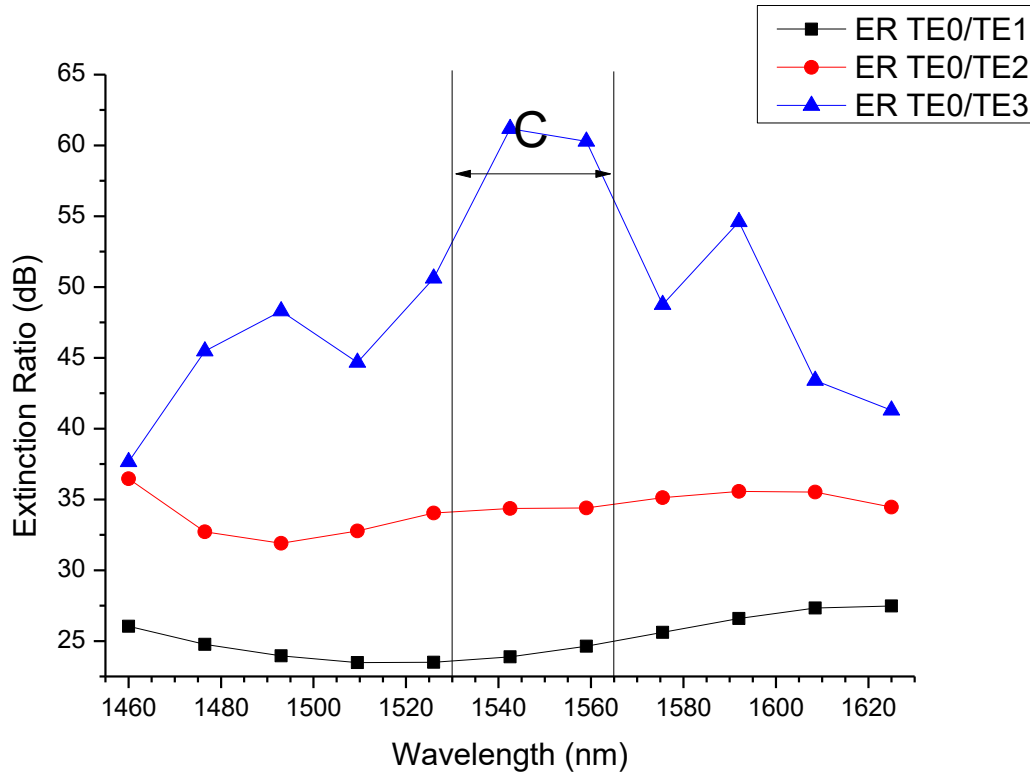


Figure 4-24 Four-Mode ER TE₀

4.3.3 Input from Port 3

To conduct TE₀ to TE₁ mode conversion, optical power of TE₀ mode is injected from port 3. After mode conversion, TE₁ mode is obtained at the end of the device.

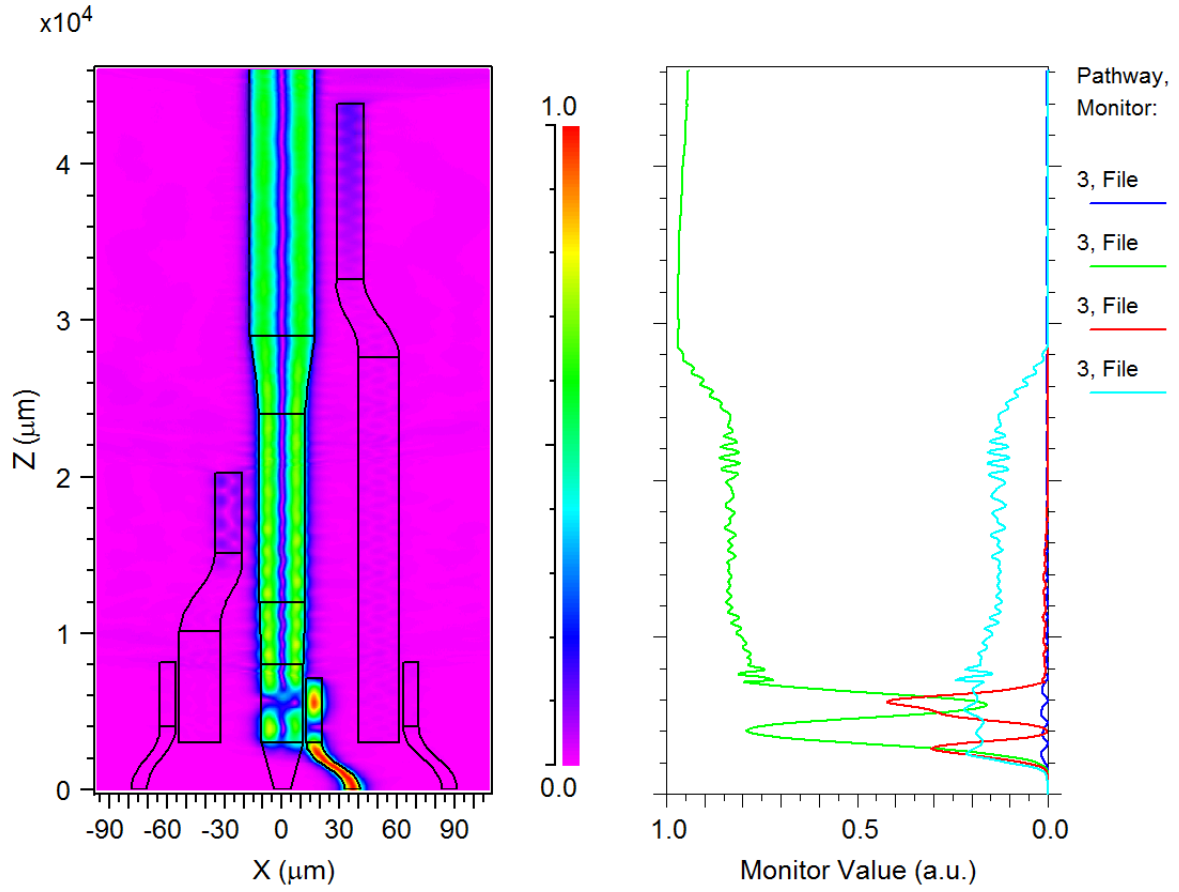


Figure 4-25 Four-Mode input at port 3

As explained before, by increasing gap width, the conversion length is also increased. So, we had to find a balance, after multiple rounds of optimization, between obtaining a good enough result through a longer conversion length and controlling power leakage of reverse-transfer arose from modifications as much as possible.

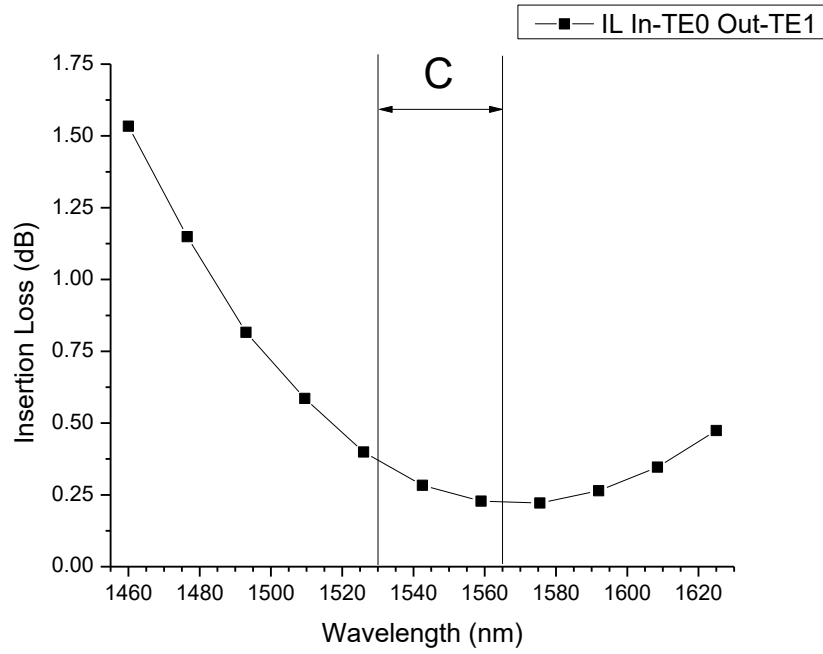


Figure 4-26 Four-Mode IL In-TE₀ Out-TE₁

Figure 4-26 shows the insertion loss results after several wavelength scan simulations when TE₀ mode is inputted at port 3 and TE₁ mode received at the end of the device. The value is below 1.6 dB over the S, C, L-band and is below 0.4 dB for the C-band.

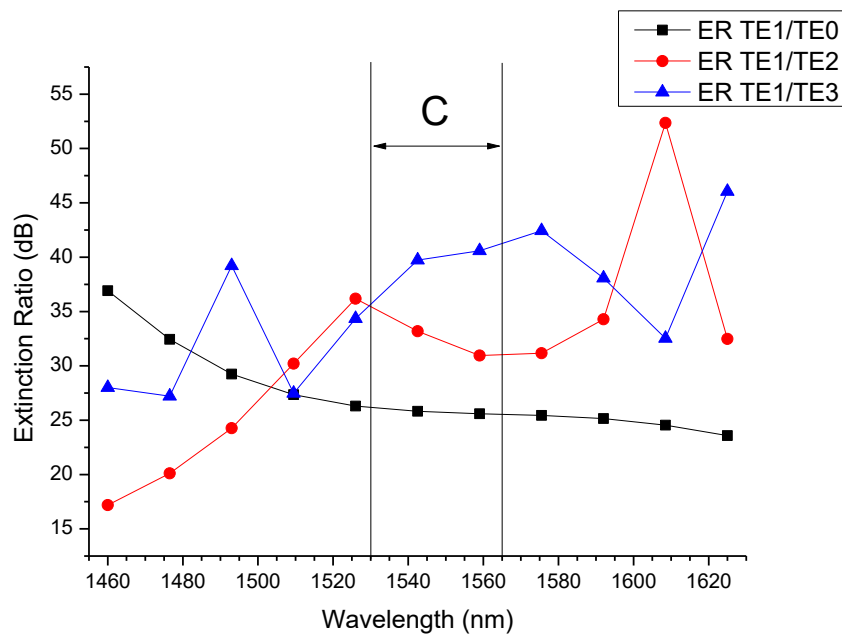


Figure 4-27 Four-Mode ER TE₁

From Figure 4-27 it can be found that the extinction ratio is above 17 dB over the entire S, C, L-band and is higher than 25 dB over the C-band. Furthermore, for the TE₁/TE₂ mode and TE₁/TE₃ mode, the extinction ratio is higher than 23 dB over the S, C, L-band.

4.3.4 Input from Port 4

To evaluate the performance of mode conversion from TE₀ to TE₃ mode, optical power is injected at port 4 as shown in Figure 4-28 to measure the results for this case.

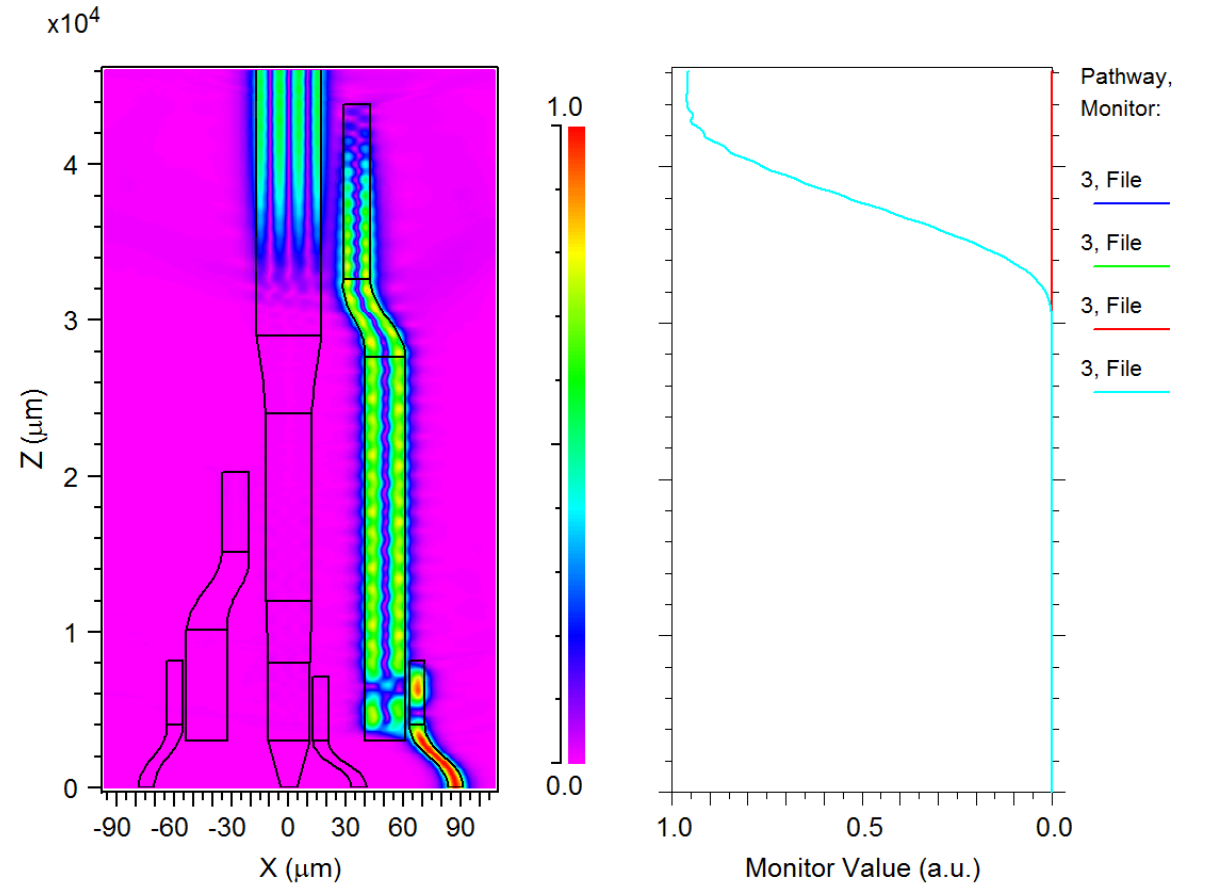


Figure 4-28 Four-Mode input at port 4

For each of the extensive simulations with wavelength scan, the insertion loss is measured and its relationship with wavelength is presented in Figure 4-29 below.

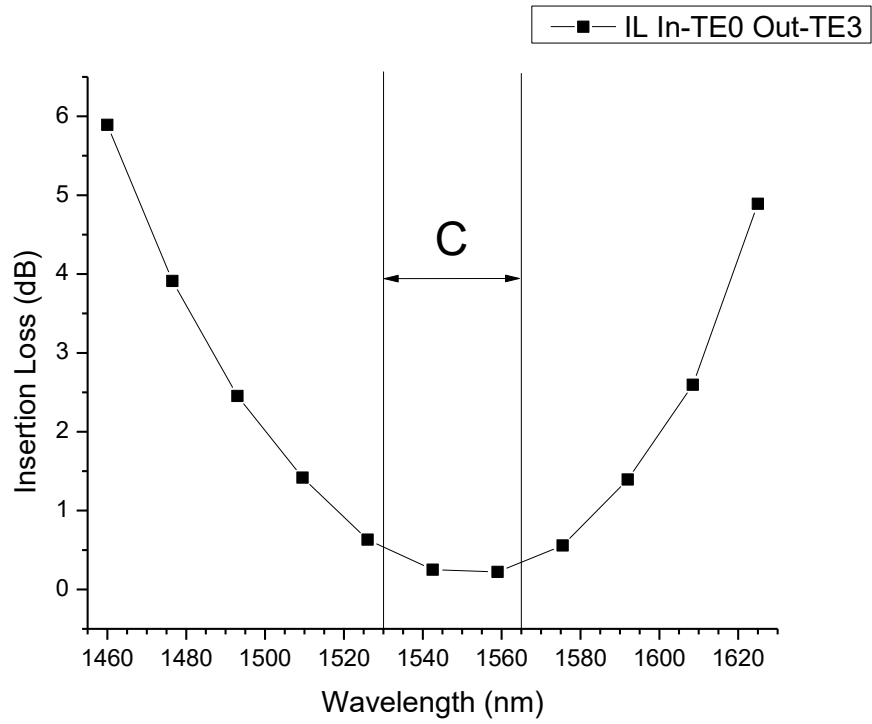


Figure 4-29 Four-Mode IL In-TE₀ Out-TE₃

From Figure 4-29 we can see that the insertion loss is less than 6 dB over the S, C, L-band, and below 0.5 dB over the C-band.

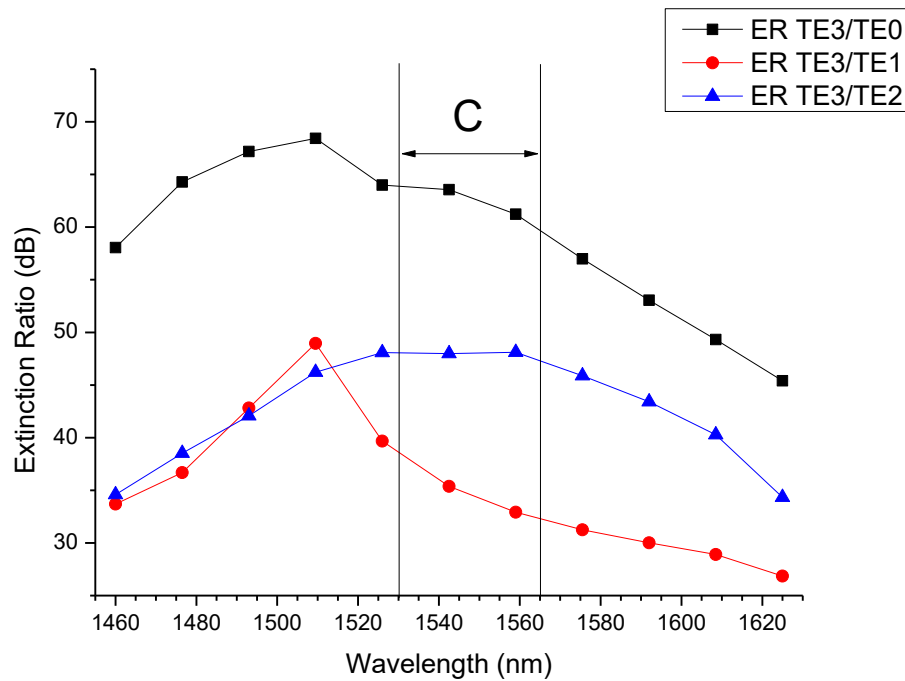


Figure 4-30 Four-Mode ER TE₃

The extinction ratio of each simulation is also measured and displayed in relation to wavelength in Figure 4-30. Over the entire S, C, L-band, the overall extinction ratio is above 26 dB, and within the C-band, the extinction ratio is higher than 32 dB. Moreover, for the TE_3/TE_0 mode and TE_3/TE_2 mode, the result is higher than 34 dB over the S, C, L-band and 46 dB over the C-band.

4.3.5 Input from All 4 Ports

Furthermore, to monitor and measure the crosstalk between all working modes, TE_0 modes are injected to all four input ports simultaneously. Figure 4-31 shows the result of the simulations with wavelength scan. As introduced in the last chapter, when there are four inputs in the system, the measured mode power is normalized to 25% each by RSoft. That is, for every output mode, a quarter in the meter is equivalent to 100% original power for each input mode.

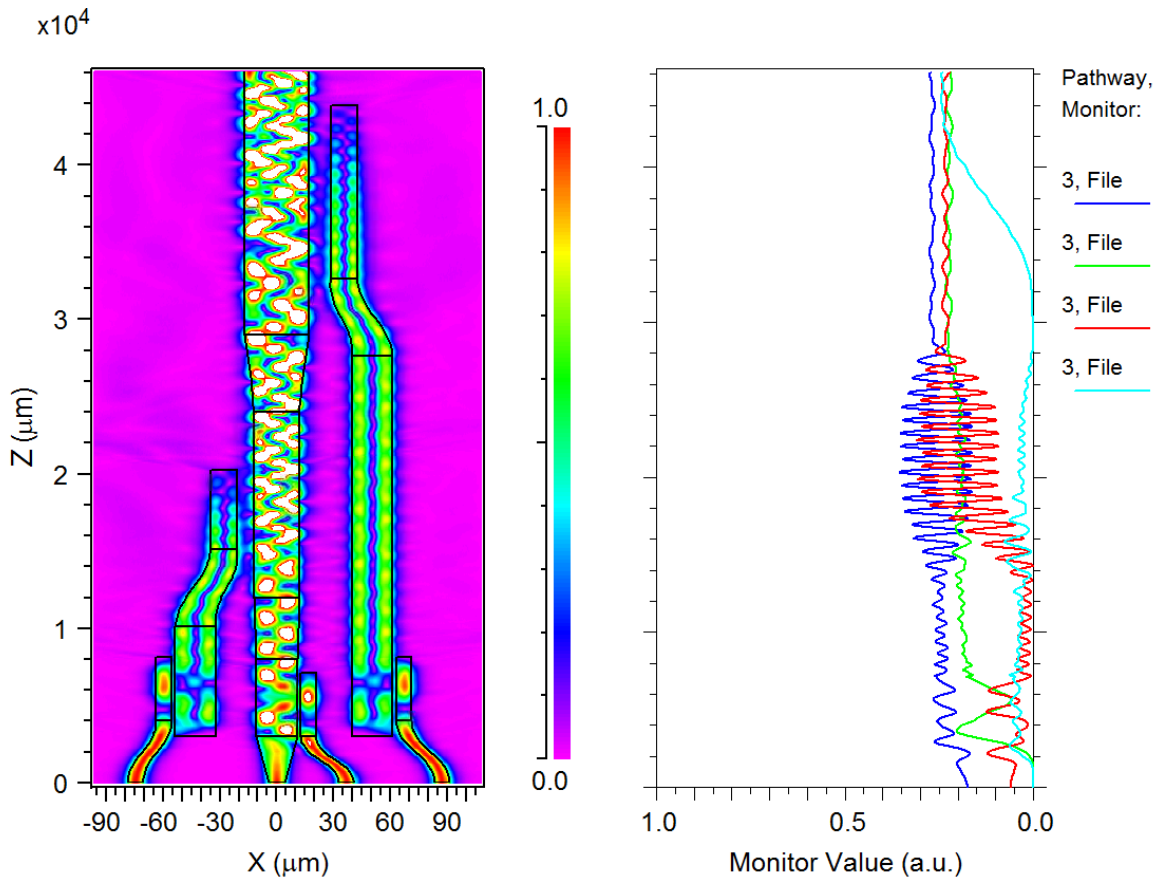


Figure 4-31 Four-Mode input all

And by using the same method introduced in the last chapter, calculated results for crosstalk can be found in the following figures.

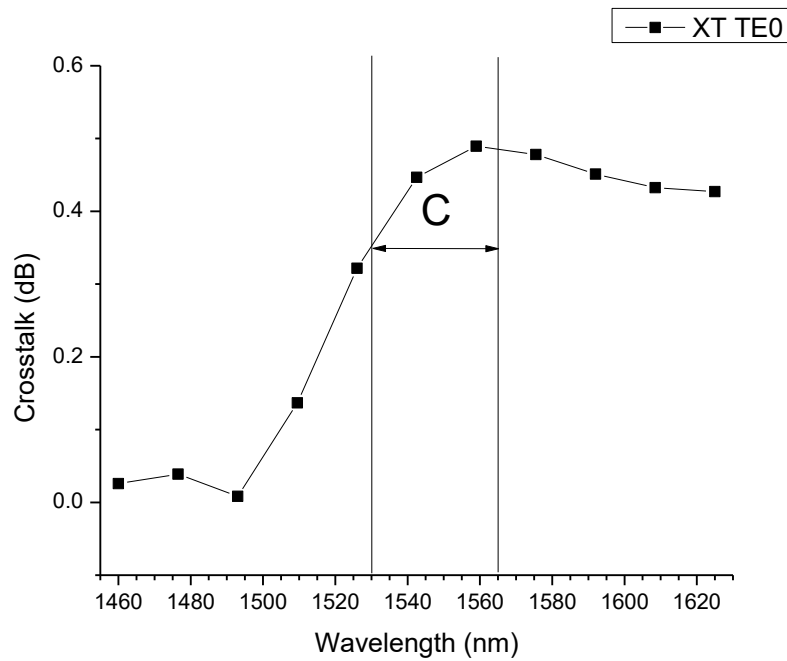


Figure 4-32 Four-Mode XT TE₀

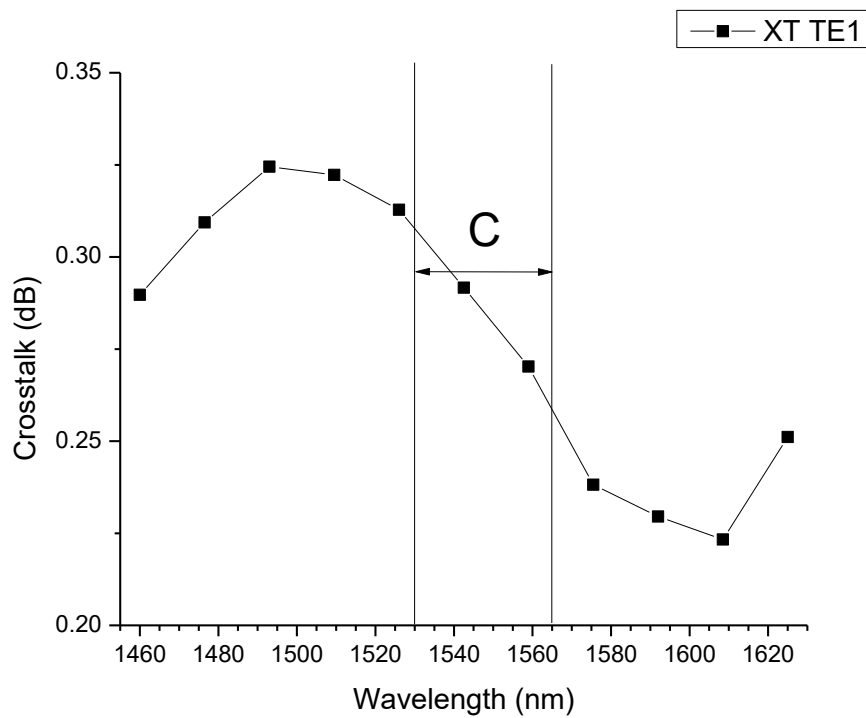


Figure 4-33 Four-Mode XT TE₁

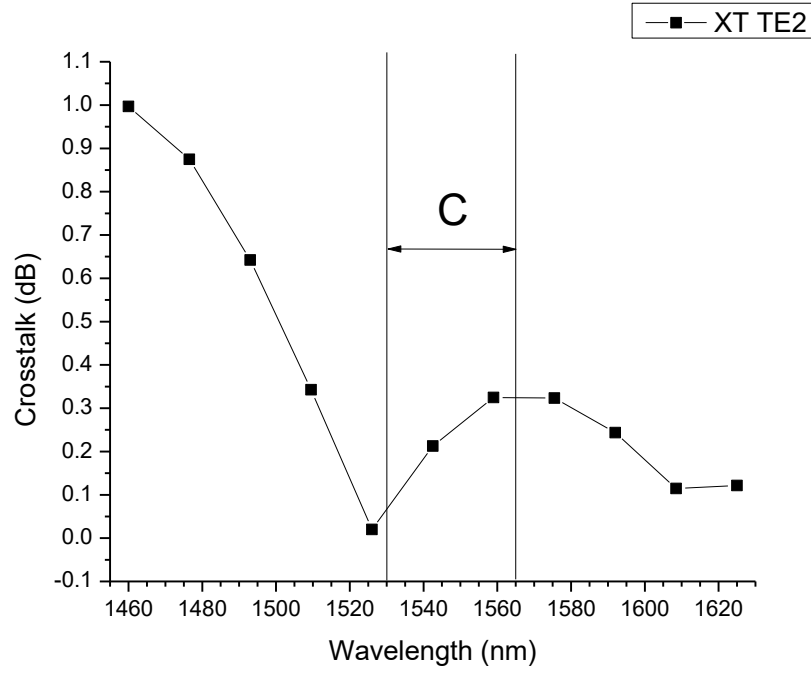


Figure 4-34 Four-Mode XT TE₂

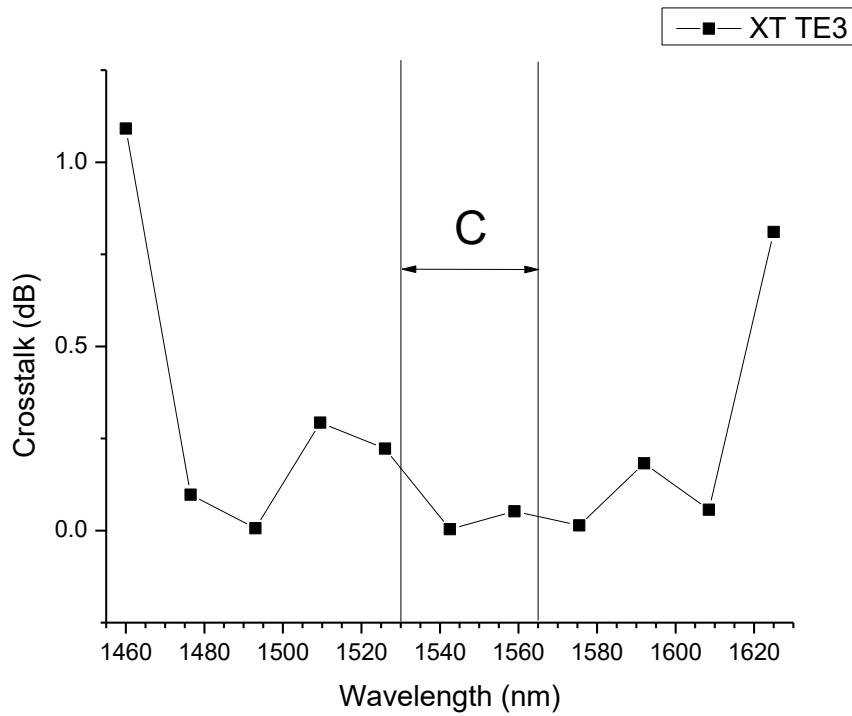


Figure 4-35 Four-Mode XT TE₃

Figure 4-32 to Figure 4-35 illustrate the crosstalk in the mode converting-multiplexing process. For TE₀ mode the crosstalk is below 0.5 dB for the S, C, L-band, and the crosstalk for

TE₁ mode is also less than 0.33 dB for the same broadband. The same metric is measured at below 1 dB and 1.1 dB for TE₂ mode and TE₃ mode respectively over the S, C, L-band. Over the C-band, it is below 0.4 dB for TE₂ mode and 0.3 dB for TE₃ mode.

4.3.6 Four-Mode Backward Conversion and Demux

Lastly, the proposed device can also be used for the reciprocal process when injecting light backwards, as shown in Figure 4-36 below. This design is functioned as a mode converter-demultiplexer. It needs to be pointed out that since the structure only supports TE in this device, the input of light should pass a polarization controller to get efficient results.

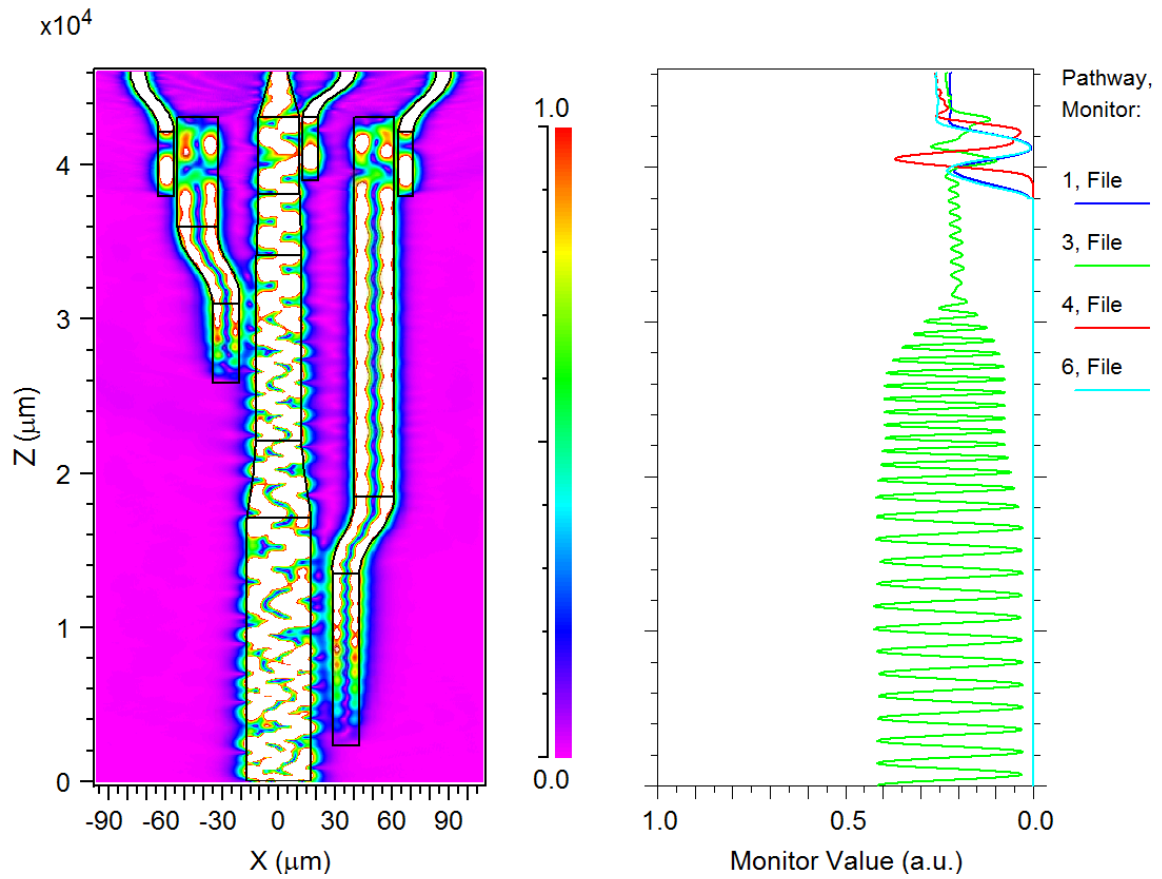


Figure 4-36 Four-Mode Demux

Figure 4-37 to Figure 4-40 below illustrate the insertion loss performance of the mode converter-demultiplexer with wavelength scan. Over the S, C, L-band, insertion loss is below 2 dB for TE₀, TE₁ and TE₂ mode input, and below 0.5 dB for all four scenarios over the C-band.

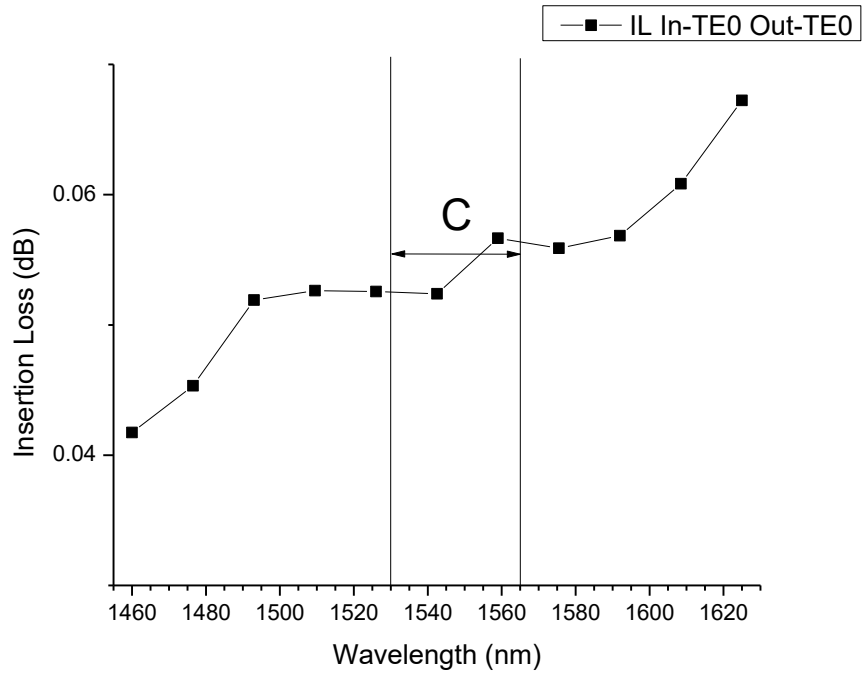


Figure 4-37 Four-Mode Demux IL In-TE₀ Out-TE₀

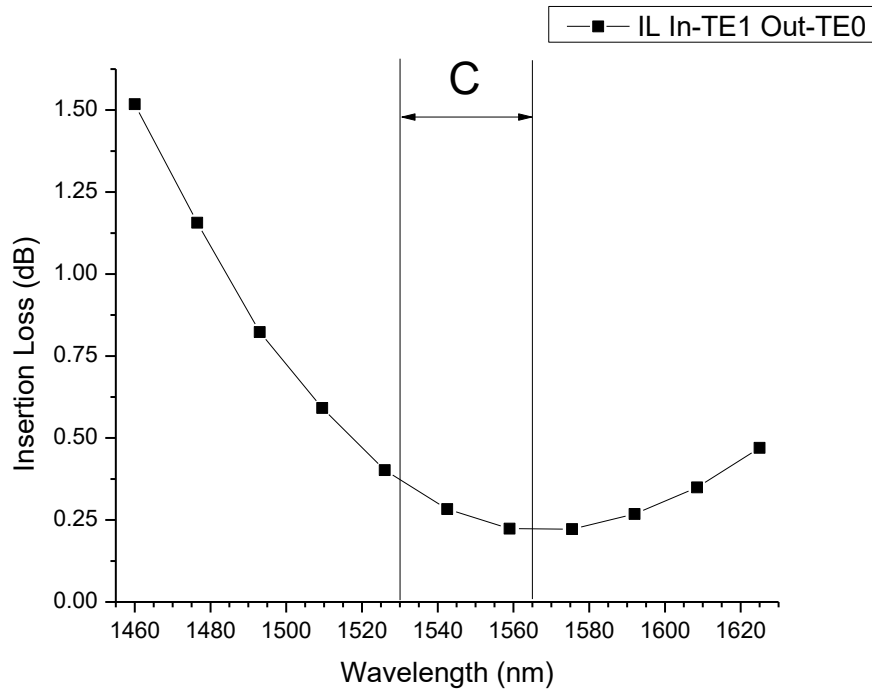


Figure 4-38 Four-Mode Demux IL In-TE₁ Out-TE₀

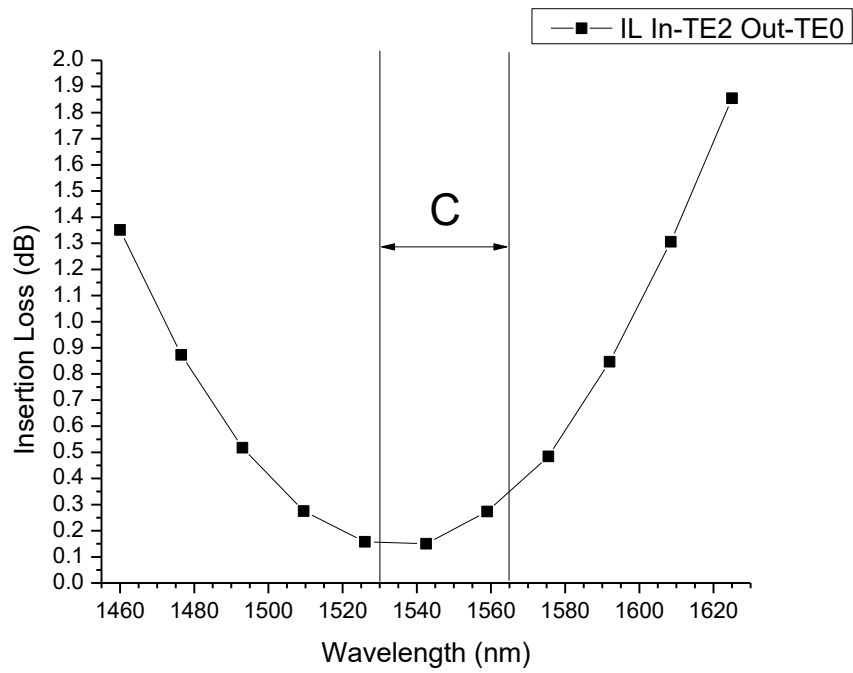


Figure 4-39 Four-Mode Demux IL In-TE₂ Out-TE₀

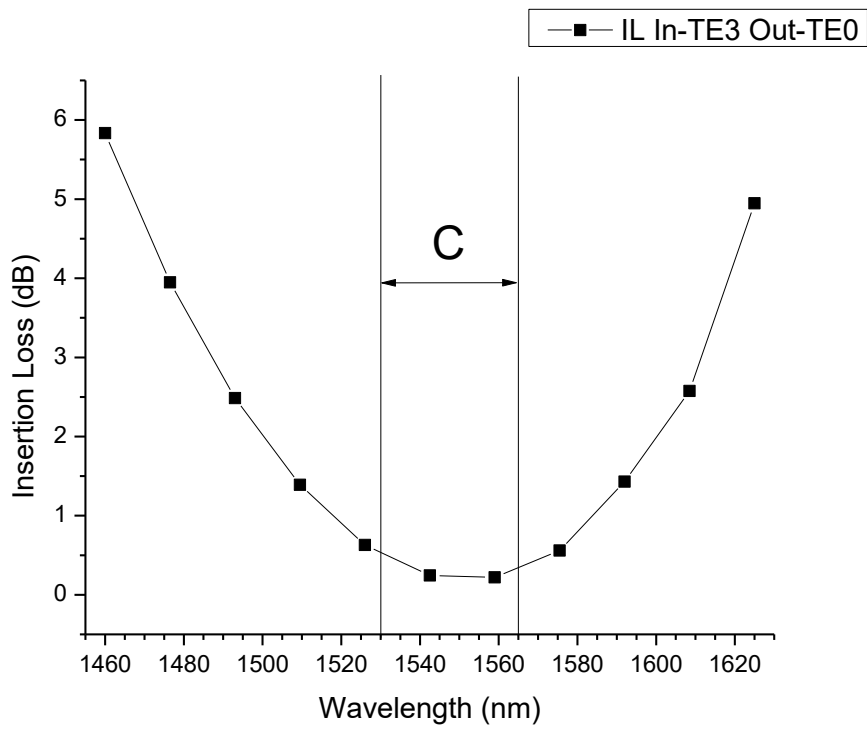


Figure 4-40 Four-Mode Demux IL In-TE₃ Out-TE₀

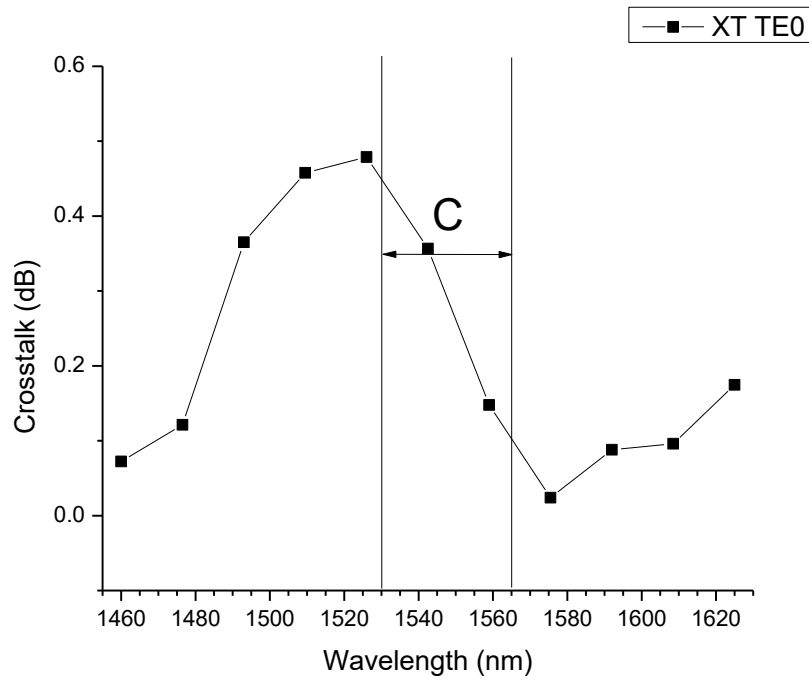


Figure 4-41 Four-Mode Demux XT TE₀

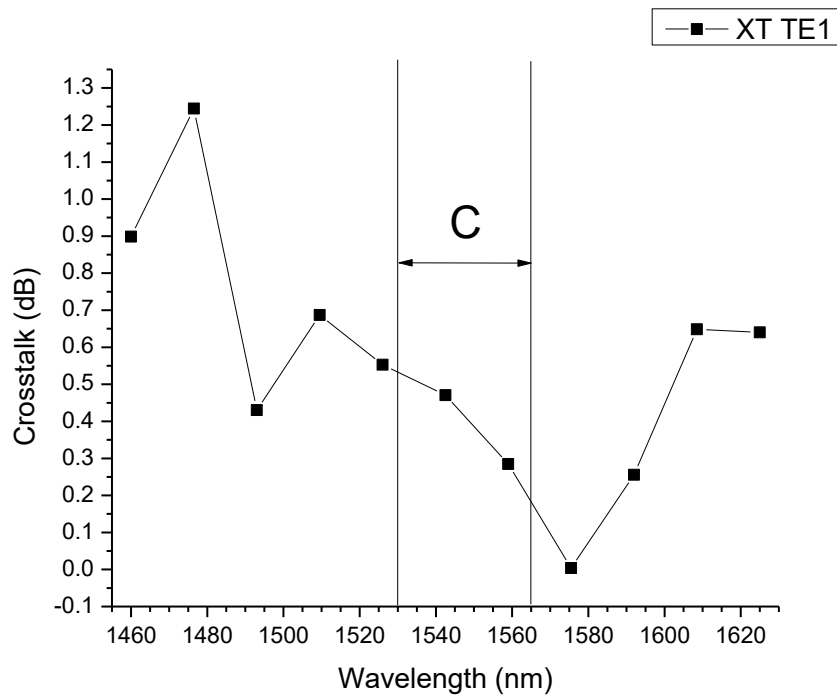


Figure 4-42 Four-Mode Demux XT TE₁

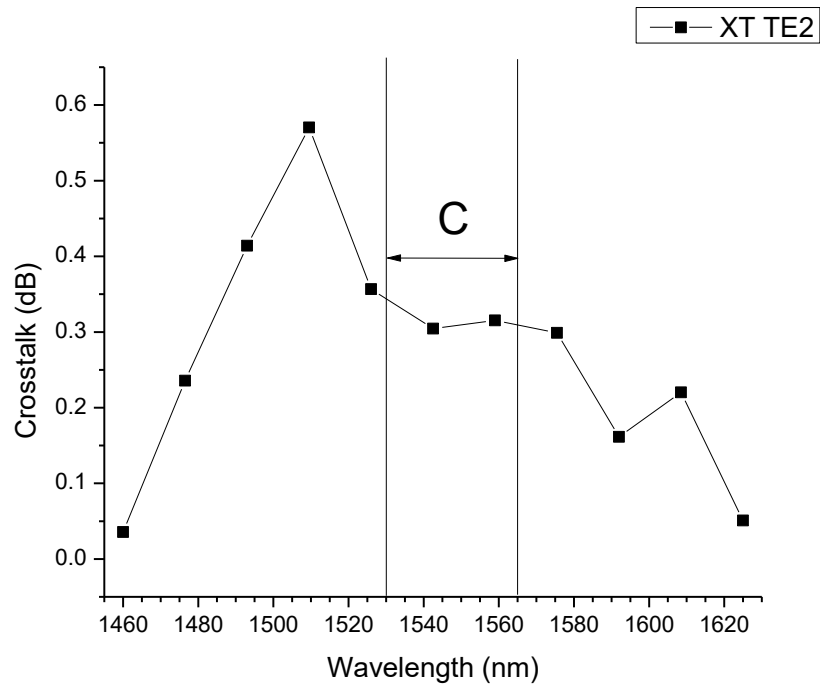


Figure 4-43 Four-Mode Demux XT TE₂

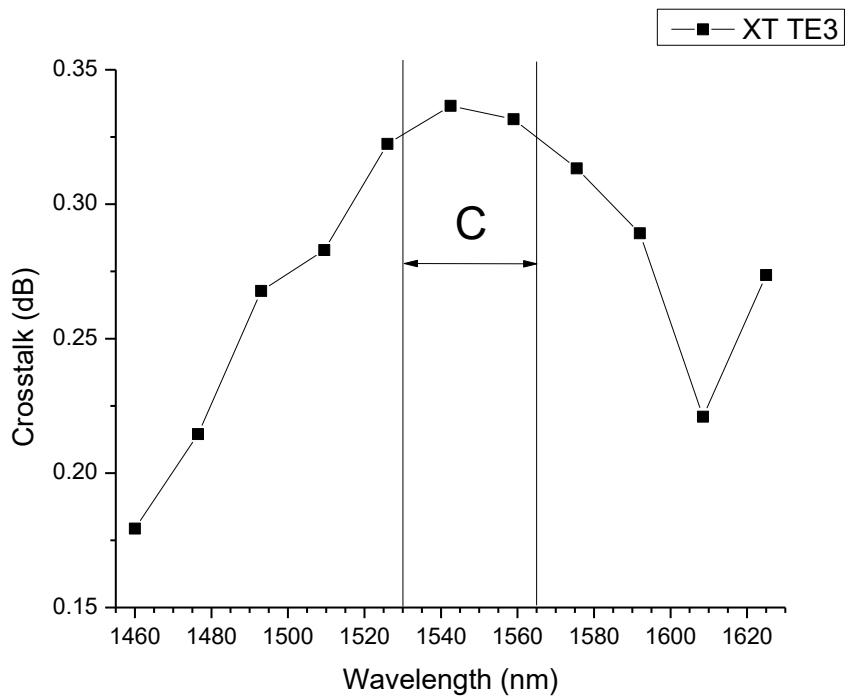


Figure 4-44 Four-Mode Demux XT TE₃

Figure 4-41 to Figure 4-44 illustrate the crosstalk in the structure by comparing output TE_0 mode power between two scenarios: one when only its dedicated input mode is injected, and the other when all input modes are injected. For TE_0 , TE_2 and TE_3 input mode, the crosstalk is less than 0.6 dB over the S, C, L-band. As for TE_1 input mode, the crosstalk is less than 1.3 dB over the same broadband and less than 0.6 dB over the C-band. Since output only supports TE_0 mode, the extinction ratio is not measured in the reciprocal operation.

Chapter 5 Conclusion

5.1 Conclusion

Optical space and mode-division multiplexing (MDM) is considered as a promising upgrade for optical transmission to increase transmission capacity. The deployment of MDM system often includes utilizing mode converter and (de)multiplexer to successfully manipulate the target modes. Fundamental mode is converted to higher mode and combined with other higher modes together. Mode converting and (de)multiplexing can be achieved through free-space optics, fibre and other waveguides-based devices.

In this thesis, a four-mode broadband planar lightwave circuit (PLC)-based mode converter-(de)multiplexer is designed and evaluated using RSoft. The design is performed starting from a two-mode device and applying the principle with multiple upgrades to a four-mode device. In the two-mode device, the TE_0 can be converted to TE_1 using two rectangular planar waveguides by matching the N_{eff} of two modes at each waveguide. Along with another unchanged TE_0 mode, overall two modes in the form of TE_0 and TE_1 can be received at output. The mode converting and multiplexing process is reciprocal so that converting and demultiplexing can also be achieved. The four-mode device is constituted by six waveguides, of which four waveguides are used to input TE_0 modes and other two waveguides are functioned as assistant waveguides. Three of the four TE_0 modes are converted to TE_1 , TE_2 and TE_3 mode and multiplexed to the central waveguide. Along with the unchanged TE_0 mode, four modes in the form of TE_0 , TE_1 , TE_2 and TE_3 can be received at output.

The two-mode device can convert and (de)multiplex between TE_0 and TE_1 mode with an insertion loss less than 1.5 dB over the entire S, C, L-band. Within the same range, the extinction ratio is higher than 22 dB, with a crosstalk under 0.5 dB.

The four-mode device inherits the same principle with multiple major changes on the waveguides to increase N_{eff} gaps for different modes at output. From TE_0 to TE_1 , the insertion

loss is less than 0.4 dB for the C-band, and less than 1.6 dB for the S, C, L-band. And the extinction ratio is higher than 17 dB for the S, C, L-band, and higher than 23 dB for the C-band. For the conversion between TE_0 and TE_2 , the insertion loss is also less than 0.4 dB for the C-band, and less than 2 dB for the S, C, L-band. The extinction ratio is above 25 dB over the whole S, C, L-band and it is over 32 dB in the C-band. Furthermore, the insertion loss between TE_0 and TE_3 is less than 0.5 dB for the C-band with the extinction ratio higher than 32 dB in the same range. The crosstalk is below 0.4 dB over the C-band and below 1.1 dB over the S, C, L-band.

5.2 Future work

With proper conditions, the device can be fabricated and tested experimentally in further research. Since the N_{eff} matching method is universal to waveguides, the same principle can be used to the silicon-based planar waveguides so that the device size can be reduced in theory.

References

- [1] D. J. Richardson, J. M. Fini and L. E. Nelson, "Space-division multiplexing in optical fibres," *Nature Photonics*, vol. 7, pp. 354-362, 5 2013.
- [2] P. P. Mitra and J. B. Stark, "Nonlinear limits to the information capacity of optical fibre communications," vol. 411, p. 4, 2001.
- [3] M. Salsi, C. Koebele, D. Sperti, P. Tran, H. Mardoyan, P. Brindel, S. Bigo, A. Boutin, F. Verluise, P. Sillard, M. Astruc, L. Provost and G. Charlet, "Mode-Division Multiplexing of 2×100 Gb/s Channels Using an LCOS-Based Spatial Modulator," *Journal of Lightwave Technology*, vol. 30, pp. 618-623, 2 2012.
- [4] R. Ryf, S. Randel, A. H. Gnauck, C. Bolle, A. Sierra, S. Mumtaz, M. Esmaeelpour, E. C. Burrows, R.-J. Essiambre, P. J. Winzer, D. W. Peckham, A. H. McCurdy and R. Lingle, "Mode-Division Multiplexing Over 96 km of Few-Mode Fiber Using Coherent 6×6 MIMO Processing," *Journal of Lightwave Technology*, vol. 30, pp. 521-531, 2 2012.
- [5] G. Yin, C. Wang, Y. Zhao, B. Jiang, T. Zhu, Y. Wang and L. Zhang, "Multi-channel mode converter based on a modal interferometer in a two-mode fiber," *Optics Letters*, vol. 42, p. 3757, 1 10 2017.
- [6] D. Garcia-Rodriguez, J. L. Corral, A. Griol and R. Llorente, "Dimensional variation tolerant mode converter/multiplexer fabricated in SOI technology for two-mode transmission at 1550 nm," *Optics Letters*, vol. 42, p. 1221, 1 4 2017.

- [7] D. Yu, S. Fu, Z. Cao, M. Tang, D. Liu, I. Giles, T. Koonen and C. Okonkwo, "Mode-dependent characterization of photonic lanterns," *Optics Letters*, vol. 41, p. 2302, 15 5 2016.
- [8] T. Fujisawa, Y. Yamashita, T. Sakamoto, T. Matsui, K. Tsujikawa, K. Nakajima and K. Saitoh, "Scrambling-Type Three-Mode PLC Multiplexer Based on Cascaded Y-Branch Waveguide With Integrated Mode Rotator," *Journal of Lightwave Technology*, vol. 36, pp. 1985-1992, 15 5 2018.
- [9] Y. Yamashita, T. Fujisawa, S. Makino, N. Hanzasa, T. Sakamoto, T. Matsui, K. Tsujikawa, F. Yamamoto, K. Nakajima and K. Saitoh, "Design and Fabrication of Broadband PLC-Based Two-Mode Multi/Demultiplexer Using a Wavefront Matching Method," *Journal of Lightwave Technology*, vol. 35, pp. 2252-2258, 1 6 2017.
- [10] A. Witkowska, S. G. Leon-Saval, A. Pham and T. A. Birks, "All-fiber LP 11 mode convertors," *Optics letters*, vol. 33, pp. 306-308, 2008.
- [11] C. P. Tsekrekos and D. Syvridis, "All-Fiber Broadband LP02 Mode Converter for Future Wavelength and Mode Division Multiplexing Systems," *IEEE Photonics Technology Letters*, vol. 24, pp. 1638-1641, 9 2012.
- [12] X. Zeng, Y. Li, W. Li, L. Zhang and J. Wu, "All-Fiber Broadband Degenerate Mode Rotator for Mode-Division Multiplexing Systems," *IEEE Photonics Technology Letters*, vol. 28, pp. 1383-1386, 1 7 2016.
- [13] H. Mellah, X. Zhang and D. Shen, "Two-stage taper fiber-based mode converters between LP 01 and LP 0m," in *Optical Communications and Networks (ICOON), 2015 14th International Conference on*, 2015.

- [14] B. Huang, H. Chen, N. K. Fontaine, R. Ryf, I. Giles and G. Li, "Large-bandwidth, low-loss, efficient mode mixing using long-period mechanical gratings," *Optics Letters*, vol. 42, p. 3594, 15 9 2017.
- [15] S. Cai, S. Yu, M. Lan, L. Gao, S. Nie and W. Gu, "Broadband Mode Converter Based on Photonic Crystal Fiber," *IEEE Photonics Technology Letters*, vol. 27, pp. 474-477, 1 3 2015.
- [16] M.-Y. Chen, G.-D. Cao, Y.-Q. Tong and L. Wang, "High-order mode conversion based on adiabatical mode evolution for mode division multiplexing applications," *Applied Optics*, vol. 56, p. 5125, 20 6 2017.
- [17] N. Hanzawa, K. Saitoh, T. Sakamoto, T. Matsui, K. Tsujikawa, M. Koshiba and F. Yamamoto, "Two-mode PLC-based mode multi/demultiplexer for mode and wavelength division multiplexed transmission," *Optics Express*, vol. 21, p. 25752, 4 11 2013.
- [18] N. Hanzawa, K. Saitoh, T. Sakamoto, T. Matsui, K. Tsujikawa, T. Uematsu and F. Yamamoto, "PLC-Based Four-Mode Multi&Demultiplexer With LP11 Mode Rotator on One Chip," *Journal of Lightwave Technology*, vol. 33, pp. 1161-1165, 15 3 2015.
- [19] N. Hanzawa, K. Saitoh, T. Sakamoto, K. Tsujikawa, T. Uematsu, M. Koshiba and F. Yamamoto, "Three-mode PLC-type multi/demultiplexer for mode-division multiplexing transmission," in *Optical Communication (ECOC 2013), 39th European Conference and Exhibition on*, 2013.
- [20] W. K. Zhao, K. X. Chen, J. Y. Wu and K. S. Chiang, "Horizontal Directional Coupler Formed With Waveguides of Different Heights for Mode-Division Multiplexing," *IEEE Photonics Journal*, vol. 9, pp. 1-9, 10 2017.

- [21] T. Uematsu, K. Saitoh, N. Hanzawa, T. Sakamoto, T. Matsui, K. Tsujikawa and M. Koshiba, "Low-loss and broadband PLC-type mode (de) multiplexer for mode-division multiplexing transmission," in *Optical Fiber Communication Conference*, 2013.
- [22] J. Wang, Y. Xuan, M. Qi, H. Huang, Y. Li, M. Li, X. Chen, Z. Sheng, A. Wu, W. Li, X. Wang, S. Zou and F. Gan, "Broadband and fabrication-tolerant on-chip scalable mode-division multiplexing based on mode-evolution counter-tapered couplers," *Optics Letters*, vol. 40, p. 1956, 1 5 2015.
- [23] Y.-J. Chang and R.-W. Feng, "Embedded-Silicon-Strip-to-Hybrid-Plasmonic Waveguide Polarization Mode Converter," *IEEE Photonics Technology Letters*, vol. 29, pp. 759-762, 1 5 2017.
- [24] V. Mere, R. Kallega and S. K. Selvaraja, "Efficient and tunable strip-to-slot fundamental mode coupling," *Optics Express*, vol. 26, p. 438, 8 1 2018.
- [25] H. Xu and Y. Shi, "On-Chip Silicon TE-Pass Polarizer Based on Asymmetrical Directional Couplers," *IEEE Photonics Technology Letters*, vol. 29, pp. 861-864, 1 6 2017.
- [26] Z. Zhang, Y. Yu and S. Fu, "Broadband On-Chip Mode-Division Multiplexer Based on Adiabatic Couplers and Symmetric Y-Junction," *IEEE Photonics Journal*, vol. 9, pp. 1-6, 4 2017.
- [27] T. Zhou, H. Jia, J. Ding, L. Zhang, X. Fu and L. Yang, "On-chip broadband silicon thermo-optic 2X2 four-mode optical switch for optical space and local mode switching," *Optics Express*, vol. 26, p. 8375, 2 4 2018.

- [28] L. Liu, "Densely packed waveguide array (DPWA) on a silicon chip for mode division multiplexing," *Optics Express*, vol. 23, p. 12135, 4 5 2015.
- [29] W. Chen, P. Wang, T. Yang, G. Wang, T. Dai, Y. Zhang, L. Zhou, X. Jiang and J. Yang, "Silicon three-mode (de)multiplexer based on cascaded asymmetric Y junctions," *Optics Letters*, vol. 41, p. 2851, 15 6 2016.
- [30] C. Li and D. Dai, "Low-loss and low-crosstalk multi-channel mode (de)multiplexer with ultrathin silicon waveguides," *Optics Letters*, vol. 42, p. 2370, 15 6 2017.
- [31] S. Wang, X. Feng, S. Gao, Y. Shi, T. Dai, H. Yu, H.-K. Tsang and D. Dai, "On-chip reconfigurable optical add-drop multiplexer for hybrid wavelength/mode-division-multiplexing systems," *Optics Letters*, vol. 42, p. 2802, 15 7 2017.
- [32] J. Wang, S. He and D. Dai, "On-chip silicon 8-channel hybrid (de)multiplexer enabling simultaneous mode- and polarization-division-multiplexing: On-chip Si 8-channel hybrid (de)multiplexer for mode-/polarization-division-multiplexing," *Laser & Photonics Reviews*, vol. 8, pp. L18-L22, 3 2014.
- [33] D. Garcia-Rodriguez, J. L. Corral and R. Llorente, "Mode Conversion for Mode Division Multiplexing at 850 nm in Standard SMF," *IEEE Photonics Technology Letters*, vol. 29, pp. 929-932, 1 6 2017.